ISOLATION AND CHARACTERIZATION OF BIOLOGICALLY ACTIVE SECONDARY METABOLITES PRODUCED BY FOLIAR ENDOPHYTES OF RED AND BLACK SPRUCE FROM THE ACADIAN FOREST

Grace Juliette Daly

A thesis submitted to the Faculty of Graduate Studies in partial fulfillment of the requirements for a degree of

Master of Science

Chemistry with a Specialization in Chemical and Environmental Toxicology

Department of Chemistry

Carleton University

Abstract

The spruce budworm is the most economically important destructive insect pest affecting North American forests. Some endophytes, isolated from the Acadian forest, produce secondary metabolites, toxic to the spruce budworm *in planta*. The aim of this study was to investigate the biologically active extracts of endophytes of red (*Picea rubens*) and black spruce (*P. mariana*). This was hypothesized to result in the isolation of antifungal and antiinsectan metabolites with structural similarities to related pathogenic toxins. From this investigation, 13 secondary metabolites were isolated. Three macrocyclic lactones (**1-3**) were characterized from *Nectria dacryocarpa*. Five aromatic polyketides (**4-8**) were isolated from two unique species of *Penicillium* cf. *glaucoalbidum* belonging to the Thysanophora sect. One small amino acid derived molecule, tyrosol (**9**) was isolated from the endophyitc *P*. cf. *glaucoalbidum.* Four lachnellulone related compounds (**10-13**) were isolated from *Lachnellula* cf. *calyciformis* including two new compounds (**12, 13**). Most purified secondary metabolites inhibited the growth of test microorganisms *in vitro*, including *Saccharomyces cerevisiae, Bacillus subtilis*, *Escherichia coli*, and *Microbotryum violaceum*.

Acknowledgements

I will first thank my supervisor Dr. David Miller, for giving me the opportunity to work on several interdisciplinary projects related to fungal endophytes of conifers. Thank you for allowing me to visit the J.D. Irving forestry research labs in Sussex, New Brunswick. This experience let me put our research into better context, and witness the impact we have on the real world. I am also grateful for having the opportunity to attend two Gordon Research Conferences and Seminars on Mycotoxins and Phycotoxins. These events emphasized the importance of collaboration, and working together as a scientific community.

Thank you to David McMullin for mentoring me during my graduate degree, and helping edit this thesis. Your expertise in the area of fungal metabolites has been absolutely invaluable, and I will remember and build upon your teachings as I move forward in my scientific career. With that, I also thank Blake Green who taught me a great deal about metabolite isolation and HPLC. Thank you both for welcoming me into the group in 2015, and for instilling a sense of lab tradition.

Thank you to Joey Tanney for all your hard work collecting, isolating, and taxonomically classifying all of the fungal specimens in this study. I am especially grateful for your help depositing the strains reported in this thesis. I also extend a thank you to Justin Renaud for your HRMS expertise.

I cannot forget to acknowledge the help of my undergraduate students and friends, Kimberlynn McDonald and Robert Pap. Keep up the good work!

I also want to thank all my fellow graduate students in the chemistry department for their support and for providing such an amazing atmosphere and student life. From our epic softball teams, garden plots, Mike's Place Trivia, LDLs, donut breaks, etc. You made this experience truly unforgettable.

To both my parents, thank you for your love and support. Thank you for teaching me to be curious, and to value the natural world and the wonders it holds if you look closely.

Table of Contents

List of Figures

List of Tables

List of Abbreviations

ATP= adenosine tri-phosphate

ACP=acyl carrier protein

ACN= acetonitrile

Apn2= DNA lyase barcode

BLAST= basic local alignment search tool

$CDCl_3$= deuterated chloroform

CD_3OD= deuterated methanol

$(CD_3)_2SO$= deuterated DMSO

$CHCl_3$= chloroform

CoA= coenzyme-A

DAD= diode array detector

DAHP= D-arabino-heptulosonic acid 7-phosphate

DAOMC= Canadian collection of fungal cultures

ddH_2O= distilled de-ionized water

DMAP= dimethyl phosphate

DMAPP= dimethylallyl diphosphate

DXP= deoxyxylulose phosphate pathways

EF1-α=translation elongation factor 1-α

EM= Embden-Meyerhof

EtOAc= ethyl acetate

FA= formic acid

FADH= flavin adenine dinucleotide

HA= heptidillic acid

Hex= hexanes

HM= hexose monophosphate

HMBC= heteronuclear multiple bond correlation experiment

HPLC= high performance liquid chromatography

Hsp90= heat shock protein

HSQC= heteronuclear single quantum correlation experiment

IPP= isopentenyl diphosphate

ITS= internal transcribed spacer

LC-HRMS= liquid chromatography high resolution mass spectrometry

LC-UV-MS= liquid chromatography ultraviolet mass spectrometry

LSD= least significant difference

MEA= malt extract agar

MeOH= methanol

ME= malt extract

MIC= minimum inhibitory concentration

MVA= mevalonic acid pathway

NaClO= sodium hypochlorite

Na_2SO_4= sodium sulphate

NADH= nicotinamide adenine dinucleotide

NADPH= nicotinamide adenine dinucleotide phosphate

NCBI= National Center for Biotechnology Information

NMR= nuclear magnetic resonance

NRPS= non-ribosomal peptide synthase

NRPs= non-ribosomal peptides

OR= optical rotation

Sect.= section

PEP= phosphoenolpyruvate

PKS= polyketide synthase

PTFE= polytetrafluoroethylene

SM(s)= secondary metabolite(s)

TCA= tricarboxylic acid cycle

TUB= beta-tubulin

UV= ultraviolet

ZEA= zearalenone

Introduction

1.1 Plants and Fungi

Fungi belong to the one of the five eukaryotic kingdoms, and are ubiquitous colonizers of the natural and built environments (Adams et al., 2013; Kendrick, 1992). The ability of fungi to metabolize complex sources of carbon and nitrogen, enable them to survive in virtually every ecological niche on the planet. Fungi are heterotrophic microorganisms that rely on complex physical and chemical associations with plants to survive within the terrestrial environment. A complex series of evolutionary adaptations has resulted in an immensely diverse collection of morphologically and chemically adapted fungal species.

Fungi within the natural environment can be classified by their roles in nutrient cycling and host interactions. They can belong to one or more of three groups including saprophytes, pathogens, and endophytes (Kendrick, 1992). Most fungi are saprophytes that decompose dead or decaying organic matter. By contrast, endophytes and pathogens survive by physical associations with living organisms. Pathogens can occasionally produce visible host disease symptoms, potentially leading to plant mortality. The current definition of an endophyte is somewhat ambiguous, and represents a group of phylogenetically diverse fungi which inhabit healthy plant tissue, without producing disease symptoms (Carroll, 1988; Tanney, 2016). Endophytes have been discovered in all plants on the planet to date (Carroll, 1988; Rodriguez et al., 2009). Pathogenic and endophytic fungi appear to exist somewhere on a spectrum between mutualism, commensalism, and parasitism depending on environmental and host conditions (Figure 1.1; Carroll, 1995; Tanney et al., 2016). Schulz theorized fungal pathogenesis is an

example of ‘unbalanced antagonism’ between the plant and fungus resulting in plant disease (Figure 1.1). Often, endophyte-plant associations lack visible disease symptoms possibly due to ‘balanced antagonism’. In this scenario, both the plant defenses and endophyte virulence factors are balanced, and the two organisms exist harmoniously (Figure 1.1). The foraging ascomycete theory suggests some ascomycetes exist as saprobes on their primary hosts, but survive as endophytes for parts of their life cycles (Thomas et al., 2016). The endophytic stage may serve as an adaptive mechanism to survive times of low moisture, until they can infect their primary hosts and reproduce in their saprophytic form (Thomas et al., 2016). Fungi can therefore belong to one or more of three groups based on their host-interactions at the time of observation, making them difficult to define.

Endophytic mutualism is commonly associated with the production of biologically active chemicals that confer fitness benefits including tolerance to biotic and abiotic stressors, nutrient acquisition, and increased biomass (Rodriguez et al., 2009). The study of endophytic mutualism has historically lead to the discovery of novel bioactive metabolites with applications in the areas of agriculture, medicine, and public health (Gloer, 1995). Carroll (1988) suggested there are five central characteristics of endophytic mutualism. The first being the endophyte must be ubiquitous over a given geographical region, and cause minimal pathogenic responses in the host. Second, the endophyte must be transmitted between hosts either vertically via the seed, or horizontally from plant-to-plant. The endophyte must propagate throughout the host

tissues, and produce SMs, which likely serve as chemical defenses. Lastly, the endophyte is closely related to herbivore or pathogen antagonists.

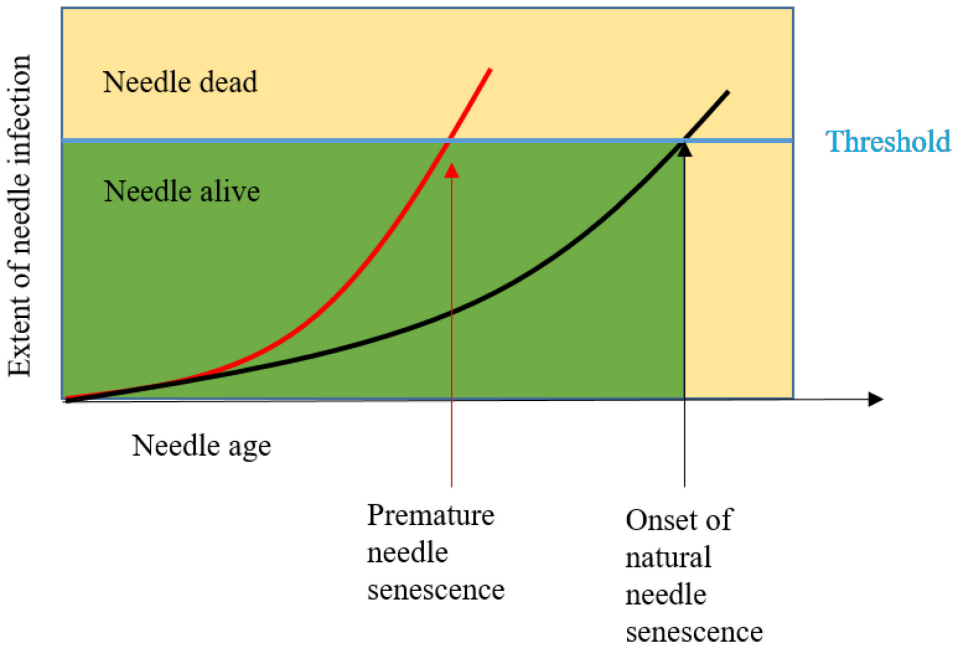

Figure 1.1: Development of senescence leading to needle death, as a function of endophytic colonization density. The black line represents normal needle senescence progression and low infection density. The red line represents premature needle senescence caused by an increase in endophytic infection, possibly due to environmental or host cues (after Sieber, 2007).

The majority of endophytes belong to the group of filamentous fungi within the phylum Dikaryomycota, which includes the subphyla Ascomycota and Basidiomycota (Kendrick, 1992). Endophytes that survive within the leaves and stems belong to the group termed 'mycophylla' compared to mycorrhiza which inhabit root systems. Within the mycophylla, there are the Claviciptaceous and non-Claviciptaceous endophytes (Sieber, 2007). The existence of fungi living inside plant tissue was not documented until the end of the 19th century (Guerin, 1898). According to fossil records, endophytes were present within some of the first recorded land plants, 500 million years ago (Redecker, 2000).

Claviciptaceous endophytes inhabit cool season grasses, and represent the longest recognized and best understood model of herbivore resistance conferred by fungal endophytes (Bacon et al., 1977; Clay, 1984; Siegel, 1987; Breen, 1994). Endophyte-symbiotic grasses were discovered by their toxic effects on grazing livestock (Clay, 1988, Porter, 1995). Early observations suggest grasses with systemic endophyte infections are less susceptible to herbivory and possess a higher degree of fitness compared to uninfected plants (Clay, 1988).

Grass endophytes are strictly host specific, and produce unique collections of alkaloid toxins. Species from the genus *Neotyphodium* specifically *N. coenophialum* are systemic symbionts of cool-season grasses, and are commonly associated with tall fescue, *Lollium arundinaceum*. Cattle grazing on tall fescue can develop gangrene of the extremities, known as 'fescue foot' and summer syndrome (Powell & Petroski, 1993). Summer syndrome is characterized by symptoms of heat intolerance, reduced weight gain, excessive salivation, rough coat, and reduced rates of pregnancy and milk production (Powell & Petroski, 1993). Perennial ryegrass (*L. perenne*) is commonly associated with strains of *N. lolii*. Sheep and cattle grazing on perennial ryegrass can develop a neurological disease characterized by severe muscular spasms leading to falls or drownings (Siegel, 1987). Grass endophytes are widespread in nature and known to propagate vertically through endophyte-infected seed. The natural occurrence of endophyte infection in wild grass is increasing over time (Clay, 1990). Grass endophytes are known to infect at least eighty plant genera, which reflects the selective advantage conferred to plants capable of harboring endophytes. Systemic endophyte infections of

grasses appear to increase plant biomass production by up to 30%. The beneficial effects conferred by grass endophytes to their hosts prompted their application as turf grass-seed inoculum (Breen, 1994). This model motivated extensive research into the endophytes of woody plants, including conifers (Sherwood-Pike et al., 1986; Carroll, 1995; Findlay et al., 2003; Sumarah & Miller, 2009). Clay (1990) provides a concise review of the Clavicipitaceae, and the nature of their ecological relationships with their hosts and herbivores. Clay (1990) emphasizes the need for more large-scale surveys of endophyte communities throughout the world to better understand the nature of these fungal infections, the co-evolutionary origin of mutualisms from pathogenic association, and the role of herbivory.

Endophytes of conifers, and woody herbaceous angiosperms cover a large geographical range from tropical to boreal and Arctic/Antarctic forest communities (Rodriguez et al., 2009). Endophytes of woody plants display increased phylogenetic diversity, decreased host specificity, non-systemic infections, and methods of horizontal transmission compared to grass endophytes. Colonization of most tree endophytes is a relatively rapid process when inoculum is airborne and the humidity is high or the foliage surfaces is wet by dew, rain or fog (Rodriguez et al., 2009). Studies on geographically separated endophyte communities of trees indicate they are species, location, and age dependent (Carroll, 1995; Espinosa-Garcia et al., 1990; Petrini, 1991). The extent of endophytic infection is a function of tree age (Espinosa-Garcia et al., 1990; Petrini, 1991). It is not fully understood if and how endophytes affect needle senescence. One theory states that under normal endophyte infection conditions, a commensal or mutualistic relationship is

maintained (Figure 1.1; Rodriguez et al. 2009). Under certain environmental and host conditions, the endophyte mycelium remains below a critical threshold, the needle senesces normally, and the endophyte sporulates on senescing or dead needle tissue. However, if conditions change, and the endophyte mycelium propagates above the critical infection threshold, it can trigger early needle senescence and subsequent sporulation (Figure 1.1; Sieber, 2007)

Fossil records indicate endophytes and angiosperms/gymnosperms have co-existed for the past 300 million years, since trees colonized land (Sieber, 2007; Rodriguez et al., 2009). Seed-grown conifer seedlings under nursery conditions completely lack endophytes (Sumarah & Miller, 2009). All natural forest trees in temperate regions are host to a diverse community of endophytes, which are angiosperm and gymnosperm specific (Petrini, 1991). Angiosperms are flat leafed trees known to host species primarily belonging to the *Diaporthales* (order), compared to the *Heoliates* (order) in angiosperms with needle-like leaves (Carroll, 1995). It is speculated that trees would not have survived millions of years without accompanying endophytes (Sieber, 2007). Trees have very long lifespans, 100-1000 years in some cases, and despite selection pressures they possess a fixed genotype over a long time period (Carroll, 1988). Carroll (1988) proposed that the short life cycles of endophytes and insects permitted heterogeneity within long-lived plants. He suggests that host plants might accommodate specific endophytes in the event of inducible mutualism and the endophytes could deter herbivorous insects by producing toxins (Carroll, 1988).

Pirozynski and Malloch postulated a similar theory that attempted to explain how plants colonized the terrestrial environment. These authors hypothesized the symbiotic relationship between algae and fungi is what formed the foundations for the first land plants (Pirozynski & Malloch, 1975). Since the origin of life approximately 450 million years ago, gradual accumulations of mutations led to the evolution of photosynthesizing bacteria into algae, and ultimately into the first land plants (Pirozynski & Malloch, 1975). Those bacteria, which lost their photosynthetic mechanisms, diverged into the first aquatic fungi; the oomycetes. The oomycete was unable to manufacture carbohydrates, and both were unable to complete their life cycles in the absence of water. Pirozynski and Malloch (1975) suggested the algae and the oomycete collaborated in a mutualistic relationship to overcome evolutionary constraints, and the first terrestrial plant and symbiotic mycorrhizal fungus emerged.

Exploring endophyte diversity relies on expert investigation into their taxonomy and phylogeny, combined with consideration of the interactions within their natural habitat. Fungi are extremely biodiverse occupants of plants, and therefore plant tissue is a multilayered (spatially and temporally) fungal habitat. There are an estimated 1.5 million fungal species on the planet, based on the estimated ratio of vascular plants to fungal species ratio (1:6), with an estimated one million undiscovered endophytic fungi (Sun & Guo, 2012). Endophytes are identified using a morphotaxonomic approach that combines morphological and molecular identification methods. First healthy needles are collected, surface sterilized, and mycelium is sub-cultured once it emerges from a needle section on solid growth medium. Sporulation can occur spontaneously, or it can be induced which

sometimes involves labour intensive protocols (Tanney, 2016). Sporulation facilitates morphological comparisons and provides taxonomically important information. This step is complicated by the difficulty in differentiating morphologically similar taxa, which may be phylogenetically distinct (Tanney et al., 2015). Endophytes are frequently sterile in culture, and therefore cannot be identified based on characteristic sporulation morphologies (Tanney, 2016). If the axenic culture is sterile and sporulation cannot be induced, DNA is extracted and the ITS barcode is sequenced. The resulting sequence is searched in GenBank BLAST, and matched to an accessioned sequence and name. If endophytes are unidentifiable based on the available sequence data, they can be connected to identifiable specimens using other DNA barcodes. DNA sequencing of various conserved fungal genome regions, including the four unlinked genetic loci ITS, Apn2, EF1-a, and TUB loci can be used as DNA barcodes. Using the ITS region alone is questionable, as it cannot differentiate between closely related taxa (Schoch et al., 2012; Sun & Guo, 2012). Identifying endophytes based on genetic sequence information is also complicated due to their enormous phylogenetic diversity, and absence of reference sequences in public databases and scientific literature (Tanney, 2016). There are currently more than 30, 000 unidentified endophyte ITS sequences published in GenBank, which can be attributed to these difficulties in identification. DNA extraction and sequencing methods can also be performed directly from plant material to avoid missing fungi which do not grow under lab culture conditions (Sun & Guo, 2012). This method is challenged by the generation of numerous unidentifiable sequences, most of which have not been studied. In practice, these methods are optimized for the respective plant species, tissues and fungi.

From a taxonomic perspective, some endophytes are related to pathogens from the same, or closely related hosts (Carroll, 1988). There are several lines of evidence to support this evolutionary progression of some pathogens to endophytes. Pathogens of agricultural crops are pre-adapted for mutualism due to their host-latency and ability to produce compounds that are toxic towards both vertebrates and insects, including herbivores (Carroll, 1988). Pathogens are known to exist endophytically within weeds growing in the same fields as important agricultural crops, adding to the difficulty in discerning the difference between a latent pathogen or endophyte (Carroll, 1988). Some endophytes may also produce virulence factors and disease symptoms (Figure 1.1) when the host becomes stressed (Carroll, 1988). Wicklow (1981) hypothesized that pathogens evolved into endophytes, which were capable of co-existing with plants without diminishing the resource by 'interference competition' (Wicklow, 1981; Carroll, 1988). When two different species are exploiting the same resource for survival, and there are not limitless resources to support both parties, interspecific competition occurs. He proposed that fungi exploit mechanisms of antibiosis to ensure that levels of their resource do not deplete. Endophytes fit into this theory because they are using the host plant as a resource, and occasionally defend it through antibiosis (Wicklow, 1981). This idea is supported by taxonomic evidence whereby the grass endophyte *N. coenophialum* is closely related to fungal pathogen *N. typhiba* (Clay, 1988). Secondly, the *Rhabdocline parkeri* endophyte of Douglas-fir is morphologically similar to fungal pathogens *R. wierrii* and *R. pseudotsugae* (Carroll, 1988).

1.2 Metabolism

Primary metabolism is accomplished through a series of catabolic and anabolic reactions that break down carbohydrates for cellular energy in the form of (ATP) (Drew & Demain, 1977). In addition to ATP, these reactions yield reduced NADH and NADPH which power the production of ATP in the final stage of primary metabolism. Alternatively, other products of metabolism function as biosynthetic intermediates for amino acids, nucleotides, vitamins, carbohydrates, and fatty acids which give fungi structure and biological function. Collectively, these reactions exist within a network of enzymatically-regulated metabolic pathways, which enable fungi to grow, reproduce, and respond to their environment. Secondary metabolic processes rely on anabolic reactions which harness free energy to build more complex molecules. Small molecular weight metabolites are produced from a few precursors (primary metabolites) formed during primary metabolism, after all cell growth conditions have been satisfied. The fundamental building blocks of fungal metabolites include three primary metabolites; acetyl-CoA, shikimic acid, and mevalonic acid (Drew & Demain, 1977).

Carbohydrates are the main source of energy for fungi, and are oxidized by several primary metabolic pathways including glycolysis, the TCA cycle, and oxidative phosphorylation (Dewick, 2002). Initially, glucose is first converted to pyruvate and ATP before it enters the TCA cycle via the EM glycolytic pathway. Simultaneously, fungi exploit the HM pathway to generate NADPH, the primary reducing agent in the biosynthesis of fatty acids, sugars, alcohols, and nucleotides (RNA, DNA). In the second and third stages of primary metabolism, pyruvate is aerobically converted to CO_2 by the

TCA cycle. The pyruvate dehydrogenase complex is a multi-enzyme system, which catalyzes the oxidation of pyruvate to CO_2 and acetyl-CoA. This metabolic process is an essential source of energy for the cell, and yields two CO_2, three NADH, one $FADH_2$, and one GTP molecules for each acetyl-CoA oxidized. Acetyl-CoA is a critical primary metabolite intermediate molecule produced during the catabolism of carbohydrates, lipids, and amino acids. It is energy rich due to the thiol ester bond connecting the CoA and acetate moieties. Reducing equivalents (NADH and $FADH_2$) contribute to the formation of ATP in the final step of primary metabolism, the electron transport chain and oxidative phosphorylation. As reducing equivalents are oxidized and electrons are passed to O_2, energy is stored in the form of a differential proton electrochemical gradient across the inner mitochondrial membrane. Oxidative phosphorylation takes advantage of this electrochemical gradient, and powers the reverse hydrolysis of ATP.

Primary metabolites are products and intermediates of primary metabolism whereas secondary metabolites are products of secondary metabolism. Secondary metabolites can be classified into three groups, according to the primary metabolite starting material. Polyketides are assembled from units of acetate, terpenes are biosynthesized by either the mevalonic acid dependent or independent route, and non-ribosomal peptides rely on amino acids. Secondary metabolites may also arise from mixed biosynthetic pathways. The biosynthetic machinery required for the production of secondary metabolites are uniquely encoded in biosynthetic gene clusters, which are often separated by approximately 2-kb (Walton, 2000). Biosynthetic clusters contain the regulatory genes that control the pathway, and genes for conferring self-resistance (Walton, 2000).

Clustering of biosynthetic genes has been attributed to some selective pressure (Walton, 2000; Spatafora et al., 2002). This clustering also supports the mechanism of horizontal gene transfer, which would be more effective by movement of small contiguous clustered DNA fragments.

Polyketides and NRPs are predominantly produced by ascomycetous fungi, as revealed to date (Schmidt-Dannert, 2015). Based on genomic studies, ascomycetes contain between 20 and 40 non-ribosomal peptide and PKS biosynthetic gene clusters per genome. By comparison, Basidiomycetes may possess less than ten, very few of which have been investigated closely. This would suggest these two groups of fungi have evolved to produce different collections of natural products Ascomycetes produce polyketides, non-ribosomal peptides, and indole derived compounds, whereas Basiomycetes produce more terpenoid based compounds (Schmidt-Dannert, 2015).

Polyketides are the most abundant group of natural products, are produced primarily by ascomycetes, and include phenols, prostaglandins, and macrolides (Dewick, 2002). Both aromatic and non-aromatic polyketides have been identified from fungal ascomycetes, and most are products of iterative type I PKS enzyme. Type I PKS enzymes are multi-domain protein complexes, similar to eukaryotic fatty-acid synthases. Iterative type I PKS enzymes, catalyze the formation of a growing poly-β-keto ester from acetyl-CoA or propionyl-CoA starter units, and malonyl-CoA or methylmalonyl-CoA extender units (Figure 1.2). This growing chain is extremely reactive, and is stabilized by an enzyme until chain elongation is complete. Type 1 PKS enzymes are one or more large

multifunctional proteins with distinct active sites. Type I PKS enzymes can modify the beta-ketone to a hydroxyl, methnyl, or methylene if it has ketoreductase, dehydratase, or

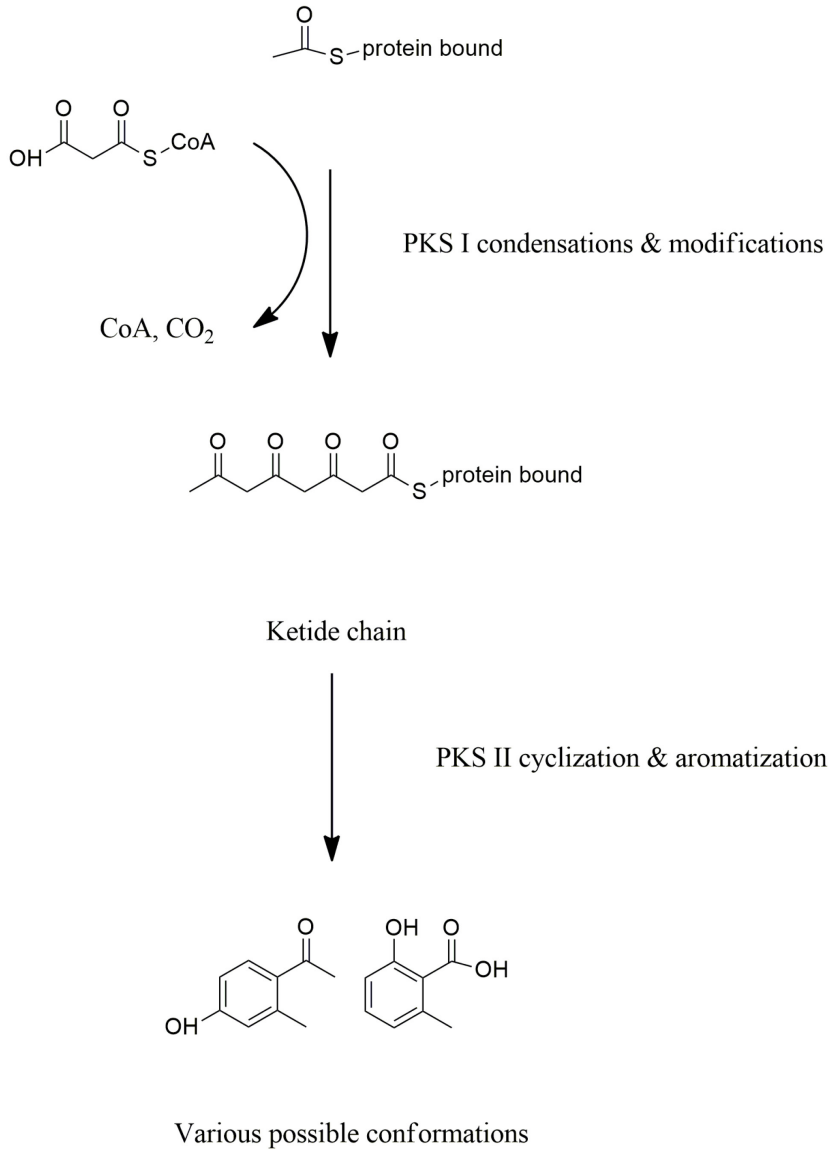

Figure 1.2: Figure illustrating the condensation of acetyl-CoA and malonyl-CoA producing a poly-β-keto ester via multiple Claisen reactions (after Dewick, 2002; Green, 2016).

enoylreductase domains (Dewick, 2002). Once the appropriate chain length is synthesized, the metabolite intermediate may undergo cyclization and aromatization by type II PKS enzymes. First, the molecule folds in one of several possible sterically

favorable conformations dependent on the chain length, branch points, and degree of reduced functional groups. In all cases, methylenes flanked by two carbonyls are activated (electrophilic), permitting intramolecular Claisen and/or Aldol reactions. This generates intermediate carbanions/enolates that may react with ketone or ester carbonyl functionalities, producing an energetically favorable aromatic ring. In the final step, the final product is released from the CoA or ACP via thioester bond hydrolysis. Type III PKS enzymes add cinnamoyl-CoA starter units to a select group of alkaloids, and form a distinct group of PKS enzymes (Dewick, 2002). Very few reducing domains in PKS I often results in the production of cyclic polyketides and pigments. In contrast, certain PKS I enzymes rich in reducing groups yield molecules similar to fumonisin, a linear polyketide. Notable polyketides include the mycotoxin aflatoxin B1, and the pharmacologically important cholesterol-lowering compound lovastatin (Keller et al., 2005). This immense number of reduction reactions, the identity of the carbon extender unit, the number of extender units, and potential for cyclization reactions directly influences the degree of variation present in this family of natural products (Keller et al., 2005).

The primary metabolites shikimic acid is the building block for aromatic compounds (Hermann, 1995). Shikimic acid is synthesized from PEP and erythrose 4-phosphate, intermediate molecules from the glycolytic and HM pathways, respectively. The shikimic acid pathway is an alternative route by which microorganisms and plants generate a variety of phenolic acids and lignin derivatives (Dewick, 2002). First, PEP and D-erythrose 4-phosphate are enzymatically condensed to produce DAHP. Phosphoric acid is

subsequently eliminated from DAHP, and an intramolecular aldol reaction generates 3-dehydroquinic acid. A series of enzyme catalyzed dehydration and reduction steps ultimately yield shikimic acid. Three aromatic amino acids including phenylalanine, tyrosine, and tryptophan, are biosynthesized by the shikimate pathway, where shikimic acid is converted to chorismic acid, and further enzymatically transformed into either L-Phe, L-Tyr, or L-Trp.

Terpenes are characteristically odoriferous and composed of several isoprene units in a linear, cyclic, saturated or unsaturated organization (Dewick, 2002). Some examples of fungal terpenes include aristolochenes, carotenoids, gibberellins, and trichothecenes (Keller et al., 2005). Terpenes or isoprenoid natural products are synthesized from isoprenoid precursor molecules that are converted into complex biomolecules such as sesquiterpenoids, diterpenoids, and triterpenoids. The foundations of the isoprenoid precursor molecules are IPP and DMAPP, and are generated by one of two pathways; MVA or DXP. The MVA pathway relies on mevalonic acid, a product of acetate metabolism. The DXP pathway is an alternative way to IPP and DMAPP, and is likely more frequently occurring in nature than the MVA pathway (Dewick, 2002). Terpenes are formed by the combination of IPP and DMAPP into longer prenyl chains by the head to tail condensations catalyzed by isoprenyl diphosphate synthases. This yields linear prenyl chains of ten, fifteen, twenty or more carbons in length. Further modifications include the processing of the linear chains by enzymes that transfer prenyl chains to other molecules, typically an aromatic compound. Prenyl chain cyclization, which is less common in fungi, can also occur. Many different combinations and variations of prenyl

transferases and cyclases generate the vast structural diversity of isoprenoid-derived metabolites (Schmidt-Dannert, 2015). Giberellin is a notable terpene molecule which functions as a plant growth hormone and is produced by plants and various phytopathogens including *Gibberella fujikuroi*. Tricothecenes are a family of metabolites produced by *Fusarium* and other related genera. *Fusarium* tricothecenes inhibit eukaryotic protein biosynthesis and their contamination of agricultural contaminants present serious negative health impacts on humans and livestock.

Indole alkaloids are an example of mixed pathway biosynthesis that involves both aromatic moieties and prenylated aromatic moieties derived from tryptophan and DMAPP. The biosynthesis of indole alkaloids generally begin with the region- and stereoselective transfer of DMAPP to a tryptophan-derived indole ring via condensation of the prenyl chain. Other enzymes catalyze this reaction of prenyl chains to other aromatic substrates including polycyclic polyketides and phenols, or O- and N-functionalities of aromatics. This group contains several pharmaceuticals and toxins produced by strains if *Aspergillus, Penicllium, Claviceps, and Neosartorya* (Schmidt-Dannert, 2015). An example indole alkaloid is ergotamine produced by *Claviceps purpurea* (Hoffmeister & Keller, 2007). Ergotamine synthesis begins with the addition of prenyl groups, then methylation and a series of oxidation steps to yield agroclavine which converts to lysergic acid. A tripeptide is added onto the lysergic acid, with ergotamine as the final product (Hoffmeister & Keller, 2007).

NRPs are non-ribosomally assembled by the multimodular enzymes termed NRPSs (Hoffmeister & Keller, 2007). NRPS enzymes have specific catalytic domains, which together catalyze the formation of NRPs. The resulting polypeptides can be combined with polyketide structures, producing NRPS and PKS hybrid SMs. Due to the immense pharmacological impact of penicillin and cephalosporins, they are the most well understood models of NRPS biosynthesis pathways. β-lactam antibiotic, such as penicillin and cephalosporin, are assembled from a linear tripeptide containing L-α-aminoadipic acid, L-cysteine and L-valine (Hoffmeister & Keller, 2007).

1.3 Fungal Secondary Metabolism

Humans have been experimenting with the biochemical processes of microorganisms for thousands of years. Ancient Egyptians (4000 BC) used Brewer's yeast to leaven bread, eventually leading to their application as food and drink preservation and fermentation methods (Demain & Fang, 2000a). Penicillin, the antibiotic produced by several species of penicillium, was identified by its antagonistic behaviour towards *Staphylococcus aureus* after it accidentally contaminated Fleming's culture dishes (Fleming, 1929). The optimization of penicillin fermentation in the 1940's initiated the 'golden age' of industrial microbiology, leading to the identification of thousands of new molecules with applications in the areas of medicine, agriculture, and basic scientific research. The selective action of metabolites against other organisms including bacteria, fungi, and mammals make them antibacterial, antifungal, and antitumor chemotherapy agents. Over 40% of filamentous ascomycetes including fungal endophytes produce antibiotics *in vitro*, making them the largest secondary metabolite producing group of fungi (Demain &

Fang, 2000). Acquired chemical defenses are the most common and well understood basis for endophytic mutualism within plants (Carroll, 1988).

It is widely accepted that secondary metabolites provide other competitive advantages to the producing organism; however, in most cases the benefits are unknown. It is theorized that fungi produce metabolites for purposes including weapons against other organisms competing for resources within the same environment, metal chelators, agents of symbiosis, sex hormones, and effectors of morphological differentiation (Carroll, 1988; Wicklow, 1981). Fungal metabolites have also been shown to be cytotoxic, mutagenic, carcinogenic, teratogenic, immunosuppressant, enzyme inhibitors, and allelopathic (Keller et al., 2005). Most fungal natural products are biologically active and many inhibit the growth of bacteria, fungi, protozoa, insects and viruses (Keller et al., 2005). Notably, more than half of the 1500 compounds discovered between 1993 and 2001 had either antifungal, antibacterial, or antitumour activities (Tudzynski, 2014). The vast structural and functional diversity of fungal secondary metabolites make them ideal candidates for targeted isolations and characterizations.

The biochemical association of fungi with plants occur by the production of SMs. Primary metabolism produces cellular energy and universal primary metabolites including amino acids, nucleotides, vitamins, carbohydrates and fatty acids. Secondary metabolism is much more limited in nature and is not essential for growth and reproduction. Only specific organisms or strains with the proper genetic machinery, under nutrient limitation, occupying specific environmental conditions at certain life stages may

produce true secondary metabolites (Miller, 1984). At the micro level *in vivo*, only the few cells immediately behind the advancing mycelium actively produce secondary metabolites from thread like structures (3-4 μM) (Sumarah & Miller, 2009). *In planta*, the metabolite concentration must reach a threshold for it to have specific activity on its molecular target. Secondary metabolism by fungi *in planta* occurs the interstitial spaces of the cells in the foliage (Sumarah & Miller, 2009). In conifers, freeze fracture scanning electron microscopy images depicts the hyphae of a *A. balsamea* endophyte present in the intercellular spaces, associating with the outer walls of parenchyma cells without cellular penetration (Johnson & Whitney, 1989). Water content and the water-available volumes of specific tissue architectures limit mycelial growth within plant tissues. Additionally, toxin production represents a small amount of toxin per penultimate cell instead of continuous production. This likely reflects a biomass to toxin ratio dependence like that of deoxynivalenol production in corn (Miller et al., 1983). In controlled fermentations, billions of cells grow in a synchrony, yielding predictable and measurable ratios of metabolite production to dry weight, nutrient depletion, and respiration (as described in Sumarah & Miller, 2009).

In vitro, fungal secondary metabolism only occurs during the 'unbalanced' cellular growth phase. This follows the 'balanced' phase, when all nutrients are supplied and the growth of the fungus is rapid and linear. The unbalanced phase begins when one or more nutrients in the medium become limiting or is exhausted, the mycelial growth ceases but the cells begin producing SMs. Nitrogen limitation is what most fungi encounter most frequently *in vivo*, and is known to induce the production of polyketides such as

zearalenone and deoxynivalenol, and other toxins in conifers (Miller, 1984; Krnjaja et al., 2015; Sumarah & Miller, 2009). Other fungi including several *Penicillium* species produce penicillin when carbon limited (Kluge et al., 1992). The *in vitro* carbon to nitrogen ratio is an important determinant for secondary metabolite production. It is important to emphasize that the same fungus can produce different metabolite mixtures depending on the environmental conditions, meaning this process is highly variable and influenced by external factors. Additionally, the biosynthesis of secondary metabolites is energetically expensive, and are therefore produced to provide an overall competitive benefit.

Fungi that inhabit competitive environments experience unique selection pressures, which influence their secondary metabolic processes. Plant pathogens are well known producers of phytotoxic and antifungal compounds active against host plants and other competing fungi, respectively. Endophytes within stems and leaves experience selective pressures from the host, insect pests, herbivores, and fungal pathogens leading to the production of defensive compounds for specific scenarios (Miller, 1984; Williams & Vickers, 1986). Carroll and Carroll proposed the idea that foliar endophytes antagonize leaf pathogens by way of decreasing leaf palatability. Gloer rationalized that since mycelia and fruiting structures are avoided by insects and arthropods, secondary metabolites are likely responsible (Gloer, 1995). Gloer found that the sclerotia and ascostromata contained antiinsectan metabolites, which may serve to protect the fungus against insect predation. Wicklow (1981) provided compelling evidence that secondary metabolism functioned within the context of what he termed ‘interference

competition'(Wicklow, 1981). There are many examples of this type of ecological relationship, specifically in trees and wood. *Trichoderma viride* produces a collection of metabolites capable of limiting the growth of other wood decomposing fungi (Wicklow, 1981). Some lignicolous marine fungi are also capable of producing molecules which combat the growth of competing fungi in the environment (Miller, 1984; Carroll, 1988). Mycorrhizal fungi protect plants from root pathogens by the production of antibiotics in the local environment (Marx, 1972).

1.4 Anti-insect Toxins

Investigation into the biologically active metabolites of *Picea* (spruce) endophytes has resulted in the discovery of several anti-insect toxins (Calhoun et al., 1992, Findlay et al., 1997; Findlay et al., 2003; Sumarah & Miller, 2009; Sumarah et al., 2010). The first reported antiinsectan metabolites from conifers include three sesquiterpene lactones from endophytes of *Aibes balsamea* (Calhoun et al., 1992). The sesquiterpenes isolated included HA, two HA chlorohydrin derivatives, and a hydro-HA, which were toxic towards *Choristoneura fumiferana* (spruce budworm) larvae between 5-15 μM concentrations (Figure 1.3).

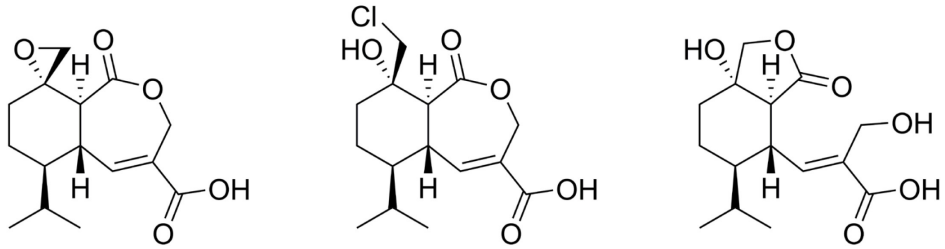

Figure 1.3: Chemical structures of the initially discovered antiinsectan sesquiterpenes isolated from Douglas-fir endophytes.

The collections of endophytes from the Acadian forest (New Brunswick) made in 1984 and 1987-88, resulted in the collection of *Phialocephala scopiformis* isolated from white spruce (*Picea glauca*) and produced the antiinsectan compound rugulosin, as well as closely related skyrin and emodin (Figure 1.4; Miller et al. 2002). This metabolite was acutely toxic to the spruce budworm at dietary concentrations of 10-25 μM (reduced growth rate). At concentrations of 50 μM, this toxin produced equivalent effects towards other *Picea* pests (Calhoun et al., 1992; Miller et al., 2008). When the endophyte was present in needles, rugulosin concentrations as low as 0.5 μg g^{-1} of needle resulted in reduced growth rates of spruce budworm larvae (Miller et al., 2008).

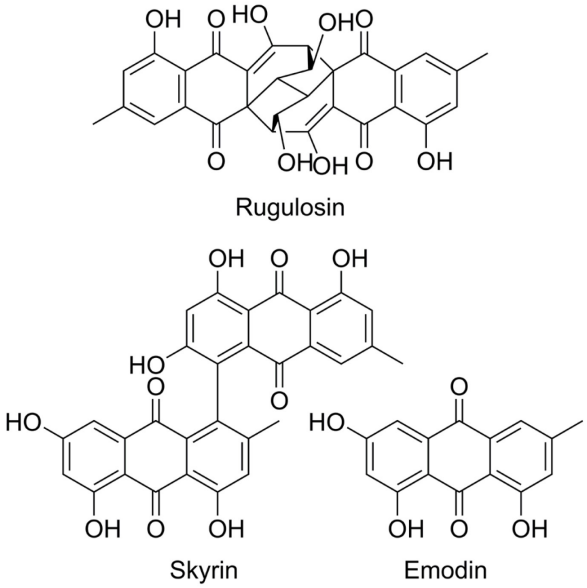

Figure 1.4: Chemical structure of rugulosin and related natural products produced by *Phialocephala scopiformis* DAOM229536.

The polyketides illustrated in Figure 1.5 were characterized from an undescribed *Mycosphaerella* species collected independently from black (*P. mariana*) and red spruce

(*P. rubens*). These polyketides are toxic towards the spruce budworm (Findlay et al., 1995; McMullin et al., 2017).

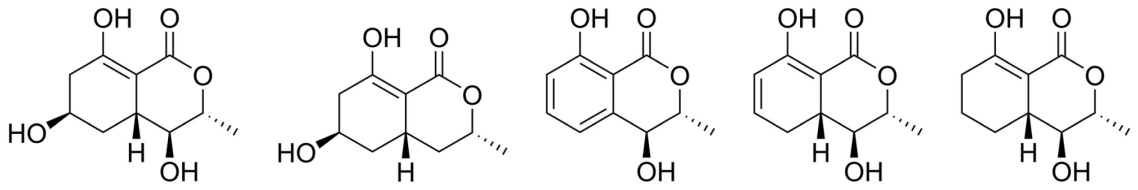

Figure 1.5: Chemical structures of isocoumarin polyketides isolated from a black spruce endophyte from the *Mycosphaerellaceae*.

More recently, two new polyketides (Figure 1.6) were isolated from a black spruce endophyte in the Rhytismataceae (Family) (McMullin et al., 2017). However, only rhytismatone B exhibited moderate antifungal activity, inhibiting the growth of *Saccharomyces cerevisiae* at 25 μg mL^{-1} concentrations (Figure 1.6). The rhytismatone metabolites did co-occur with other known biologically active compounds including two pthalides, two isocoumarins, and one amino-acid derived compound known to inhibit the growth of spruce budworm larvae (McMullin et al., 2017).

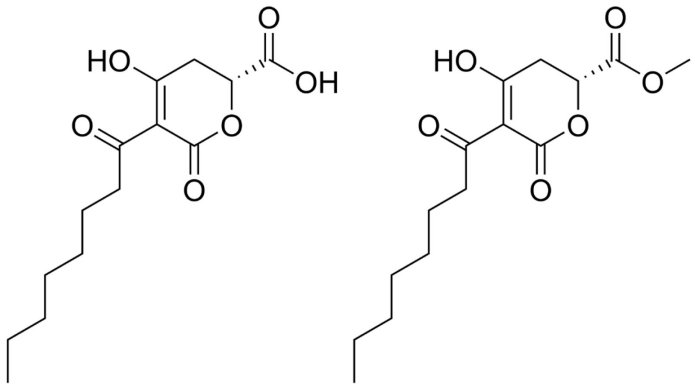

(**A**) (**B**)

Figure 1.6: Chemical structures of rhytismatones (**A**) and (**B**) isolated from *Rhytismataceae* sp. DAOMC 251461.

1.5 The Acadian Forest

The Acadian forest is concentrated in Maine, New Brunswick, Nova Scotia, Prince Edward Island, and includes parts of eastern Quebec (Miller, 2011). The forest is comprised of red (*Picea rubens*), black (*P. mariana*), and white spruce (*P. glauca*), balsam fir (*Abies balsamea*), yellow birch (*Betula alleghaniensis*) and sugar maple (*Acer saccharum*). Additional trees include red pine (*Pinus resinosa*), eastern white pine (*P. strobus*), eastern hemlock (*Tsuga canadensis*), and beech (*Fagus* sp.).

The spruce budworm the most economically important insect pest threatening North Americas coniferous forests (Gray & MacKinnon, 2006; Royama et al., 2005). Balsam fir (*A. balsamea*) is the most susceptible to spruce budworm defoliation. Several other spruce species are vulnerable to infestation including *P. glauca, P. rubens,* and *P. mariana* with 70%, 40% and 30% favorability, respectively (Royama, 1984). Since 300 years ago, the 20th century has experienced the most frequent spruce budworm outbreaks in 9 forest regions in eastern Canada (Blais, 1983). Instead of only localized regions being affected by the insect pest, nine regions seem to have coalesced into a larger affected areas of 10, 25, and 55 million ha in the outbreaks of 1910, 1940, and 1970, respectively. Reasons for the increase in frequency and intensity of outbreaks is attributed to anthropogenic forest changes such as clear cutting of pulpwood stands, fire protection, and pesticides use against the budworm (Blais, 1983).

Macrofossil analysis suggests the Acadian forest has been uniquely susceptible to spruce budworm outbreaks for the last 8240 years (Miller, 2011). The Acadian forest has been

the central unit of study and measure for understanding spruce budworm life cycles and population dynamics. *C. fumiferana* reach critical population levels to be considered epidemic every 35 years, and have been re-occurring in a cyclical pattern for the past five centuries (Royama, 1984; Royama et al., 2005). In 1952, the Canadian Forest Service-Atlantic Forestry Centre began surveying spruce budworm populations, and since 1982 by the New Brunswick Department of Natural Resources (Royama et al., 2005). This survey information is continuously providing ecologists with a wealth of data to probe for more information on the insects' complex life cycle. Moths lay their eggs in masses on the needles of susceptible trees, and within ten days the larvae have dispersed and commenced their first life stage, termed the first-instar. It is not until late April or May of the following year that the larvae begin to consume the foliage of their 1-2 year old seedling hosts, pupating into their final moth stage (Royama et al., 2005). In 1984 during Royama's quest for understanding the factors influencing the population dynamics of the insect, he postulated the existence of a 'fifth agent' (Royama, 1984). He elaborated on the theory calling it an "intriguing complex of unknown causes", whereby a large number of larvae exhibiting no distinct symptoms of disease died during the population decline which took place in the 1950's. The most significant decrease in population was the proportion of budworm surviving from the fifth to sixth instars. He also noted in his study that his results relied on observations made from host trees, known to survive budworm defoliation. It is hypothesized by Royama that this cycling pattern will repeat itself and the spruce budworm population will rise again.

Endophytes of conifers were proposed as the fifth agent affecting the cyclical epidemic of the spruce budworm in the Acadian forest (Miller, 1986). This was further supported by the observations that defensive terpenoids produced by conifers weren't sufficiently toxic towards insects to deter their herbivory. By contrast, many fungal endophytes have been shown to produce antiinsectan SMs, toxic towards the spruce budworm at effective concentrations *in planta* (Miller et al., 2008; Frasz et al., 2014). Miller (1984) collected fungi from budworm-infected and non-budworm-infected conifers between May to July in 1983 and 1984. Samples selected from budworm-infected needles resulted in a doubling in diversity of isolated fungal specimens. Specific fungal isolates were systematically selected based on their frequency of isolation from needles, and their association with infected and uninfected trees. Metabolite extracts were generated from culture filtrate following *in vitro* fermentations of the isolates. Some extracts were shown to reduce the growth rate of spruce budworm larvae, HeLa cells, and other fungi (Miller, 1984). It was also demonstrated that fungal endophytes are horizontally transmitted between trees, and therefore modern re-forestation processes (i.e. production of seedlings in greenhouses) have probably reduced endophyte diversity in the natural environment (Miller et al., 2009). Since then, conifer endophytes have been studied in great detail using a holistic approach and modern taxonomic identification methods, with special focus on their secondary metabolites (Miller, 2011).

The needles of Douglas-fir trees were one of the first examples of endophyte-mediated antagonism towards insect pests in conifers (Carroll, 1988). In regions of the Pacific Northwest, *R. parkeri* accounts for 90% of the endophytic infections observed in

Douglas-fir (Sherwood-Pike et al., 1986). Douglas-fir trees are particularly susceptible to attack by any of three species of gall midges from the genus *Contarinia*. The flies emerge from eggs and subsequently damage the young needles by chewing holes through them. Multi-year studies performed by Carroll shed light on the theory of antagonism between *R. parkeri* and the gall midge insect (Carroll, 1988). Prof. Carroll suggested that the mortality of the flies was due to fungal toxins, which were shown to be toxic to the spruce budworm *in vitro* (Miller, 1986). Carroll was also able to show the diversity of coniferous needle endophytes in Oregon and forested areas in the Pacific Northwest. This further supports the existence of a diverse array of conifer endophytes, heavily dependent on climate and geographical region (Carroll & Carroll, 1978).

The best-studied foliar endophyte from the Acadian forest is *Phialocephala scopiformis* DAOMC 229536 collected from *P. glauca*. Multiple studies have shown it produces rugulosin both *in vitro* and *in planta*, as the primary metabolite with insect toxicity towards the spruce budworm, and other insect pests of spruce including *Lambdina fiscellaria* (hemlock looper) and *Zeiaphere canadensis* (spruce budmoth) (Calhoun et al., 1992; Miller et al., 2002, 2008; Sumarah et al., 2008). Dose response relationships have been recorded *in vivo* when spruce budworm ingest endophyte inoculated and toxin sprayed needles (Miller et al., 2008). In both nursery and field experiments, the endophyte and its toxin (average concentration of 1μg g^{-1}) was shown to persist in the foliage for more than a decade after nursery inoculation (Miller et al., 2008; Frasz et al., 2014). The extent of fungal infection and toxin productions appears to be throughout the

crown of the tree, at biologically effective concentrations to reduce spruce budworm growth rate (Frasz et al., 2014).

The Douglas fir and spruce endophyte scenarios meet all the criteria postulated by Carroll for relationships of endophytic mutualisms, which supports their role as the fifth agent proposed by Royama (Carroll, 1988). It would suggest that mature trees, which withstood defoliation for hundreds of years, contained toxigenic endophytes, which would account for their survival amidst complete forest defoliation (Miller, 2011). The cyclical damage caused by the spruce budworm in the Acadian forest affirms the pressing need to improve the tolerance of seedlings to the spruce budworm. Enhancing trees by re-introducing beneficial endophyte diversity presents a more widespread reforestation solution when compared to the costly, labour intensive approaches of chemical spraying and pruning techniques. Current outbreak reports show the spruce budworm outbreak in the Mackenzie River delta in the Northwest Territories, the highest latitude every recorded, suggesting climate change is affecting the outbreak areas (National Resources Canada, 2016). It is not known whether climate change will enhance or decrease outbreak extent and severity; however, the insect seems to be migrating more north than ever before. The spruce budworm appears to be moving out of the range of its currently preferred host tree, balsam fir. In 2014, it was reported that the eastern spruce budworm has increased to 3.4 million ha undergoing moderate to severe defoliation. Certain areas centering on the origin of this most current outbreak are now in their 7th to 8th years of annual defoliation, and significant tree mortality has started. This outbreak is expected to continue, increasing to 6 million ha in 2015, and 10 million ha in 2016 (National Resources

Canada, 2016). For perspective, Canada's forests cumulatively encompass 347 million ha of land. Insects have damaged 20.3 million ha, and 0.03 million ha have been completely deforested as of 2014 (National Resources Canada, 2016).

1.6 Project Aim

The study of foliar fungal endophytes of conifers has yielded a rich collection of secondary metabolites with diverse biological activities. Field research revealed the existence of 'superior' trees, which originated by natural forest regeneration, and harbour endophytic fungal mutualists. Studies suggest beneficial symbiotic associations allowed superior trees to withstand several spruce budworm epidemics. Further research has shown seed grown nursery seedlings lack cultivable endophytes, because endophytes transmit horizontally. This means endophytes propagate from infected trees, to younger seedlings only in close spatial proximity. Since foliar conifer endophytes transmit horizontally, seed grown trees lack all endophytic fungi. Large-scale endophytic-inoculation experiments support the ability of *Picea* endophytes to improve tree insect tolerance to the spruce budworm.

This thesis aims to elucidate more of the secondary metabolite producing capabilities of red and black spruce endophytes. Ultimately, the goal is to identify more anti-insect producing genotypes for field inoculation studies in red and black spruce seedlings. Future field experiments could determine if the red and black endophytes provide increased host tolerance against the spruce budworm herbivory. For this work, a collection of 46 endophytes of red and black spruce was screened to facilitate targeted isolations of their biologically active SMs. This is hypothesized to result in the isolation

and characterization of bioactive (antibacterial and antifungal) metabolites, which are structurally related to known toxins produced by better-studied phylogenetically related pathogens.

2.0 Materials and Methods

2.1 Fungal Material & Identifications

A systematic survey of conifer endophytes was performed in areas of New Brunswick and Ontario, Canada (Appendix I). Branches of healthy *P. mariana* (black spruce), *P. rubens* (red spruce) and *P. glacua* (white spruce) trees of varying ages were collected and stored in plastic bags at 4°C. Individual needles were removed with forceps and surface sterilized by briefly submerging them in 70% ethanol (1 min), 3% NaClO (7.5 min), and 70 % ethanol (30 s), sequentially. Needles were rinsed in ddH_2O, blotted on Kimwipes and cut longitudinally into 2 mm sections. Needle sections were inoculated onto 2% MEA (20 g of Bacto malt extract, Difco Laboratories, Sparks MD; 15 g agar, EMD Chemicals Inc., NJ; 100 mL of ddH_2O) Petri dishes (9 cm), and incubated at 16°C in the dark according to (Tanney et al., 2016). Upon observing sufficient mycelial growth emerging from the needle tissue, biomass was transferred and sub-cultured on MEA Petri dishes (6 cm). A collection of 46 endophytes were selected for preliminary investigation of natural products, and were stored at 8°C on MEA.

Initially, fungal strains were identified by sequencing their ITS and TUB region as described by Tanney (2016). Total DNA was extracted (Mo Bio Laboratories Carlsbad, CA, USA) from 4-12 week-old cultures on MEA, and the ITS sequences amplified and

sequenced. ITS sequences were amplified using the primers ITS4 and ITS5 (Tanney et al., 2016; McMullin et al., 2017). Partial 28S nuclear ribosomal LSU rRNA gene region was amplified to confirm identifications, using the amplification primer pairs LR0R and LR5 (Tanney et al., 2016; McMullin et al., 2017). Sequences were assembled and compared to NCBI GenBank using the BLASTN algorithm.

2.2 Fermentation, Extraction & Isolation

The 46 endophyte candidates were incubated on a small scale (1L cultures) to evaluate their antimicrobial potential and chemical profiles by LC-UV-MS. For inoculation, a portion of a 2% MEA plate for each endophyte was macerated in sterile ddH_2O under aseptic conditions. Glaxo culture bottles containing 1L of 2% ME broth were inoculated with the macerated cell suspension (5%, v/v). Cultures were left to grow at 25˚C in darkness stationary for 8 weeks before extraction.

After 8 weeks, the resulting biomass were separated from the culture medium by vacuum filtration through Whatman #4 (240 mm) filter papers (Whatman GE Healthcare, UK). Mycelium were frozen and stored at -20˚C. Prior to extraction the pH and volume of each culture filtrate were recorded. Each aqueous filtrate was saturated with sodium chloride (20-40 g L^{-1}) to aid in the prevention of emulsions. This resulting culture filtrate was extracted twice with EtOAc in a 2L separatory funnel. The liquid-liquid extraction was performed first with 60% the total volume of EtOAc (600 mL), followed by 50% the total volume (500 mL). The organic phases were combined and filtered through anhydrous Na_2SO_4 to remove traces of water prior to rotary evaporation. Extracts were dissolved in

HPLC grade MeOH, and passed through 0.2 μm PTFE 13 mm syringe filters into amber vials (PTFE lids) and stored at -20˚C until LC-UV-MS chemical profiling and antimicrobial assays. Resulting extracts had masses between 10-300 mg L^{-1} of culture filtrate depending on the endophyte.

After considering the chemical profiles, bioactivity, and mass of crude extract, four endophytes were selected for natural product isolation and characterization (Appendix I). In order to produce sufficient material for structural elucidation, larger fermentations (15L) were performed. Prior to inoculating Glaxo bottles, 50 mL starter flasks (2% ME broth) were inoculated with 5% (v/v) of macerated agar culture in sterile ddH_2O. These were grown with agitation (100 rpm, rotary shaker) for 2 days then left to grow without agitation until sufficient mycelium was present (another 5-7 days). Starter flasks were macerated under aseptic conditions and transferred to 15 Glaxo bottles each containing 1L 2% ME broth, and incubated for 8 weeks in the dark at 25 ˚C. The same filtration and extraction process described above was used for the bulk material. Resulting culture filtrate extracts had a mass between 0.5-3 g depending on the endophyte.

Crude culture filtrate extracts of selected endophytes were generally separated by flash column chromatography prior to semi-preparative HPLC as described above. Metabolites were purified by single injections as described below, until adequate material was obtained for structural elucidation by NMR, OR, UV experiments and comparisons to the literature.

2.3 Nectria dacryocarpa (NB-236-7B; DAOMC 251709)

Figure 2.1: *Nectria dacryocarpa* (NB-236-7B, DAOMC 251709) growing on 2% MEA.

Bulk fermentations yielded 50 mg L^{-1} and 1.5 g of total of EtOAc soluble crude extract. The crude extract was separated by silica gel flash chromatography into 14 like fractions. LC-UV-MS analysis indicated fraction 6 (105.0 mg), 10 (247.8 mg), and 11 (68.7 mg) contained the dominant metabolites of interest. Fraction 6 eluted with 30% Hex:EtOAc, and metabolites were purified by HPLC using a 20 minute linear elution gradient from 20-100% ACN:ddH_2O (Appendix II, A1). The peak at 11 minutes required a second HPLC purification to isolate compound **1** (4.5 mg). Fraction 10 eluted with 90% EtOAc:MeOH and was separated by HPLC using a 25 minute linear gradient from 15-60% ACN:ddH_2O (Appendix II, A2). This resulted in the isolation of compounds **2** (19 mg) and **3** (30 mg). Fraction 11 eluted with 85% EtOAc:MeOH, and was separated using an 25 minute HPLC gradient from 10-100% ACN:ddH_2O (Appendix II, A3).

2.4 *Penicillium* cf. *glaucoalbidum* (RS10-14G; DAOMC 251707)

Figure 2.2: *Penicillium glaucoalbidum* (RS10-14G, DAOMC 251707) growing on 2% MEA.

Large-scale culture filtrates of this endophyte produced 33.3 mg L^{-1}, and 1.22 g total of EtOAc soluble crude extract. A normal phase silica gel column was used to separate the crude extract into 13 TLC-guided combined fractions. Four major metabolites were purified from fraction 7 including compounds **4**, **5** (6.3 mg), **6** (9.6 mg), **7, 8** (2 mg), and (**9**) (6.3 mg). Fraction 7 was separated using a linear gradient programmed from 5 to 60% ACN:ddH_2O over 25 minutes (Appendix II, A4). Secondary HPLC purification were required in all cases, using the same gradient, over 10 minutes.

2.5 *Penicillium* cf. *glacuoalbidum* (NB-589; DAOMC 251708)

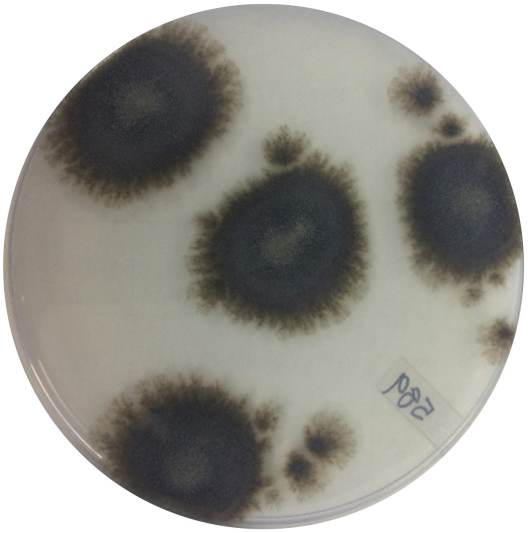

Figure 2.3: *Penicillium glaucoalbidum* (NB-589, DAOMC 251708) growing on 2%MEA.

This fungus produced 139.7 mg L^{-1} culture filtrate, and 1.2 g in total. The chemical profile as determined by LC-UV-MS indicated the extract was a complex mixture of all molecular weight metabolites (<200 Da). Only one metabolite was purified in sufficient amounts. A normal phase silica gel column was employed over a larger range of polarity to completely separate the extract. The only changes to the solvent gradient was the addition of a step gradient from 40-100% EtOAc:MeOH. Eluate was combined into 12 fractions in total, where fraction 7 was the most promising (Appendix II, A5). HPLC fractionation of fraction 7 (eluted at 100% EtOAc) was performed using a linear gradient from 10-100% ACN:ddH_2O for 17 minutes. This permitted the isolation of compounds **4** and **5** (7 mg).

2.6 *Lachnellula* cf. *calyciformis* (RS10-3B; DAOMC 251710)

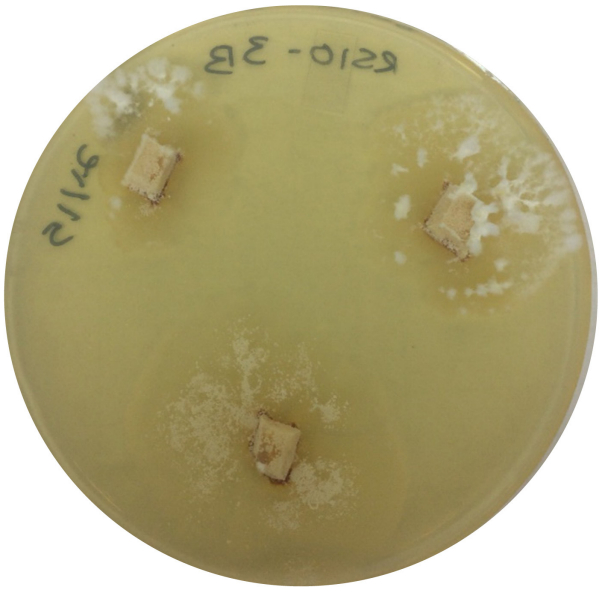

Figure 2.4: *Lachnellula* cf. *calyciformis* (RS10-3B, DAOMC 251710) growing on 2% MEA.

This endophyte produced 120 mg L^{-1}culture filtrate, and 5L of culture yielded 450 mg of crude EtOAc soluble material. According to LC-UV-MS analysis, this extract contained two major metabolites, which were suspected structural analogues. The crude extract was separated using a normal phase silica gel column as described above, yielding 10 fractions. Fraction 4 eluted with 90% EtOAc: Hex, and 5 eluted with 100% EtOAc. These fractions were combined because LC-UV-MS analysis showed they contained the same major metabolites. Preliminary HPLC purifications required a 17 minute gradient method, from 10 to 100% ACN:ddH_2O (Appendix II, A6). The resulting isolates required a secondary HPLC purification using the same method. A chiral column was used in attempt to separate the suspected diastereomers; however, they would spontaneously re-

interconvert in organic solvent following separation. Metabolites isolated included compounds **10**, **11** (35 mg) and **12** and **13** (4.9 mg).

2.7. General Experimental Procedures

NMR experiments were performed on a JEOL ECZS 400 MHz NMR spectrometer (Akishima, Tokyo, Japan) using an autotuning broadband probe for both ^{1}H and ^{13}C experiments. Purified natural products were diluted to 4cm from the bottom of the NMR tube, in either $CDCl_3$, $(CD_3)_2SO$, or CD_3OD purchased from CDN Isotopes (Point Claire, Quebec). Each spectrum was referenced to the corresponding solvent peaks for either $CDCl_3$ (δ_H 7.26, δ_C 77.16), $(CD_3)_2SO$ (δ_H 2.50, δ_C 39.52), or CD_3OD (δ_H 3.31, δ_C 49.00) (Gottlieb et al., 1997). Homonuclear (^{1}H, ^{13}C, COSY, and DEPT-135) and heteronuclear (HSQC, and HMBC) spectra were used to elucidate the structures of isolated compounds.

LC-HRMS data was acquired using a Thermo Q-Exactive Orbitrap Mass Spectrometer (Thermo Scientific, Waltham, MA, USA), coupled to an Agilent 1290 HPLC system. Metabolites were separated with an Agilent Zorbax Eclipse Plus RRHD C18 column (2.1 x 50 mm, 1.8 μm) with a flow rate of 0.3 mL min^{-1}. The solvent gradient utilized was 100% ddH_2O (0.1% FA) to 100% ACN (0.1% FA) over 5 minutes.

LC-UV-MS analysis was performed with a Waters 2795 separations module, Waters 996 DAD, and Waters MicroMass Quatro Ultima triple quadrupole mass spectrometer (Waters Corporation, Milford, MA, USA). Ten μL injections of crude extracts were separated by a Kinetex C18 (100 x 4.6 mm, 2.6 mm) column (Phenomenex Inc.,

Torrance, CA, USA) at 1 mL min^{-1}. The linear solvent gradient was programmed from 95% ddH_2O (0.1% FA) to 100% ACN (0.1% FA) over 12 minutes. A post-column splitter (80:20) between the DAD and MS diverted 200 µL of solvent to the source per minute. The DAD was set to detect absorbance between 200-600 nm for the 12-minute period. MS product ion scans using positive ESI conditions were as follows: capillary voltage 3.00 kV, cone voltage 30 V, source temperature 80°C, desolvation temperature 180˚C, cone gas flow (N_2) 90 L h^{-1}, desolvation gas flow (N_2) 540 L h^{-1}, and multiplier voltage of 650 V.

Normal phase gel silica columns were prepared using silica (Silicycle; 40-60 µm, 50 mg silica per gram crude extract) to fractionate complex mixtures prior to metabolite purification by HPLC. Typically, flash chromatography followed a step gradient elution system of Hex-EtOAc (0-100% v/v) in 10% increments followed by 5, 10, 20, and 50% EtOAc-MeOH (v/v). Eluate was collected in test tubes (20 mL), and subsequently combined into like fractions based on metabolite polarity and TLC plate observations. TLC plates (0.2 mm silica gel 60 F_{254} pre-coated) were used to monitor eluting metabolites with 10% (v/v) MeOH in $CHCl_3$ as the mobile phase. Plates were visualized in the dark, under both long (365 nm) and short wave UV (254 nm). After fractionation, the solvent was removed by rotary evaporation and extracts were dissolved in MeOH prior to filtration through 0.2 µm PTFE syringe filters (Pall Corporation, New York). Samples were dried under a gentle stream of nitrogen and stored at -20˚C in amber vials with PTFE caps. Fractions generated from the silica column were subsequently analyzed by LC-UV-MS.

Compounds were purified by preparative HPLC using an Agilent 1100 HPLC system (Agilent Technologies, Palo Alto, CA, USA), connected to a DAD with Kinetix C18 column (250 x 10mm, 5µm; Phenomenex). Fractions were dissolved in MeOH at a concentration of 50 mg mL^{-1}, and injected in 50 uL volumes at a constant flow rate of 4 mL min^{-1}. The mobile phase comprised of ACN and ddH_2O. HPLC elution gradients were fraction, and metabolite specific. Optical rotation measurements of purified metabolites were acquired using an Autopol IV polarimeter (Rudolph Analytical, Hackettstown, NJ, USA). UV spectra of purified metabolites were determined using a Varian Cary 3 UV-visible spectrophotometer.

2.8 Antimicrobial Assays

Prior to their inoculation and fermentation in bulk, a collection of foliar endophytes from various regions in New Brunswick and Ontario were incubated in 1L fermentations and screened for antimicrobial activity (Appendix I). This was accomplished using a modified Oxford disc diffusion assay (Vincent & Vincent, 1944). Each conifer endophyte extract generated from the screening (1L) was dried under nitrogen, weighed, diluted in MeOH to 50 mg mL^{-1}, and transferred via pipette (10 µL) to 10 mm sterile Whatman discs. Nystatin was used as the positive control at a concentration of 1 mg mL^{-1}. Discs were left in a sterile chamber overnight to ensure complete solvent evaporation. *Saccharomyces cerevisiae* and *Microbotryum violaceum* were used as test organisms for the modified Oxford disc assays. *S. cerevisiae* was inoculated in media containing yeast extract (1g L^{-1}) and glucose (10g L^{-1}), whereas the rust media contained malt extract (20 g L^{-1}),

peptone (2.5 g L^{-1}), and yeast extract (2.5 g L^{-1}). *S. cerevisiae* was left to grow overnight, and *M. violaceum* was left to grow for 3-5 days prior to beginning the assay. Cultures were spread on 2% MEA plates once the OD of their culture filtrate reached 0.10 (600 nm). Spread plates were left to dry aseptically for three hours. Spread plates were split into four quadrants. On each plate, two test extracts, one positive (nystatin), and one negative (evaporated MeOH) control were placed face-down. Zones of inhibition were observed every 12 hours for two days. Zones of inhibition were measured radially (in mm), from the outside of the disc.

Purified metabolites were tested for *in vitro* antimicrobial activity by monitoring the growth curve and the MIC for 4 test organisms were determined. *M. violaceum* and *S. cerevisiae* were maintained in the same growth medium as described above. Nystatin was serially diluted (2x) in DMSO from 20 to 0.024 μg mL^{-1} and used as the positive control for the fungi. *Bacillus subtilis* and *Escherichia coli* were grown in media containing yeast extract (5g L^{-1}) and peptone (10 g L^{-1}). Chloramphenicol was used as the positive control for the bacteria in dilutions as described for nystatin. Metabolite stock solutions were diluted in DMSO from a working solution of 5 mg mL^{-1}. Using sterile 96 well microplates (Falcon 353072), 10 μL stock solution aliquots were added to the first wells containing 90 μL of media, and serially diluted (2x) over seven concentrations (125.0, 62.5, 31.2, 15.6, 7.8, 3.9, 1.9 μg mL^{-1}). Negative controls using 10 μL aliquots of DMSO were included with every dilution series as a comparison. All wells were mixed and diluted to a final volume of 200 μL by pipetting with 150 μL of cell suspension standardized to 0.100 OD 600 nm for each test organism. Assays were performed in

triplicate and incubated at 26˚C on a rotary shaker (500 RPM) for 48 hours. Measurements at 600nm were recorded every two hours for all test organisms. Optical density measurements were taken using a Molecular Devices Spectra Max 340PC reader (Sunnyvale, CA, USA). Bioassay data was analyzed by ANOVA followed by Tukey's test (p <0.05) for significant differences between treatments and controls (Systat V13.1: Systat Software Inc. Chicago, IL, USA).

3.0 Results

3.1 Preliminary Antimicrobial Screening

Of the 46 crude extracts assessed for antifungal activity using a modified Oxford disc diffusion assay, 3 (7%) isolates exhibited potent antifungal activity towards *M. violaceum*. By comparison, 2 (5%) isolates reduced the growth of *S. cerevisiae*. For the detailed results of the preliminary collection and screening, refer to Appendix I. A single endophyte was studied thoroughly for the production of natural products from this survey; *Lachnellula* cf. *calyciformis* DAOMC 251710. Three additional endophyte strains from a previous homologous survey of *P. rubens* and *P. mariana* were investigated for biologically active compounds as well; *Nectria dacrocarpa* DAOMC 251709, and two *Penicillium* cf. *glaucoalbidum* stains (DAOMC 251707 and 251709; Appendix I). The results of this study pertain to the structural elucidation and antimicrobial characterization of the dominant metabolites produced by these conifer endophytes *in vitro*.

3.2 Metabolites of *Nectria dacryocarpa* (NB-236-7B; DAOMC 251709)

The dominant metabolites isolated from *N. dacryocarpa* DAOMC 251709 showed approximate 3:1 isotopic peak distributions of $[M+H]^+$:$[M+H+2]^+$ in their HRMS spectra, suggesting they were chlorinated. These metabolites displayed UV absorption maxima at 220 and 265 nm. Examination of the NMR and physiochemical data indicated metabolites (**1-3**) were structurally similar to previously characterized chlorinated resorcyclic acid lactones, in accord with reports in the literature (Table 3.1, 3.2; Mejia et al., 2014; Shinonaga et al., 2009). The three metabolites isolated from this endophyte shared a core structure and structural diversity arose from differential substitutions of their 14 membered rings (**1-3**) (Figure 3.1).

Compound (**1**) was purified as a colourless solid (4.5 mg) with the molecular formula $C_{18}H_{17}ClO_6$ determined by an $[M+H]^+$ peak at *m/z* 365.0787. The NMR spectra for both ^1H and ^{13}C nuclei were in agreement with the published spectra of radicicol (Figure 3.1, Table 3.2; Shinonaga et al., 2009). The ester connectivity within the molecule was confirmed by the HMBC correlation between the aromatic methine δ 6.58 (H-15) and the deshielded carbon at δ 168.9 (C-18). The epoxide functionality was confirmed by the deshielding effect of the oxygen on δ 3.04 (H-4) and δ 3.31 (H-5), and one more degree of unsaturation compared to compound (**2**). COSY correlations were observed between H-4 and H-5. The specific optical rotations were also in agreement with previous reports, supporting the reported stereochemistry (Table 3.1; Shinonaga et al., 2009). Here we report the specific optical rotation as +175.7 ($[\alpha]^{25}_D$, c 0.03, $CHCl_3$) compared to +216 (c 0.05, $CHCl_3$; Mirrington & Taylor, 1964), +194 (c 1.0, $CHCl_3$; Shinonaga et al, 2009)

and +108 ($[\alpha]^{20}_{D}$ c 0.05, $CHCl_3$; Hellwig et al., 2003). Together, the NMR and physiochemical data support the isolation of compound (**1**), radicicol (Figure 3.1, Table 3.1, 3.2).

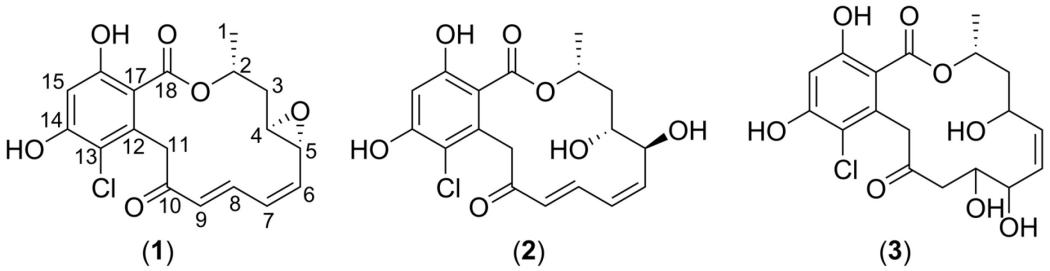

(**1**) (**2**) (**3**)

Figure 3.1: Structures of radicicols (**1-3**) isolated from *N. dacryocarpa* DAOMC 251709.

Table 3.1: ^{1}H (400 MHz) and ^{13}C (100 MHz) NMR data for radicicols (**1-3**) isolated from *N. dacryocarpa* DAOMC 251709 in *acetone-d6.*

		(1)		**(2)**		**(3)**
position	δ_C	δ_H (***J*** **in Hz)**	δ_C	δ_H (***J*** **in Hz)**	δ_C	δ_H (***J*** **in Hz)**
1	18.6	1.56, d (6.8)	21.3	1.46, d (6.4)	20.6	1.37, d (6.5)
2	71.9	5.43, qt (3.7, 6.8)	70.6	5.63, m	71.6	5.56, m
3	37.1	2.43, m	38.4	2.10, m	43.0	2.10, m
		1.79, m		1.87, m		
4	56.2	3.04, dt (2.8, 8.6)	71.8	3.62, ddd (2.3, 5.0, 8.7)	70.1	4.27, m
5	55.8	3.31, m	69.3	4.50, ddd (1.1, 5.0, 8.7)	135.9	5.47, dd (8.5, 15.5)
6	136.0	5.76, dd (3.5, 10.6)	143.3	5.87, dd (8.7, 10.9)	131.7	5.39, dd (8.5, 15.5)
7	130.5	6.25, dd (9.4 10.6)	127.0	6.16, t (10.9)	78.6	3.60, t (8.7)
8	139.1	7.51, dd (9.4, 16.1)	139.6	7.42, dd (10.9, 16.2)	69.0	3.92, ddd (3.0, 6.5, 9.2)
9	131.3	6.13, d (16.1)	131.2	5.96, d (16.2)	46.8	2.56, m
10	196.7		196.7		204.3	
11	46.7	4.43, d (16.1)	44.5	4.46, d (15.5)	47.5	4.24, d (17.6)
		3.90, d (16.1)		4.04, d (15.5)		4.00, d (17.6)
12	136.4		136.6		137.7	
13	115.7		115.8		116.1	
14	160.5		158.0		159.4	
15	103.8	6.58, s	103.8	6.59, s	104.1	6.65, s
16	158.3		159.4		164.1	
17	111.0		111.4		107.4	
18	168.9		168.1		171.3	

Table 3.2: Physiochemical properties of radicicols (**1-3**) isolated from *N. dacryocarpa* DAOMC 251709.

properties	**radicicol (1)**	**radicicol B (2)**	**radicicol C (3)**
appearance	colourless solid	colourless solid	colourless solid
molecular formula	$C_{18}H_{17}ClO_6$	$C_{18}H_{19}ClO_7$	$C_{18}H_{21}ClO_8$
HRMS	365.0785 $[M+H]^+$	383.0889 $[M+H]^+$	423.0815 $[M+Na]^+$
calculated	365.0786 $[M+H]^+$	383.0892 $[M+H]^+$	423.0817 $[M+Na]^+$
OR $[\alpha]^{25}_D$ $CHCl_3$, c 0.03	175.8	30.3	-42.4
UV (MeOH) λ_{max} nm (log ε)	207 (4.20) 220 (4.14) 267 (4.01) 323 (3.36)	215 (4.04) 264 (3.86) 282 (3.79)	220 (3.98) 264 (3.57) 234 (3.71) 315 (3.46)

Compound (**2**) was also isolated as a colourless solid (19 mg) with the molecular formula $C_{18}H_{19}ClO_7$ determined by an $[M+H]^+$ peak at *m/z* 383.0892. The nine units of unsaturation are one less compared to radicicol (**1**). This and the larger molecular weight suggest the presence of a H_2O equivalent in place of the epoxide. The hydrolysis of the epoxide agrees with new δ 71.8 (C-4) and δ 69.3 (C-5) shifts compared to the δ 56.2 (C-4) and δ 55.8 (C-5) in compound (**1**) (Table 3.1). This is further supported by the COSY correlations between δ 2.10 (H-3) and δ 3.62 (H-4), δ 3.62 (H-4) and δ 4.50 (H-5), and δ 4.50 (H-5) and δ 5.87 (H-6). The NMR data matched the literature values published for radicicol B (**2**) (Mejia et al., 2014) The specific optical rotations measured in this study $[\alpha]^{25}_D$ +30 (c 0.3, MeOH) also were in accordance with the reported literature value of +32 (c. 0.8 MeOH, Mejia et al., 2014; Table 3.2).

Compound (**3**) was isolated as a colourless solid from *N. dacryocarpa* DAOMC 251709 in the largest amounts (30 mg). It had a molecular formula of $C_{18}H_{21}ClO_8$ determined by an $[M+Na]^+$ peak at *m/z* 423.0815. This molecular formula indicated eight double bond equivalents due to the presence of one less non-aromatic double bond compared to

radicicol B (**2**) (Figure 3.1, Table 3.1). COSY correlations between δ 5.47 (H-5) and δ 5.39 (H-6) support the reduction of a double bond in (**3**) compared to compound (**2**). Compound (**3**) lacks double bonds between δ 131.7 (C-6) and δ 78.6 (C-7), as well as between δ 69.0 (C-8) and δ 46.8 (C-9). Instead, C-7 and C-8 are hydroxylated, confirmed by the oxygenated proton chemical shifts at δ 3.60 (H-7) and δ 3.92 (H-8), which correlate with each other based on COSY data. The NMR spectral data and physiochemical data reported here for (**3**), are in accordance with the literature values for radicicol C (Figure 3.1, Tables 3.1 and 3.2, Mejia et al., 2014). The specific optical rotations measured for this compound, $[\alpha]^{25}_{D}$ -42 (c 0.03, MeOH; Table 3.2), agrees with the reported value -69 (c. 0.8 MeOH; Mejia et al., 2014,). The relative stereochemical configurations of the three secondary alcohols could not be assigned based on NOESY correlations due to the flexible structure of (**3**) (Mejia et al., 2014). The UV spectra showed absorption maxima at 220, 264, and 315, which agrees with reported findings (Table 3.2 data; Mejia et al., 2014).

3.3 Metabolites of *Penicillium* cf. *glaucoalbidum* (RS10-14G; DAOMC 251707)

All the *P*. cf. *glaucoalbidum* species studied here produced different mixtures of metabolites. *P*. cf. *glaucoalbidum* DAOMC 251707 produced the largest array of compounds under the culture conditions used and exhibited the most bioactivity in the preliminary screening.

Purification of (**4**) and (**5**) resulted in the isolation of a white solid with the molecular formula $C_{10}H_{10}O_4$ based on the $[M+H]^+$ peak of *m/z* 195.0654. The molecular formula of

indicated six degrees of unsaturation, accounting for an aromatic ring, a carbonyl, and an additional ring (Figure 3.2). Aromatic carbons were confirmed by their ^{13}C NMR chemical shifts at δ 109.9 (C-5), δ 166.4 (C-6), δ 101.9 (C-7), δ 167.3 (C-8), δ 111.4 (C-9), and δ 146.1 (C-10). The aromatic carbons which were hydroxylated, C-6 and C-8, were more deshielded. The ketone carbonyl at C-1 was confirmed by its shift at δ 202.4, and the hydroxylated chiral center was observed at δ 66.9 (C-3). The methine at δ 4.25 (H-3) displayed a COSY correlation with the methylene protons at δ 2.81, 2.61 (H-2). The ^{1}H and ^{13}C NMR data for compounds (**4**) and (**5**) are in agreement with literature values for scytalone (Table 3.3, 3.4 and Figure 3.2; Findlay & Kwan, 1972). The UV spectra showed absorption maxima at 220, 237, 281, and 324, which is in accordance with the original reported literature values (Findlay & Kwan, 1972). The presence of enantiomers in a 1:1 mixture was confirmed by HPLC elution of two equally integrating peaks (220 nm) through a chiral HPLC column, as well as a specific optical rotation $[\alpha]^{25}_{D}$ of 0 (c 0.03, $CHCl_3$; Table 3.4). These physiochemical properties agree with similar reports in the literature (Fabrice et al.,1990).

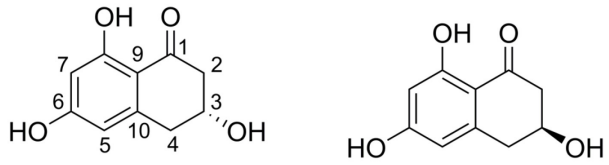

(**4**) (**5**)

Figure 3.2: Structures of (*R*)-scytalone (**4**) and (*S*)-scytalone (**5**) produced in equal amounts by *P. glaucoalbidum* DAOMC 251707.

Table 3.3: ^{1}H (400 MHz) and ^{13}C (100 MHz) NMR data for scytalone (**4**, **5**) isolated from *P.* cf. *glaucoalbidum* DAOMC 251707 in CD_3OD.

position	δ_C	δ_H (*J* in Hz)
1	202.4	
2	47.4	2.81, m
		2.59, dd (7.8, 16.9)
3	66.9	4.23, m
4	39.1	3.06, dd (3.7, 15.6)
		2.81, m
5	109.9	6.21, s
6	166.4	
7	101.8	6.09, d (2.1)
8	167.3	
9	111.4	
10	145.9	

Table 3.4: Physiochemical properties of for (*R*) and (*S*)- scytalone (**4**, **5)** isolated from *P.* cf. *glaucoalbidum* DAOMC 251707.

properties	scytalone (4,5)
appearance	white solid
molecular formula	$C_{10}H_{10}O_4$
HRMS	195.0654 $[M+H]^+$
calculated	195.0652 $[M+H]^+$
OR $[\alpha]^{25}_D$ $CHCl_3$, c 0.03	0
	220 (2.99)
UV (MeOH)	237 (2.90)
λ_{max} nm (log ε)	281 (3.11)
	324 (2.66)

Compound (**6**) was isolated as a yellow oil with the molecular formula $C_{14}H_{10}O_7$ determined from the $[M+H]^+$ peak at *m/z* 291.0497. Compound (**6**) and other dominant metabolites in the chemical profile absorbed at 324 nm strongly, suggesting conjugated structural features. The molecular formula indicated ten degrees of unsaturation, afforded by five double bonds, three rings and two carbonyls (Figure 3.3). Methine protons in the

aromatic regions displayed signals at δ 6.08 (H-3) and δ 6.33 (H-10). HMBC correlations between H-3 and δ 164.6 (C-2) and δ 175.1 (C-4) supported the presence of conjugated ring structure. Additional HMBC correlations were observed between the aromatic methylene at δ 6.33 (H-10) and δ 151.8 (C-11), δ 157.9 (C-9), and δ 148.9 (C-12). Interpretation of the ^{1}H and ^{13}C NMR spectra indicated compound (**6**) was citromycetin as it aligned with published NMR data (Figure 3.3, Table 3.6 Capon et al., 2007). The physiochemical data also supports the identity of compound when compared to literature values (Table 3.6; Capon et al., 2007).

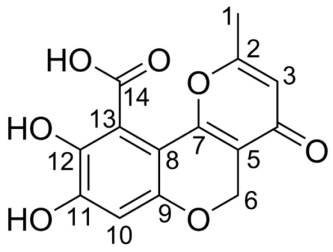

(**6**)

Figure 3.3: Structure of citromycetin (**6**) isolated from *P.* cf. *glaucoalbidum* DAOMC 251707.

Table 3.5: ^{1}H (400 MHz) and ^{13}C (100 MHz) NMR data for citromycetin (**6**) isolated from *P.* cf. *glaucoalbidum* DAOMC 251707 in DMSO-*d6*.

position	δ_C	δ_H (*J* **in Hz**)
1	19.2	2.18, s
2	164.6	
3	112.6	6.08, s
4	175.1	
5	110.5	
6	61.5	4.74, s
7	150.2	
8	106.0	
9	157.9	
10	102.9	6.33, s
11	151.8	
12	148.9	
13	116.4	
14	168.9	

Table 3.6: Physiochemical properties measured for citromycetin (**6**) isolated from *P.* cf. *glaucoalbdium* DAOMC 251707.

properties	**citromycetin (6)**
appearance	yellow oil
molecular formula	$C_{14}H_{10}O_7$
HRMS	291.0497 $[M+H]^+$
calculated	291.0499 $[M+H]^+$
UV (MeOH) λ_{max} nm (log ε)	216 (3.71) 259 (3.38) 307 (3.25) 380 (3.40)

Compound (**7**) and (**8**) were isolated as a yellow solid with the molecular formula $C_{14}H_{12}O_8$ as determined by a $[M+H]^+$ peak at *m/z* 309.0608. This molecule displayed UV absorption maxima at 216, 258, 329, and 400 nm, suggesting the presence of a conjugated structural component. Upon inspection of the NMR spectra, the compound was successfully identified as fulvic acid (Figure 3.4). Two-dimensional correlations support the identity of the secondary metabolite as fulvic acid, evident by the HMBC correlations from the methyl group δ 1.56 to δ 95.7 (C-3) and δ 37.8 (C-4). The benzene ring conformation was confirmed due to HMBC correlations between the methine at δ 7.01 (H-6) and δ 152.5 (C-5a), δ 112.5 (C-9, C-9a). The connectivity between the three cyclic moieties was confirmed by the HMBC correlations between the methine at H-6 to C-5a, and between the inequivalent methylene protons at δ 4.65 (H-1) and δ 115.5 (C-10a). COSY correlations between the inequivalent methylene protons displayed J^2 coupling typical of germinal coupling constants (18.1 Hz), suggesting the molecule was present as cyclic fulvic acid. Together, the ^1H and ^{13}C NMR data matched the reported spectra for fulvic acid, with the exception of a few unidentified ^1H signals, in CD_3OD (Capon et al., 2007). This is possible due to the known solvent dependent tendency for fulvic acid to equilibrate with its acyclic form, and eventually dehydrate into

anhydrofulvic acid (Figure 3.5). However, no distinct peaks were identified as belonging to either acyclic, or anhydo- forms (Appendix III, Figure 3.5). Optical rotation was measured as -0.5 ($[\alpha]^{20.9}_{D}$ DMSO, c 0.01) which closely matches the reference value of 0 (Capon et al., 2007). Upon HPLC elution using a chiral column, 2 compounds (approx.. 1:1 integration) eluted at 270 nm. This molecule can tautomerize at the C-2 position, which supports the existence of two enantiomers, in roughly equivalent ratios. The UV absorption profile of this compound did not match the available literature data, suggesting the molecule is present as a mixture with small amounts of degradation, acyclic, or dehydrated analogues.

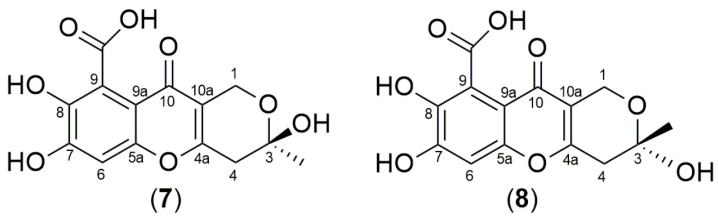

Figure 3.4: Structures of (*S*)-fulvic acid (**7**) and (*R*)-fulvic acid (**8**) produced in equal amounts by *P.* cf. *glaucoalbdium* DAOMC 251707.

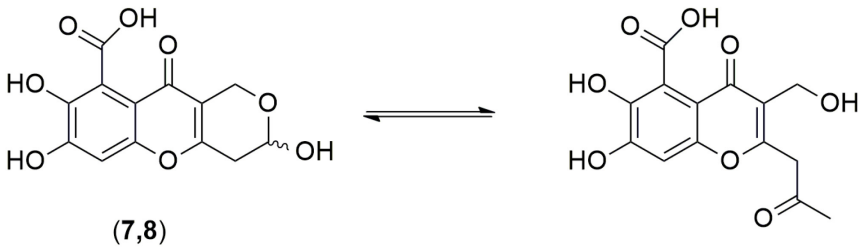

Figure 3.5: Solvent dependent equilibrium between cyclic and acyclic isomers of fulvic acid (**7**, **8**).

Table 3.7: ^{1}H (400 MHz) and ^{13}C (100 MHz) NMR data for fulvic acid (**7, 8**) isolated from *P.* cf. *glaucoalbidum* DAOMC 251707 in CD_3OD.

position	δ_C	δ_H (*J* in Hz)
1	57.8	4.65, s
3	95.7	
4	37.8	2.98 (d, 18.1)
		2.76 (d, 18.2)
4a	161.5	
5a	152.5	
6	106.0	7.01, s
7	155.3	
8	157.2	
9	112.5	
9a	112.5	
10	176.4	
10a	115.5	
COOH	174.7	
CH_3	28.6	1.56, s

Table 3.8: Physiochemical properties for fulvic acid (**7, 8**) isolated from *P.* cf. *glaucoalbidum* DAOMC 251707.

properties	fulvic acid (7, 8)
appearance	yellow solid
molecular formula	$C_{14}H_{12}O_8$
HRMS	309.0608 [M+H]
calculated	309.0605 [M+H]
OR $[\alpha]^{20.9}_D$ DMSO, c 0.01	-0.5
UV (DMSO)	216 (3.80)
λ_{max} nm (log ε)	258 (3.01)
	329 (5.90)
	400 (2.77)

Compound (**9**) was isolated as a colourless powder (6.3 mg) with the molecular formula $C_8H_{10}O_2$ based on a HRMS peak at *m/z* 121.0651 $[M\text{-}H_2O+H]^+$. This formula indicates four degrees of unsaturation, consistent with one aromatic ring. The loss of a water (Δ *m/z* 18) from the molecular ion is a very common fragment (Nielsen et al., 2011). Loss of

water from an alcohol group often occurs when the proton attached to the α-carbon is available to participate in an elimination reaction (Nielsen et al., 2011). The ^{13}C spectrum suggested the molecule had some degree of symmetry, permitting two equivalent carbon signals, appearing as doublets at δ 116.2 (C-2) and δ 130.9 (C-3). Two peaks integrate for two methine protons each at δ 6.69, and 7.02 ppm, suggesting aromatic symmetry, and a *para*-substituted aromatic ring. The COSY coupling systems were consistent with two separate systems. The first COSY coupled system consists of two methylene groups at δ 2.71 (H-5) and δ 3.68 (H-6) with coupling constants of 8.2 Hz, indicative of vicinal ^{3}J coupling. The second contained four aromatic methines at δ 6.69 (H-2) and δ 7.02 (H-3). The ^{1}H and ^{13}C NMR spectra for this compound **9** are in accordance with tyrosol reported from other conifer enodphytes (Table 3.9; Figure 3.6; McMullin et al., 2017). This molecule displayed UV absorption maxima at 201, 224, and 272 nm which agree with the literature (McMullin et al., 2017).

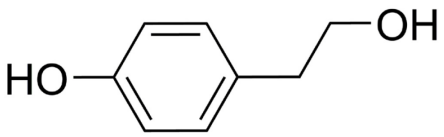

(**9**)

Figure 3.6: Structure of tyrosol (**9**), isolated from *P.* cf. *glaucoalbidum* DAOMC 251707.

Table 3.9: ^{1}H (400 MHz) and ^{13}C (100 MHz) NMR data for tyrosol (**9**) isolated from *P.* cf. *glaucoalbidum* DAOMC 251707 in CD_3OD.

position	δ_C	δ_H (*J* in Hz)
1	156.9	
2	116.2	6.69, d (8.2)
3	130.9	7.02, d (8.2)
4	131.1	
5	39.5	2.72, t (7.3)
6	64.7	3.68, t (7.3)

Table 3.10: Physiochemical properties measured for tyrosol (**9**) isolated from *P.* cf. *glaucoalbdium* DAOMC 251707.

properties	tyrosol (9)
appearance	white solid
molecular formula	$C_8H_{10}O_2$
HRMS	121.0651 $[M\text{-}H_2O+H]^+$
calculated	121.0653 $[M\text{-}H_2O+H]^+$
UV (MeOH)	201 (3.81)
λ_{max} nm (log ε)	224 (3.52)
	272 (3.00)

3.4 Metabolites of *Penicillium* cf. *glaucoalbidum* (NB-589; DAOMC 251708)

The only metabolites isolated in sufficient amounts from *P.* cf. *glaucoalbidum* DAOMC 251708 were a racemic mixture of compounds (**4**) and (**5**) (7 mg). The isolated metabolites were present in equal amounts of both *R* and *S* enantiomers based on equally integrated HPLC signals at 224 nm when eluting through a chiral column, and an observed optical rotation of zero. The NMR and physiochemical data from this strain

matched the data collected from the *P.* cf. *glaucoalbidum* DAOMC 251707, and the reported literature values (Findlay & Kwan, 1972).

3.5 Metabolites of *Lachnellula* cf. *calyciformis* (RS10-3B; DAOMC 251710)

Compounds (**10**) and (**11**) were isolated as white solids in the largest amounts (approximately 25 mg L^{-1} culture filtrate). Their molecular formula were determined to be $C_{18}H_{28}O_5$ according to the $[M+H]^+$ peak at *m/z* 325.2006. It became apparent that the isolated compound was present as a mixture of two inter-converting isomers (**10**, **11**) in a solvent and time dependent equilibrium (Figure 3.8). When NMR spectra were collected in $CDCl_3$, one set of signals was observed in both the ^1H and ^{13}C spectra, which equilibrated into two sets of signals after 24 hours (Appendix II). In CD_3OD, two sets of 1:1 signals were observed when spectra were recorded right after the compound was dissolved (Appendix III). The unique physiochemical properties, isomer equilibrium, and the NMR shifts corresponded to lachnellulone and isolachnelulone (Figure 3.7, 3.8, Table 3.11, 3.12; Ayer et al., 1988). Notable features in their ^{13}C spectra include the appearance of symmetrical signals from both linear aliphatic chains attached to δ 77.5 C-6 and δ 91.3 (C-15) (Table 3.11). COSY cross-peaks between δ 4.43 (H-5), δ 4.56 (H-6), and the oxygenated protons δ 3.85 (OH) confirm the presence of the hydroxyl moiety in compounds (**10**) and (**11**) (Figure 3.7). COSY correlations between δ 3.76 and 3.28 (H-13), δ 1.86 (H-14) and δ 4.99 (H-15), confirm the six-membered ring structure. HMBC correlations between δ 4.43 (H-5) and δ 191.2 (C-4), δ 99.9 (C-5), and δ 188.9 (C-12), confirm the double bond connection between the two ring systems (Figure 3.7). Extensive COSY coupling between methylene groups is visible in both aliphatic chains.

The measured optical rotation in MeOH and UV spectra match reported literature findings (Table 3.12; Ayer et al., 1988).

Compounds (**12**) and (**13**) were isolated as a white solid (4.9 mg) with the molecular formula $C_{18}H_{28}O_4$ based on the HRMS $[M+H]^+$ peak at *m/z* 309.2056. These compounds were also isolated as an interconverting mixture of isomers, similar to that of compounds (**10**) and (**11**). Unlike compounds (**10**) and (**11**), compounds (**12**) and (**13)** were present in equal amounts, immediately upon dissolution in both $CDCl_3$ and CD_3OD (Appendix III). The molecular weight change from compound **10** is in accordance with the loss of an oxygen atom. The NMR spectral data for the two compounds supports this structural change as the loss of the oxygen at C-5 which caused the ^{13}C signal to shift from δ 71.6 ppm in compounds (**10**) and (**11**), to δ 43.9 ppm in compounds **(12**) and (**13**) (Table 3.11). Additionally, the hydroxyl proton was no longer visible in the ^1H spectrum at δ 3.85 ppm. COSY correlations were conserved between δ 2.51 (H-5) and δ 4.34 (H-6). The major COSY correlations between the methylenes of the aliphatic chains were still observed. HMBC correlations from δ 2.51 (H-5) to δ 191.2 (C-4), δ 101.9 (C-3) and δ 187.9 (C-12) suggest the same core structure as compounds (**10**) and (**11**). Compounds (**10**), (**11**), (**12**), and (**13**) had the same UV absorption maxima (Table 3.12). However, the specific optical rotations differed because (**12**) and **(13**) lack one stereocenter, attributing to a different observed $[\alpha]^{25}_D$ -2.5 ($CHCl_3$, c 0.03).

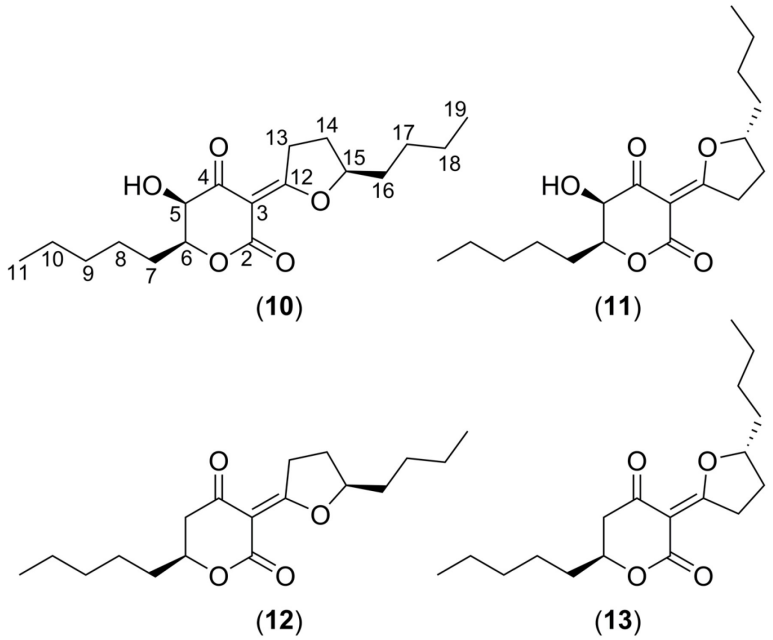

Figure 3.7: Structures of lachnellulone (**10**), isolachnellulone (**11**), and related lachnellulone isomers (**12, 13**) isolated from *L.* cf. *calyciformis* DAOMC 251710.

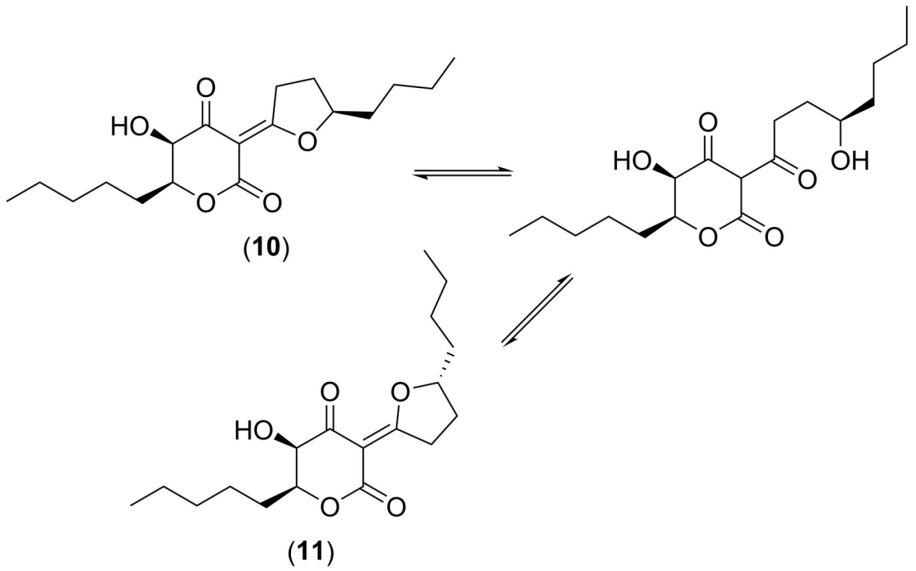

Figure 3.8: Isomerization of lachnellulone (**10**) via intermediate hydrolytic ring opening, followed by ring closure to produce isolachnellulone (**11**), as proposed by Ayer et al., 1988.

Table 3.11: ^{1}H and ^{13}C NMR data for lachnellulone (**11**, **12**) and related compounds (**12, 13**) isolated from *L.* cf. *calyciformis* DAOMC 251710, in $CDCl_3$.

	(10, 11)		**(12, 13)**	
position	δ_C	δ_H (*J* in Hz)	δ_C	δ_H (*J* in Hz)
2	165.3		167.9	
3	99.9		101.9	
4	191.2		191.2	
5	71.6	4.43, dd (2.6, 6.4)	43.9	2.51, m
6	77.5	4.56, ddd (2.6, 6.4, 10.7)	74.3	4.34, m
7	28.5	1.68, m	34.7	1.74, m
		1.28, m		
8	27.7	1.48, m	27.7	1.45
9	31.5	1.28, m	31.7	1.27
10	22.6	1.26, m	22.6	1.26, m
11	14.0	0.87, t (6.8)	14.2	0.86, m
12	188.9		187.9	
13	36.2	3.76, ddd (5.8, 9.5, 20.3)	36.4	3.38, m
		3.28, ddd (7.0, 9.5, 20.3)		3.24, m
14	34.7	1.86, m	34.8	1.90, m
		1.67, m		1.65, m
15	91.3	4.99, p (6.7)	90.9	4.83, m
16	26.9	2.31, dddd (5.8, 7.3, 9.6, 13.0)	27.7	2.26, m
		1.83, m		1.68, m
17	25.5	1.63, m	24.6	1.46, m
18	22.7	1.38, m	22.7	1.35, m
19	14.1	0.91, t (6.8)	14.2	0.86, m

Table 3.12: Physiochemical properties observed for lachnellulone (**10**, **11**) and related compounds (**12**, **13**) isolated from *L.* cf. *calyciformis* DAOMC 251710.

properties	**(10, 11)**	**(12, 13)**
appearance	white solid	white solid
molecular formula	$C_{18}H_{28}O_5$	$C_{18}H_{28}O_6$
HRMS [M+H]	325.2006	309.2056
calculated	325.2001	309.2061
OR $[\alpha]^{27}_D$ $CHCl_3$, c 0.03	37.5	-2.5
UV (MeOH)	215 (3.66)	216 (2.87)
λ_{max} nm (log ε)	273 (3.83)	274 (3.28)

3.6 Antimicrobial Activities

Compounds (**1-13**) were tested for antimicrobial activity against *S. cerevisiae*, *M. violaceum*, *E.coli* (ATCC 67878), and *B. subtilis* (ATCC 23857). The antibiotic data at 10 hours, and antifungal data at 22 hours for *M. violaceum* and *S. cerevisiae* were used for statistical analysis by ANOVA followed by Tukey's test and Fisher's least significant difference test (Systat V13.1), compared to the negative control (DMSO). An effect was observed when the *p*-value fell below 0.05, and the treatment was considered significantly different than the control (DMSO). Nystatin effectively inhibited the growth of *S. cerveviseae* at MICs of 6.2 μg mL^{-1} and chloramphenicol inhibited the growth bacteria with an MIC of 3.1 μg mL^{-1}. When Tukey's test gave non-significant results, the Fisher's LSD test was considered.

Antimicrobial activity exhibited by macrocyclic lactones (**1-3**) was limited to compound (**1**), radicicol. This lactone inhibited the growth of *M. violaceum*, with an MIC of 15.6 μg mL^{-1} (Table 3.13). Radicicol (**1**) was also antibacterial towards both the gram-negative and gram-positive bacteria, with MIC values of 125 μg mL^{-1} (Table 3.13). No growth inhibition was observed towards *S. cerevisiae* by radicicol (**1**) and compounds (**2-3**) did not exhibit any antimicrobial activity even at the highest concentration tested (125.0 μg mL^{-1}; Table 3.13).

Table 3.13: Growth inhibition observed when test organisms were treated with radicicol (**1**), and compared to the absence of treatment (DMSO), where a + indicates significantly inhibited growth ($p < 0.05$ according to ANOVA).

	radicicol (1) concentration (μg mL^{-1})				
test organism	**125.0**	**62.5**	**31.2**	**15.6**	**7.8**
S. cerevisiae	-	-	-	-	-
M. violaceum	+	+	+	+	-
B. subtilis	+	-	-	-	-
E. coli	+	-	-	-	-

The mixtures of racemic scytalone (**4**, **5**) produced by both *P.* cf *glaucoalbidum* (DAOMC 251707 and 251708) species exhibited no biological activity (Appendix I). Citromycetin (**6**) produced by *P.* cf. *glaucoalbidum* DAOMC 251707 inhibited the growth of *S. cerevisiae*, with an MIC of 62.5.0 μg mL^{-1} (Table 3.14). However, citromycetin (**6**) was not active against any other test organisms even at the highest concentration (Table 3.14). Fulvic acid (**7**) inhibited the growth of *S. sereviseae*, *B. subtilis*, and *E. coli* with MIC's of 62.5, 125.0, and 15.6 μg g^{-1}, respectively (Table 3.15). Tyrosol (**9**) from DAOMC 251707 also showed inhibitory effects at concentrations ranging between 125-3.9 μg mL^{-1} against *S. cerevisiae*, and moderate antifungal activity against *M. violaceum* with an MIC of 62.5 μg mL^{-1} (Table 3.16).

Table 3.14: Growth inhibition observed when organisms were treated with citromycetin (**6**), and compared to the absence of treatment (DMSO), where a + indicates significantly inhibited growth ($p < 0.05$ according to ANOVA).

	citromycetin (6) concentration (μg mL^{-1})				
test organism	**125.0**	**62.5**	**31.2**	**15.6**	**7.8**
S. cerevisiae	+	+	-	-	-
M. violaceum	-	-	-	-	-
B. subtilis	-	-	-	-	-
E. coli	-	-	-	-	-

Table 3.15. Growth inhibition observed when test organisms were treated with fulvic acid (**7, 8**), and compared to the absence of treatment (DMSO), where a + indicates significantly inhibited growth ($p < 0.05$ according to ANOVA).

	fulvic acid (7, 8) concentration (μg mL^{-1})				
test organism	**125.0**	**62.5**	**31.2**	**15.6**	**7.8**
S. cerevisiae	+	+	-	-	-
M. violaceum	-	-	-	-	-
B. subtilis	+	-	-	-	-
E. coli	+	+	+	+	-

Table 3.16: Growth inhibition observed when organisms were treated with tyrosol (**9**), and compared to the absence of treatment (DMSO), where a + indicates significantly inhibited growth ($p < 0.05$ according to ANOVA).

	tyrosol (9) concentration (μg mL^{-1})						
test organism	**125.0**	**62.5**	**31.2**	**15.6**	**7.8**	**3.9**	**1.9**
S. cerevisiae	+	+	+	+	+	+	-
M. violaceum	+	+	-	-	-	-	-
B. subtilis	-	-	-	-	-	-	-
E. coli	-	-	-	-	-	-	-

All metabolites (**10-13**) isolated from *Lachnellula* cf. *calyciformis* DAOMC 251710 exhibited some form of antimicrobial activity in the performed assays (Tables 3.17-3.18). Metabolites (**10**) and (**11**), were potently antifungal towards *M. violaceum*, with a MIC of 15.6 μg mL^{-1} (Table 3.17). The lachnellulones (**10,11**) moderately inhibited the growth of both *B. subtilis* and *E. coli* with MICs of 62.5 μg mL^{-1} (Table 3.17). Compounds (**10**) and (**11**) inhibited the growth of *S. cerevisiae* at the highest treatment concentration 125.0 μg mL^{-1} (Table 3.17).

Table 3.17: Growth inhibition observed when organism were treated with lachnellulone and isolachneullone (**10**, **11)** and compared to the absence of treatment (DMSO), where a + indicates significantly inhibited growth ($p < 0.05$ according to ANOVA).

	lachnellulone & iso-lachnellulone (10, 11) concentrations (μg mL^{-1})				
test organism	**125.0**	**62.5**	**31.2**	**15.6**	**7.8**
S. cerevisiae	+	-	-	-	-
M. violaceum	+	+	+	+	-
B. subtilis	+	+	-	-	-
E. coli	+	+	-	-	-

Related lachnellulones (**12**) and (**13**) produced by *L*. cf. *calyciformis* DAOMC 251710 were antifungal at lower treatment concentrations compared to compound (**10**) and (**11**). These compounds exhibited antifungal activity with an MIC of 7.8 μg mL^{-1} (Table 3.18). Compound (**12**) and (**13**) showed more potent antibacterial activity than compounds (**10**) and (**11**). The MIC against *B. subtilis* and *E. coli* were 31.2 and 15.6 μg mL^{-1}, respectively (Table 3.18). By comparison, metabolite (**12**) and (**13**) were not active against *S. cerevisiae* even at the highest concentration tested (Table 3.18).

Table 3.18: Growth inhibition observed when organisms were treated with compounds (**12**, **13**) and compared to the absence of treatment (DMSO), where a + indicates significantly inhibited growth ($p < 0.05$ according to ANOVA).

	1:1 compounds (12, 13) concentrations (μg mL^{-1})					
test organism	**125.0**	**62.5**	**31.2**	**15.6**	**7.8**	**3.9**
S. cerevisiae	-	-	-	-	-	-
M. violaceum	+*	+*	+*	+*	+*	-
B. subtilis	+	+	+	-	-	-
E. coli	+*	+*	+*	+*	-	-

Statistically significant by Fisher's LSD test

4.0 Discussion

The results presented in this thesis describe thirteen secondary metabolites not previously isolated from endophytes of conifers. The findings support the hypothesis that some conifer endophytes produce antifungal, antiinsectan, and antibacterial metabolites. As expected, some of these biologically active molecules were related to toxins produced by phylogenetically related pathogens including some *Penicillium* and *Fusarium* species. Some of fungi examined are phylogenetically related to fungi with well-established plant-insect associations such as the insect vectors for Dutch Elm disease (*Ophiostoma ulmi*; Tanney et al., 2016). These data further demonstrate that the bioassay-targeted study of endophytes results in the identification of bioactive molecules. This work supports the further investigation into the antiinsectan properties of the thirteen secondary metabolites and subsequent inoculation into spruce seedlings for field studies.

4.1 *Nectria dacryocarpa* (NB-236-7B; DAOMC 251709) metabolites

Three resorcyclic acid lactones (**1-3**) were isolated from the *P. mariana* (black spruce) endophyte *Nectria dacrocarpa*. Only radicicol (**1**) inhibited the growth of *M. violaceum*, *B. subtilis,* and *E. coli.* The antibacterial MICs were both 125.0 μg mL^{-1} compared to 15.6 μg mL^{-1} against the biotrophic pathogen *M. violaceum*, suggesting a more potent antifungal mode of action. These results agree with other studies, which recorded bacterial MICs for both *B. subtilis* and *E. coli* of over 100 μg mL^{-1}, and between 100-0.78 μg mL^{-1} for fungi (Fujita et al., 1999). Radicicol (**1**) was first characterized in 1953, produced by the fungus *Monocillium nordinii* and again in 1963 by *Nectria radicicola* (syn. *Cylindrocarpon radicicola*), from an unreported source (Delmotte et al., 1953; Mirrington et al., 1964). In this study, the black spruce endophyte *N. dacryocapa*

DAOMC 251709 was isolated in 2014 from a living needle of *P. mariana* in Gagetown, New Brunswick. Extensive studies on the structure-function relationships and biosynthesis of macrocyclic lactones began due to radicicol's (**1**) potent Hsp90 inhibitory activity. To inhibit the Hsp90 protein, radicicol competitively binds to the ATP binding pocket (IC_{50} 20 nM), thereby inhibiting the ATPase activity, and cellular chaperoning ability. This inhibition results in the destabilization and degradation of oncogenic proteins, which has since prompted investigation into its tumor cell growth inhibition and apoptotic properties, and application as an anti-cancer drug (Schulte et al., 1998; Mejia et al., 2014). Its antifungal activity is attributed to the inhibition of chitin synthase in the early stages, followed by inhibition of nucleic acid and protein synthesis (Fujita et al., 1999). These mechanisms of action suggest the mode of action could be similar in insects, and possibly explains the antifungal activity to *M. violaceum*.

The only structural modification which makes compound (**1**) unique from the other isolates is the epoxide moiety in the 14-membered ring. This would suggest a structure-antifungal- activity dependence of this functional group. Studies have shown the *trans-cis* dienone vicinal to the epoxide dictates the 3D structure (Zhou et al., 2010). It is the 3D structure and other functional groups including the chlorine, which likely account for the observed toxicity *in vivo*. It is theorized that the halide stabilizes the electron density of the aromatic ring, thus stabilizing the overall compound (Wang et al., 2009; Zhou et al., 2010). Based on the results from this study, the epoxide group appears to be the critical structural feature which confers antifungal and antibacterial activity *in vitro.*

The *Nectria* genus is a member of the Hypocrea sect. and a detailed monograph on the species was published in 2012 (Hirooka et al., 2012). Hypocreales (Order) encompass several genera and species, including both the *Fusarium* and *Trichoderma* genera which are prolific sources of natural products. This phylogenetic grouping supports the possible association of this endophyte with insects (Dowd et al., 1989; River et al., 2017). *Fusarium graminearum* produces metabolites are toxic to caterpillars and when combined synergism has been observed (Dowd et al., 1989). This supports the possibility that mixtures of macrocyclic lactones could result in synergistic effects on insects, or other unknown functions.

Both the structure and biosynthesis of radicicol (**1**)**,** is related to the mycotoxin ZEA. ZEA is a well-established estrogenic endocrine disruptor produced by various species of *Fusarium,* typically *F. graminearum* (Mirocha & Pathre, 1979). Epidemiologic evidence suggests effects of ZEA exposure in humans can decrease male sperm count, and increase cryptorchidi and hypospadias (Shier et al., 2001) In female mammals, it can produce estrogenic effects including infertility, vulval oedema, vaginal prolapse and mammary hypertrophy (Peraica et al., 1999). In male animals it can cause atrophy of the testes and enlargement of mammary glands. In humans it has been associated precocious pubertal changes in young girls (Pitt & Miller, 2017). ZEA is known to regulate the development of perithecia in *Fusarium* (Diekman & Green, 1992; Wolf & Mirocha, 1973). Interestingly, unlike most other mycotoxins, ZEA plays an observable role for the producing fungus. It is therefore possible that the structure-activity relationship may allow these molecules (**1-3**) to serve another unknown role for the producer. To date, macrocyclic lactones have been isolated from *Colletotrichum graminicola* (unspecified

location in Michigan, USA), a systemic vascular pathogen of maize (Wicklow et al., 2009). They have also been isolated from three strains of *Humicola fuscoatra*, one being an infector or tomato roots showing non-pathogenic signs from the Fraser Valley (British Columbia, Canada), and the second was isolated from sediment (33 m depth, Tutuila, American Samoa) (Mejia et al., 2014; Menzies et al., 1998). The third producer was isolated as a mycoparasite from the sclerotia of *Aspergillus flavus* (Wicklow et al., 1998). In all cases, radicicol was present in mixtures with other macrocyclic lactones further supporting biological action as a possible synergistic mixture including compounds (**2**) and (**3**) despite the low activity observed *in vitro***.**

Like ZEA, radicicol is biosynthesised by two iterative type PKS enzymes. Two enzymes responsible for radicicol synthesis have been isolated from *Pochonia chlamydosporia* and are termed *Rdc5* (highly reducing PK I) and *Rdc*1 (non-reducing, PK II) (Zhou et al., 2010). The ensemble of keto-reductive domains of *Rdc5* include ketoreductase, dehydratase, enoyl reductase and methyltransferase domains (Wang et al., 2009; Zhou et al., 2010). They condense a series of malonyl-CoA:ACP molecules to form the preliminary β-keto-ester (Mirocha & Pathre, 1979). *Rdc1* is composed of an N-terminal starter unit (ACP transacylase), which transfers the polyketide between the two PKS enzymes. It also houses a product template domain involved in cyclizing the complete (nonaketide) to form the 14 membered ring core, and finally a terminal thioester domain to release the final product (Wang et al., 2009). The chlorination event is a critical step in the biosynthesis happens as a tailoring step by a putative chlorinase within *Rdc2*. This

suggests the *P. mariana* endophyte *N. dacryocarpa* houses the same genetic machinery to biosynthesize radicicol and related molecules (**1-3**).

4.2 *Penicillium* cf. *glaucoalbidum* (RS10-14G; DAOMC 251707) metabolites

Both species of *P. cf. glaucoalbidum* in this study belong to the phylogenetically diverse Thysanophora section (Appendix IV). Very little peer-reviewed literature exists concerning Thysanophora. The first report was published in 1961 when W.B. Kendrick first described the genus from fungal isolates recovered from decaying needles of *Tsuga canadensis* (Eastern Hemlock) (Kendrick, 1961). Despite the intense mycological and metabolite directed research into the *genus Penicillium*, there has been little investigation into the Thysanophora sect., their existence as endophytes, or their secondary metabolite profiles. In 2012, the *Penicillium* genus was modified to include species from other genera, including *Thysanophora*, and 25 other sections (McNeill et al., 2012). Members of the section *Thysanophora* are morphologically characterized by darkly pigmented stripes, and phases of secondary growth from the apical penicillus (Visagie et al., 2014). *P.* cf. *glaucoalbidum* is the name given to many members of the *Thysanohpora* section, and was accepted into the genus (Visagie et al., 2014). This group lacks intensive study both taxonomically and chemically, and is a large species complex with high degrees of genetic variation, which deserves closer attention due to its phylogenetic relatedness to the *Penicllium* genus (Dr. J. Tanney, personal communication). The *Penicillium* genus has historically produced a wealth of biologically relevant natural products, including both agrochemically (e.g. ochratoxin A) and pharmacologically (e.g. penicillin) important molecules (Nielsen & Smedsgaard, 2003).

Two distinct species of *P*. cf *glaucoalbidum* were isolated from the Acadian forest their natural products were investigated because their crude metabolite extracts exhibited antifungal activity. These species only partially aligned to the database β-tubulin sequence for *P. glaucoalbidum,* and therefore these species are likely novel, and unique (Tanney, personal communication, Appendix IV). *P*. cf. *glaucoalbidum* (DAOMC 251708, 99% TUB similarity) was not isolated as endophyte, and instead from a dead needle attached to a living twig of *P. rubens*. *P*. cf. *glaucoalbidum* (DAOMC 251707, 91% TUB similarity) was both isolated as an endophyte from living needles attached to the twigs of *P. rubens*. All were collected from Alma, New Brunswick in 2014. Interestingly, other research indicates members of the Thysanophora sect. are most commonly isolated from dead needle specimens (23.4%) and only rarely in living needles (0.3-1.1%) (Kowalski & Andruch, 2012). Endophyte collections from New Brunswick suggest many strains within the *Thysanohpora* sect. are endophytes in spruce. Following senescence or death of the individual needles they sporulate and produce visible black sclerotia, which push through the needle stomata (Tanney, personal communication).

Citromycetin (**6**) and a racemic mixture of fulvic acid (**7-8**) were also isolated from *P*. cf. *glaucoalbidum* DAOMC 251707. Citromycetin has not been reported to be antifungal nor antibacterial *in vitro* (Capon et al., 2007; Jouda et al., 2014, 2016). Historically, these metabolites co-occur in a mixture, and are prone to rearrangement and degradation (Capon et al., 2007). Both were isolated from the marine strain of *Penicillium bilaii* strain collected from the Port Huron estuary in Tasmania, and a *P. striatisporum* strain collected

near Shalvey, New South Wales (Capon et al., 2007). Antimycobacterial activity against *Mycobacterium egmatis* was reported by citromycetin extracts from a *Penicillium* sp. of a Cameroonian medicinal plant *Garcinia nobilis* (Douanla-Meli et al., 2013; Jouda et al., 2016). This would support the phylogenetic relatedness of members of the Thysanophora sect to other *Penicillium* species. Its occurrence in medicinal plants supports the production of biologically relevant metabolites, which could have other interesting applications *in vivo*, *in planta* and in mammals (Nisa et al., 2015).

Fulvic acid was originally isolated from *Penicillium griseofulvum* in 1935 (Oxford et al., 1935). Fulvic acid (**7, 8**) was isolated here as a racemic mixture with minimal amounts of its acyclic and dehydro-forms (Figure 3.5). This molecule is prone to degradation, and rearrangement in solvent which explains the unidentifiable peaks in the ^{1}H spectra, and its difficult isolation (Oxford et al., 1935; Capon et al., 2007). These experimental findings show fulvic acid (**7, 8**) was antimicrobial towards *S. cerevisiae*, *B. subtilis*, and *E. coli* with MICs of 62.5, 125.0, and 15.6 μg mL^{-1}, respectively (Table 3.15). Fulvic acid has been shown to stimulate respiration, and root formation in some plants (Canellas et al., 2015).

It is postulated that citromycetin (**6**) is biosynthesized using a similar pathway as the antifungal compound griseofulvin and fulvic acid (**7, 8**) (Birch, 1968; Vanek et al., 1962). Both citromycetin (**6**) and fulvic acid (**7, 8**) are biosynthesized from seven C2 units including one acetyl and six malonyls, forming a linear heptaketide intermediate (Kurobane & Hutchinson, 1981). Their subsequent cyclizations (intra-molecular aldol

reactions) and processing (ring-opening and closing) is organism-specific, and governs the production of either citromycetin (**6**) and fulvic acid (**7, 8**). Also shown, was the ability of *P. griseofulvum* to *P. brefeldianum* to produce either griseofulvin or fulvic acid depending on the media chosen for growth conditions (Birch, 1968). Studies on the impacts of growth conditions (media) on secondary metabolism of *Fusarium oxysporum* and the production of the bikaverin polyketide found that it was only biosynthesized during unbalanced growth in acidic media, upon nitrogen depletion and excess carbon (Brewer et al., 1973).Overall, the ratio of carbon: nitrogen in the culture medium had the largest effects on secondary metabolite production.

Tyrosol (**9**) was produced by the endophytic *P. cf. glaucoalbidum* (DAOMC 251708), and has also been isolated from the white spruce endophyte *Rhytismatales* sp. and three other white spruce endophytes (CBS 120379-120381) (Green, 2016; McMullin et al., 2017). Various other fungal genera are known to produce tyrosol, including *Diaporthe*, *Xylaria*, and *Epichloë* (Claydon et al., 1985; Koshino et al., 1988, Schneider et al., 1996; Sumarah et al., 2008b). The culture extracts of the white spruce endophyte CBS 120380 capable of producing tyrosol, were toxic to the spruce budworm larvae resulting in reduced weights and head capsule size (Sumarah et al., 2008b). In this study, tyrosol (**9**) was potently toxic towards *S. cerevisiae* down to a concentration of 1.9 μg mL^{-1}, comparable to the MIC of the control antifungal nystatin. This bioactivity would suggest possible antiinsectan activity of this molecule, and the extract produced by *P.* cf. *glaucoalbidum* (DAOMC 251708).

4.3 *Penicillium* cf. *glaucoalbidum* (NB-589; DAOMC 251708) metabolites

Both *P. cf. glaucoalbidum* strains DAOMC 251708 and 251707 produced racemic mixtures of scytalone (**4, 5)** as determined by chiral HPLC and specific optical rotation measurements. Several enantiomeric mixtures of scytalone have been isolated previously, and is well summarized by Fabrice et al. (1990). Endophytes of conifers have also been reported to produce racemic mixtures. For example, racemic mixtures of sesquiterpenoids from species of *Lophodermium* collected from *Pinus strobus* were recently characterized (McMullin et al., 2015). The mixture of enantiomers did not inhibit the growth of any of the microorganism tested, even at the highest treatment concentration. This agrees with the literature, as there are no reported antifungal or antibacterial effects recorded (Fabrice et al., 1990; Findlay & Kwan, 1972). Racemic mixtures of scytalone was isolated from *Scytalidium* species, originally isolated from the decaying wood cores of Douglas-fir electrical poles (Findlay & Kwan, 1972; Ricard and Bollen, 1967; Strunz et al., 1970). The extracts from this fungus were antagonistic towards the *Poria carbonica*, responsible for heart wood decay of Douglas fir. The antifungal activity in these experiments was attributed to the compounds scytalidin, associated with the development of yellow pigmentation of the solid agar medium (Strunz et al., 1970). Scytalidin is reported to have diverse antifungal properties, especially against fungi responsible for the decay of conifers (Stillwell et al., 1973). It is possible that this fungus classified within the form genus *Scytalidium*, belongs to the Thysanohpora sect. Scytalone isolated from DAOMC 251707 was isolated along with several other antifungal and antibacterial compounds. This could suggest the low observed activity of scytalone by itself could be due to its combined effect *in vivo* with other molecules. It could also suggest the biosynthesis of

scytalidin is possible, under other growth conditions, or possibly *in planta*. Li et al. (2012) isolated rac-scytalon with other bioactive metabolites from *Leptographium qinlingensis,* an ophiostomatoid fungus associated with a forest insect pest *Dendroctonus armandi* which causes enormous mortalities of its host trees *Pinus armandi* (Li et al., 2012). The producer *L. qinlingensis* was isolated from bark beetles collected from galleries of sapwood of *Pinus armandi* from Quinling, China. This supports the hypothesis that these metabolites are also produced by related fungal pathogens, and fungi commonly associated with insects. The metabolites isolated from *P*. cf. *glaucoalbidum* (DAOMC 251708) merit further investigation into their potential anti-insect properties.

Some aspects of the biosynthesis of scytalone were studied in *Phialophora lagerbergii* (Sankawa et al., 1977)**.** One study postulates that it is likely biosynthesized from a symmetric anthraquinone, similar to the antiinsectan compound rugulosin produced by a *Penicillum* species (Sankawa et al., 1977). Scytalone is also an intermediate in the biosynthesis of melanin, where the biosynthesis is well characterized. Briefly, malonyl-CoA is converted to 1,3,6,8-tetrahydroxynapthalene, and then reduced by specific reductase enzymes to scytalone (Langfelder et al., 2003). In experiments with fungal derived from napthalenones, it was observed that scytalone increased the growth rate of cells within the foliar lamina at low concentrations (0.1 mM), and increased growth rates of the roots (0.3 and 0.01 mM) of *Arabidopsis thaliana* (Abou-Mansour et al., 2004). These experiments would suggest a more complex biological action *in planta*. It would also suggest a possible biochemical and phylogenetic relationship to other

phytopathogenic fungi which produce melanin as a virulence factor (Langfelder et al., 2003). Melanin is specifically involved with the hyphal (appresoria) penetration into leaves, and cell walls (Langfelder et al., 2003).

4.4 *Lachnellula* cf. *calyciformis* (RS10-3B; DAOMC 251710) metabolites

The culture extract from this fungus exhibited the highest amount of growth inhibition activity in the preliminary investigation using a modified Oxford diffusion assay. Additionally, only four liters compared to 15 L for typical bulk fermentations were required to generate an adequate amount of extract to permit the isolation of the four dominant metabolites. Lachnellulone (**10**) and iso-lachnellulone (**11**) were produced in the largest quantities *in vitro* (approx. 25 mg L^{-1}). These same molecules were the same major natural product isolated from *Lachnellula fuscosanguinea* (Ayer et al., 1988). *L. fuscosanguinea* belongs to the Hyaloscyphaceae family, and is a saprophyte of pine and other conifers. Additionally, it has been shown to be antagonistic to Dutch elm disease, and other saprophobic fungi (Ayer & Villar, 1985). *Diaporthe maritima* and other *Diaporthe* species are hypothesized to naturally control the growth of Dutch elm disease due to the production of antiinsectans, and their physical associations with *Ulmus* trees, as well as *P. rubens* (Tanney et al., 2016).

This natural product has been characterized by NMR only once in 1988, and upon dissolution exists as a mixture of two isomers. The equilibrium shifts between that of (**10**) lachnellulone, and (**11**) iso-lachneullulone, which was observed in this study, and that performed by Ayer, which is solvent and time dependent (Ayer et al., 1988). When the

NMR spectrum were observed in CD_3OD, approximately 1:1 ratios of both peaks (^{13}C and ^{1}H NMR), were observed which was confirmed in this study (Appendix III). Furthermore, upon immediate NMR spectra collection in $CDCl_3$, one product is present, representative of lachnellulone (Appendix III). Over time, the ratio equilibrates to 1:1 in $CHCl_3$ after approximately 24 hours. Both of these observations are consistent with the experimental findings in this study. Interestingly, it is known upon drying the mixture it returns to 100% lachneullulone isomer, which is the less soluble of the two forms. The NMR data here is reported for lachneullulone in $CDCl_3$ (**10**). Peaks corresponding to iso-lachneullulone can be seen in Appendix III in CD_3OD.

There are only three publications to date describing natural products from the genus *Lachnellula*; lachnellulone (Ayer et al., 1988), lechnelluloic acid (Ayer and Villar, 1985), and lechnellins (Semar et al., 1996). Interestingly, reports indicate racemic scytalone has been isolated from the same lachnellin producing *Lachnellula* sp., which was also purified from two Thysanohpora sect *P*. cf. *glaucoalbidum* strains in this investigation (Semar et al., 1996). Scytalone was not produced by the *L*. cf. *calicyformis* endophyte in this study. This could indicate a shared secondary metabolic pathway between red spruce endophytes.

In addition to lachnellulone (**10**) and iso-lachnellulone (**11**), two lachnellulone related compound (**12**) and (**13**) were isolated. When the NMR spectrum (^{1}H and ^{13}C) were collected immediately after dissolution of (**12, 13**) in $CDCl_3$, two set of signals were observed. This is contrary to what is observed with lachnellulone and iso-lachnellulone

(Appendix III). This could be due to the increased freedom of rotation around the double bond, due to the absence of the hydroxyl group. Interestingly, these metabolites were more biologically active, likely due to their differing functional group at position C-5, which altered its 3D structure and physiochemical properties. The absence of the hydroxyl group at C-5 possibly added to its affinity for its molecular target. Lachneullulone and iso-lachneullulone (**10**) and (**11**) inhibited the growth of *M. violaceum*. *B. subtilis,* and *E. coli* down to levels of 31.2, 62.5, and 62.5 μg mL^{-1}, respectively. By comparison, compounds (**12**) and (**13**) possessed MIC values of 7.8, 31.2, and 15.6 μg mL^{-1} against *M. violaceum*, *B. subtilis*, and *E. coli,* respectively.

5.0 Conclusion

These experiments contributed to a better understanding of the fungal ecology, phylogeny, and secondary metabolism of endophytes of black and red spruce. It resulted in the isolation and characterization of 13 secondary metabolites produced by the black spruce endophytes *Nectria dacryocarpa* DAOMC 251709, red spruce endophytes *Lachneullula* cf. *calyciformis* DAOMC 251710, and two distantly related species of the Thysanophora sect. grouped as *Penicillium* cf. *glaucoalbidum* (DAOMC 251707, 251708). All of the metabolites reported here were polyketides except for one amino acid derived molecule, tyrosol (**9**). Not all endophytes in this study produced bioactive metabolites under the fermentation conditions tested. For several endophytes studied here, a number of mixtures were also present. This could suggest various implications of chemical synergy, or more complex biological modes of action, as is the case with other fungal toxins (Dowd, 1988). It also permitted distant comparisons between fungal

species, and between strains. In most cases, the endophytes produced toxins related to those produced by pathogenic, or insect associated fungi.

References

Abou-Mansour, E., Couché, E., Tabacchi, R., 2004. Do fungal naphthalenones have a role in the development of esca symptoms. Phytopathol. Mediterr. 43, 75–82.

Adams, R.I., Miletto, M., Taylor, J.W., Bruns, T.D., 2013. The diversity and distribution of fungi on residential surfaces. PLoS One 8.

Ayer, W.A, Figueroa, J. D., Migak, B., 1988. Metabolites of *Lachnellula fucosanguinea* (Rehm). Part 2. The structure of lachnellulone. Can. J. Chem. 66, 506–512.

Ayer, W.A., Villar, J.D.F., 1985. Metabolites of *Lachnellula fucosanguinea* (Rehm). Part 1. The isolation, structure determination, and synthesis of lechnelluloic acid. Can. J. Chem. 63, 1161–1165.

Bacon, C.W., Porter, J.K., Robbins, J.D., Luttrell, E.S., 1977. *Epichloe typhina* from toxic tall fescue grasses. Appl. Environ. Microbiol. 34, 576–581.

Birch, A.J., 1968. Polyketide metabolism. Annu. Rev. Plant Physiol. 19, 321–332.

Blais, J.R., 1983. Trends in the frequency, extent, and severity of spruce budworm outbreaks in eastern Canada. Can. J. For. Res. 13, 539–547.

Breen, J.P., 1994. *Acremonium* endophyte interactions with enhanced plant resistance to insects. Annu. Rev. Entomol. 39, 401–423.

Brewer, D., Arsenault, G.P., Wright, J.L.C., Vining, L.C., 1973. Production of bikaverin by Fusarium oxysporum and its identity with lycopersin. Journal of Antibiotics XXVI, 778-781.

Calhoun, L.A., Findlay, J.A., Miller, J.D., Whitney, N.J., 1992. Metabolites toxic to spruce budworm from balsam fir needle endophytes. Mycol. Res. 96, 281–286.

Canellas, L.P., Olivares, F.L., Aguiar, N.O., Jones, D.L., Nebbioso, A., Mazzei, P., Piccolo, A., 2015. Humic and fulvic acids as biostimulants in horticulture. Sci. Hortic. 196, 15–27.

Capon, R.J., Stewart, M., Ratnayake, R., Lacey, E., Gill, J.H., 2007. Citromycetins and bilains A-C: New aromatic polyketides and diketopiperazines from Australian marine-derived and terrestrial *Penicillium* spp. J. Nat. Prod. 70, 1746–1752.

Carroll, G., 1995. Forest endophytes: pattern and process. Can. J. Bot. 73, 1316–1324.

Carroll, G., 1988. Fungal endophytes in stems and leaves : From latent pathogen to mutualistic symbiont. Ecol. 69, 2–9.

Carroll, G.C., Carroll, F.E., 1978. Studies on the incidence of coniferous needle endophytes in the Pacific Northwest. Can. J. Bot. 56, 3034–3043.

Clay, K., 1990. Fungal endophytes of grasses. Annu. Rev. Ecol. Syst. 21, 257–297.

Clay, K., 1988. Fungal endophytes of grasses : A defensive mutualism between plants and fungi. Ecol. 69, 10–16.

Clay, K., 1984. The effect of the fungus *Atkinsonella hypoxylon* (Clavicipitaceae) on the reproductive system and demography of the grass *Danthonia spicata.* New Phytol. 98, 165–175.

Claydon, N., Grove, J.F., Pople, M., 1985. Elm bark beetle boring and feeding deterrents from *Phomopsis oblanga*. Phytochem. 24, 937-943.

Demain, A.L., Fang, A., 2000. The natural functions of secondary metabolites. Adv. Biochem. Eng. Biotechnol. 69, 1–39.

Dewick, P.M., 2002. Medicinal natural products: a biosynthetic approach. John Wiley & Sons.

Diekman, M.A., Green, M.L., 1992. Mycotoxins and reproduction in domestic livestock. J. Anim. Sci. 70, 1615–1627.

Douanla-Meli, C., Langer, E., Talontsi Mouafo, F., 2013. Fungal endophyte diversity and community patterns in healthy and yellowing leaves of *Citrus limon*. Fungal Ecol. 6, 212–222.

Dowd, P.F., Miller, J.D., Greenhalgh, R., 1989. Toxicity and interactions of some *Fusarium graminearum* metabolites to caterpillars. Mycol. 81, 646–650.

Dowd, P.F., 1988. Synergism of aflatoxin B1 toxicity with the co-occurring fungal metabolite kojic acid to two caterpillars. Entomol. Exp. Appl. 47, 69–71.

Drew, S.W., Demain, A.L., 1977. Effect of primary metabolites on secondary metabolism. Annu. Rev. Microbiol. 31, 343–356.

Espinosa-Garcia, F.J., Langenheim, J.H., 1990. The endophytic fungal community in leaves of a coastal redwood population diversity and spatial patterns. New Phytol. 116, 89–97.

Fabrice, Viviani., Michel, G., 1990. Enantiomeric purity of scytalone from different fungal sources. Tetrahedron 46, 2827–2834.

Findlay, J.A., Kwan, D., 1972. Scytalone (3,6,8-Trihydrozytetralone), a metabolite from a

Scytalidium Species. Can. J. Chem. 51, 1617–1619.

Findlay, J.A., Buthelezi, S., Li, G., Seveck, M., 1997. Insect toxins from an endophytic fungus from wintergreen. J. Nat. Prod. 60, 1214–1215.

Findlay, J. A., Buthelezi, S., Lavoie, R., Peña-Rodriguez, L., Miller, J.D., 1995. Bioactive isocoumarins and related metabolites from conifer endophytes. J. Nat. Prod. 58, 1759–1766.

Findlay, J. A., Li, G., Miller, J.D., Womiloju, T.O., 2003. Insect toxins from spruce endophytes. Can. J. Chem. 81, 284–292.

Fleming, A., 1929. On the antibacterial action of cultures of a *Penicillium*, with specifc reference to their use in the isolation of B. Influenzae. J. Exp. Pathol. 226–236.

Frasz, S.L., Walker, A.K., Nsiama, T.K., Adams, G.W., Miller, J.D., 2014. Distribution of the foliar fungal endophyte *Phialocephala scopiformis* and its toxin in the crown of a mature white spruce tree as revealed by chemical and qPCR analyses. Can. J. For. Res. Can. Rech. For. 44, 1138–1143.

Fujita, J.I., Irie, M., Pink, X., Taniguchi, M., 1999. Antifungal activity of radicicol against *Mucor flavus* IFO 9560. J. Biosci. Bioeng. 88, 380–386.

Giordano, W., Domenech, C.E., 1999. Aeration affects acetate destination in *Gibberella fujikuroi*. FEMS Microbiol. Lett. 180, 111–116.

Gloer, J.B., 1995. The chemistry of fungal antagonism and defense. Can. J. Bot. 73, S1265–S1274.

Gottlieb, H.E., Kotlyar, V., Nudelman, A., 1997. NMR Chemical shifts of common laboratory solvents as trace impurities. J. Org. Chem. 62, 7512–7515.

Gray, D.R., MacKinnon, W.E., 2006. Outbreak patterns of the spruce budworm and their impacts in Canada. For. Chron. 82, 550–561.

Green, B.D., 2016. Characterization of secondary metabolites produced by foliar endophytes of red and black spruce. MSc Thesis, Department of Chemistry, Carleton University, Ottawa.

Guerin D. 1898. Sur la presence d'un champignon dans l'lvraie. J. Bot. 12: 230–238.

H. Marx, D., 1972. Ectomycorrhizae as biological deterrents 3558 to pathogenic root infections. Annu. Rev. Phytopathol. 10, 429–454.

Hellwig, V., Mayer-Bartschmid, A., Müller, H., Greif, G., Kleymann, G., Zitzmann, W.,

Tichy, H.-V., Stadler, M., 2003. Pochonins A−F, new antiviral and antiparasitic resorcylic acid lactones from *Pochonia c hlamydosporia* var. *c atenulata*. J. Nat. Prod. 66, 829–837.

Hirooka, Y., Rossman, A.Y., Samuels, G.J., Lechat, C., Chaverri, P., 2012. A monograph of *Allantonectria*, *Nectria*, and *Pleonectria* (Nectriaceae, Hypocreales, Ascomycota) and their pycnidial, sporodochial, and synnematous anamorphs. Stud. Mycol. 71, 1–210.

Hoffmeister, D., Keller, N.P., 2007. Natural products of filamentous fungi: enzymes, genes, and their regulation. Nat. Prod. Reports 24, 393–416.

Johnson, J.A., Whitney, N.J., 1989. A study of fungal endophytes of needles of balsam fir (*Abies balsamea*) and red spruce (*Picea rubens*) in new-brunswick, canada, using culture and electron-microscope techniques. Can. J. Bot. 67, 3513–3516.

Jouda, J.B., Kusari, S., Lamshöft, M., Mouafo Talontsi, F., Douala Meli, C., Wandji, J., Spiteller, M., 2014. Penialidins A-C with strong antibacterial activities from *Penicillium* sp.; An endophytic fungus harboring leaves of *Garcinia nobilis*. Fitoterapia 98, 209–214.

Jouda, J.B., Mawabo, I.K., Notedji, A., Mbazoa, C.D., Nkenfou, J., Wandji, J., Nkenfou, C.N., 2016. Anti-mycobacterial activity of polyketides from *Penicillium* sp. endophyte isolated from *Garcinia nobilis* against *Mycobacterium smegmatis*. Int. J. Mycobacteriology 5, 7–11.

Keller, N.P., Turner, G., Bennett, J.W., 2005. Fungal secondary metabolism-from genomics to biochemistry. Nat. Rev. Microbiol. 3, 937–947.

Kendrick, B., 1992. The Fifth Kingdom, 3rd ed. Focus Publishing, Newburyport, MA.

Kendrick, W.B., 1961. Hyphomycetes of conifer leaf litter. Can. J. Bot. 39, 817–832.

Kluge, M., Siegmund, D., Diekmann, H., Thoma, M., 1992. A model for penicillin production with and without temperature shift after the growth phase. Appl. Microbiol. Biotechnol. 36, 446–451.

Koshino, H., Terada, S., Yoshihara, T., Sakamura, S., Shimanuki, T., Sato, T., Tajimi, A., 1988. Three phenolic acid derivatives from stromata from *Epichloe typhina* on *Phleum pretense*. Phytochem. 27, 1333-1338.

Kowalski, T., Andruch, K., 2012. Mycobiota in needles of Abies alba with and without

symptoms of *Herpotrichia* needle browning. For. Pathol. 42, 183–190.

Krnjaja, V., Mandić, V., Lević, J., Stanković, S., Petrović, T., Vasić, T., Obradović, A., 2015. Influence of N-fertilization on *Fusarium* head blight and mycotoxin levels in winter wheat. Crop Prot. 67, 251–256.

Kurobane, I., Hutchinson, C.R., 1981. The biosynthesis of fulvic acid, a fungal metabolites of heptaketide origin. Tetrahedron Lett. 22, 493–496.

Langfelder, K., Streibel, M., Jahn, B., Haase, G., Brakhage, A.A., 2003. Biosynthesis of fungal melanins and their importance for human pathogenic fungi. Fungal Genet. Biol. 38, 143–158.

Li, X.J., Gao, J.M., Chen, H., Zhang, A.L., Tang, M., 2012. Toxins from a symbiotic fungus, *Leptographium qinlingensis* associated with *Dendroctonus armandi* and their in vitro toxicities to *Pinus armandi* seedlings. Eur. J. Plant Pathol. 134, 239–247.

McMullin, D.R., Green, B.D., Miller, J.D., 2015. Antifungal sesquiterpenoids and macrolides from an endophytic *Lophodermium* species of *Pinus strobus*. Phytochem. Lett. 14, 148–152.

McMullin, D.R., Green, B.D., Prince, N.C., Tanney, J.B., Miller, J.D., 2017. Natural products of *Picea* endophytes from the Acadian Forest. J. Nat. Prod.

Mcneill, J., Barrie, F.R., Buck, W.R., Demoulin, V., Greuter, W., Hawksworth, D.L., Herendeen, P.S., Knapp, S., Marhold, K., Prado, J., Prud Homme Van Reine, W.F., Smith, G.F., Wiersema, J.H., Turland, N.J., 2012. International Code of Nomenclature for algae, fungi, and plants. Koeltz Sci. Books 1–140.

Mejia, E.J., Loveridge, S.T., Stepan, G., Tsai, A., Jones, G.S., Barnes, T., White, K.N., Drakovi, M., Tenney, K., Tsiang, M., Geleziunas, R., Cihlar, T., Pagratis, N., Tian, Y., Yu, H., Crews, P., 2014. Study of marine natural products including resorcyclic acid lactones from *Humicola fuscoatra* that reactivate latent HIV-1 expression in an in vitro model of central memory CD4+ T cells. J. Nat. Prod. 77, 618–624.

Menzies, J.G., Ehret, D.L., Koch, C., Bogdanoff, C., 1998. *Humicola fuscoatra* infects tomato roots, but is not pathogenic. Eur. J. Plant Pathol. 104, 769–775.

Miller, D.J., 2011. Foliar endophytes of spruce species found in the Acadian Forest: Basis and potential for improving the tolerance of forest to spruce budworm. Endophytes

For. Trees Biol. Appl. 80, 265–294.

Miller, J.D., 1984. Toxic Metabolites of Epiphytic Fungi of Conifer Needles, in: Fokkema, NJ, Van Den Heuvel, J. (Ed.), Microbiology of the Phyllosphere. pp. 223–231.

Miller, J.D., Cherid, H., Sumarah, M.W., Adams, G.W., 2009. Horizontal transmission of the *Picea glauca* foliar endophyte *Phialocephala scopiformis* CBS 120377. Fungal Ecol. 2, 98–101.

Miller, J.D., Mackenzie, S., Foto, M., Adams, G.W., Findlay, J.A., 2002. Needles of white spruce inoculated with rugulosin-producing endophytes contain rugulosin reducing spruce budworm growth rate. Mycol. Res. 106, 471–479.

Miller, J.D., Sumarah, M.W., Adams, G.W., 2008. Effect of a rugulosin-producing endophyte in *Picea glauca* on *Choristoneura fumiferana*. J. Chem. Ecol. 34, 362–368.

Miller, J.D., Young, J.C., Trenholm, H.L., 1983. Fusarium toxins in field corn. I. Time course of fungal growth and production of deoxynivalenol and other mycotoxins. Can. J. Bot. 61, 3080–3087.

Mirocha, C.J., Pathre, S.V., 1979. Mycotoxins- Their biosynthesis in fungi; Zearalenone bioynthesis. J. Food Protection 42, 821–824.

Mirrington, R.N., Ritchie, E., Shopee, C.W., Taylor, W.C., 1964. The constitution of radicicol. Tetrahedron Lett. 7, 365–370.

Natural Resources Canada. 2016. The state of Canada's forests. Annual Report 2016. Retrieved on 06/14/17/. http://cfs.nrcan.gc.ca/pubwarehouse/pdfs/37265.pdf

Nielsen, K.F., Mansson, M., Rank, C., Frisvad, J.C., Larsen T.O., 2011. Dereplication of microbial natural products by LC-DAD-TOFMS. J. Nat. Prod. 74, 2338-2348.

Nielsen, K.F., Smedsgaard, J., 2003. Fungal metabolite screening: Database of 474 mycotoxins and fungal metabolites for dereplication by standardised liquid chromatography-UV-mass spectrometry methodology. J. Chromatogr. A 1002, 111–136.

Nisa, H., Kamili, A.N., Nawchoo, I.A., Shafim S., Shameem, N., Bandh, S.A., 2015. Fungal endophytes as prolific source of phytochemicals and other bioactive natural products: A review. Microb. Pathog. 82, 50-59.

Oxford, A.E., Raistrick, H., Simonart, P., 1935. Studies in the biochemistry of microorganisms. XLIV. Fulvic acid, a new crystalline yellow pigment, a metabolic product of *P. griseofulvum* Dierckx, *P. flexuosum* Dale and *P. brefeldianum* Dodge. Biochem. J. 29, 1102–1115.

Peraica, M., Radi, B., Luci, A., Pavlovi, M., 1999. Toxic effects of mycotoxins in humans. Bull. World Health Organ. 77, 754–766.

Petrini, O., 1991. Fungal endophytes of tree leaves, in: Microbial Ecology of Leaves. Springer, New York, NY, pp. 179–197.

Pirozynski, K.A., Malloch, D.W., 1975. The origin of land plants: A matter of mycotrophism. BioSystems 6, 153–164.

Pitt, J.I., Miller, J.D., 2017. A concise history of mycotoxin research. J. Agric. Food Chem. doi: 10.1021/acs.jafc.6b04494.

Porter, J.K., 1995. Analysis of endophyte toxins: fescue and other grasses toxic to livestock. J. Anim. Sci. 73, 871–880.

Powell, R.G., Petroski, R.J., 1993. Alkaloid toxins in endophyte-infected grasses. Nat. Toxins 1, 163–170.

Redecker, D., 2000. Glomalean fungi from the ordovician. Science 289, 1920–1921.

Ricard, J.L., Bollen, W.B., 1968. Inhibition of *Poria carbonica* by *Scytalidium* sp., an imperfect fungus isolated from Douglas-fir poles. Can. J. Bot. 46, 643-647.

Richards, T., Leonard, G., Soanes, D., Talbot, N.J., 2011. Gene transfer into the fungi. Fung. Biol. Rev. 25, 98-110.

River, K., Borneo, S.N., Foo, K., Seelan, J., Seelan, S., Dawood, M.M., 2017. Microfungi associated with *Pteroptyx bearni* (*Coleoptera lampyridae*) eggs and larvae from Kawang River, Sabah (Northern Borneo). Insects 8, 66.

Rodriguez, R.J., White, J.F., Arnold, A.E., Redman, R.S., 2009. Fungal endophytes: diversity and functional roles. New Phytol. 182, 314–330.

Royama, T., 1984. Population dynamics of the spruce budworm *Choristoneura Fumiferana*. Ecol. Monogr. 54, 429–462.

Royama, T., MacKinnon, W.E., Kettela, E.G., Carter, N.E., Hartling, L.K., 2005. Analysis of spruce budworm outbreak cycles in New Brunswick, Canada, since 1952. Ecol. 86, 1212–1224.

Sankawa, U., Shimada, H., Sato, T., Kinoshita, T., 1977. Biosyntehsis of scytalone. Tetrahedron Lett. 5, 483–486.

Schneider, G., Anke, H., Sterner, O., 1996. Xylaramide, a new antifungal compound, and other secondary metabolites from *Xylaria longipes*. Z. Naturforsch.C. 51, 802-806.

Schmidt-Dannert, C., 2015. Biosynthesis of terpenoid natural products in fungi. Adv Biochem. Eng. Biotechnol. 148, 16–61.

Schoch, C.L., Seifert, K., Huhndorf, S., Robert, V., Spouge, J.L., Levesque, C., Chen, W., Consortium, F.B., Bolchacova, E., Voigt, K., Crous, P.W., Miller, N., Wingfield, M.J., Aime, M.C., An, K.D., Bai, F.-Y., Barreto, R.W., Begerow, D., Bergeron, M.-J., Blackwell, M., Boekhout, T., Bogale, M., Boonyuen, N., Burgaz, R., Buyck, B., Cai, L., Cai, Q., Cardinali, G., Chaverri, P., Coppins, B.J., Crespo, A., Cubas, P., Cummings, C., Damm, U., De Beer, Z.W., de Hoog, G.S., Del-Prado, R., Dentinger, B., Dieguez-Uribeondo, J., Divakar, P.K., Douglas, B., Duenas, M., Duong, T. A., Eberhardt, U., Edwards, J.E., Elshahed, M.S., Fliegerova, K., Furtado, M., Garcia, M., Ge, Z.-W., Griffith, G.W., Griffiths, K., Groenewald, J.Z., Groenewald, M., Grube, M., Gryzenhout, M., Guo, L.D., Hagen, F., Hambleton, S., Hamelin, R.C., Hansen, K., Harrold, P., Heller, G., Herrera, C., Hirayama, K., Hirooka, Y., Ho, H.-M., Hoffmann, K., Hofstetter, V., Hognabba, F., Hollingsworth, P.M., Hong, S., Hosaka, K., Houbraken, J., Hughes, K., Huhtinen, S., Hyde, K.D., James, T., Johnson, E.M., Johnson, J.E., Johnston, P.R., Jones, E.B.G., Kelly, L.J., Kirk, P.M., Knapp, D.G., Koljalg, U., Kovacs, G.M., Kurtzman, C.P., Landvik, S., Leavitt, S.D., Liggenstoffer, A. S., Liimatainen, K., Lombard, L., Luangsa-ard, J.J., Lumbsch, H.T., Maganti, H., Maharachchikumbura, S.S.N., Martin, M.P., May, T.W., McTaggart, R., Methven,S., Meyer, W., Moncalvo, J.-M., Mongkolsamrit, S., Nagy, L.G., Nilsson, R.H., Niskanen, T., Nyilasi, I., Okada, G., Okane, I., Olariaga, I., Otte, J., Papp, T., Park, D., Petkovits, T., Pino-Bodas, R., Quaedvlieg, W., Raja, H. a., Redecker, D., Rintoul, T.L., Ruibal, C., Sarmiento-Ramirez, J.M., Schmitt, I., Schussler, A., Shearer, C., Sotome, K., Stefani, F.O.P., Stenroos, S., Stielow, B., Stockinger, H., Suetrong, S., Suh, S.-O., Sung, G.-H., Suzuki, M., Tanaka, K., Tedersoo, L., Telleria, M.T., Tretter, E., Untereiner, W. A., Urbina, H., Vagvolgyi, C., Vialle, A., Vu, T.D., Walther, G., Wang, Q.-M., Wang, Y., Weir, B.S., Weiss,

M., White, M.M., Xu, J., Yahr, R., Yang, Z.L., Yurkov, A., Zamora, J.C., Zhang, N., Zhuang, Y., Schindel, D., 2012. Nuclear ribosomal internal transcribed spacer (ITS) region as a universal DNA barcode marker for Fungi. Proc. Natl. Acad. Sci. U. S. A. 109, 1–6.

Schulte, T.W., Akinaga, S., Soga, S., Sullivan, W., Stensgard, B., Toft, D., Neckers, L.M., 1998. Antibiotic radicicol binds to the N-terminal domain of Hsp90 and shares important biologic activities with geldanamycin. Cell Stress Chaperones 8, 100-108.

Semar, M., Anke, H., Arendholz, W, R., Velten, R., Steglich, W., 1996. Lachnellins A, B, C, D, and naphthalene-1,3,8-triol, biologically active compounds from a *Lachnellula* species (Ascomycetes). Can. J. Biosci. 51, 500–512.

Sherwood-Pike, M., Stone, J.K., Carroll, G.C., 1986. *Rhabdocline parkeri* a ubiquitous foliar endophyte of Douglas fir. Can. J. Bot. 64, 64:1849-1855.

Shier, W.T., Shier, A.C., Xie, W., Mirocha, C.J., 2001. Structure-activity relationships for human estrogenic activity in zearalenone mycotoxins. Toxicon 39, 1435–1438.

Shinonaga, H., Kawamura, Y., Ikeda, A., Aoki, M., Sakai, N., Fujimoto, N., Kawashima, A., 2009. Pochonins K-P: new radicicol analogues from *Pochonia chlamydosporia* var. *chlamydosporia* and their WNT-5A expression inhibitory activities. Tetrahedron 65, 3446–3453.

Sieber, T.N., 2007. Endophytic fungi in forest trees : are they mutualists? Fungal Biol. Rev. 21, 75–89.

Siegel, M.R., 1987. Fungal endophytes of grasses. Ann. Rev. Phytopathol. 25, 293–315.

Stillwell, M.A., Wall, R.E., Strunz, G.M., 1973. Production, isolation, and antifungal activity of scytalidin, a metabolite of *Scytalidium* species. Can. J. Microbiol. 19, 597-602.

Strunz, G.M., Kakushima M., Stillwell, M.A., 1970. Scytalidin: a new fungitoxic metabolite produced by a *Sctalidium* species. J.C.S. Perkin Trans. 2280–2283.

Sumarah, M.W., Adams, G.W., Berghout, J., Slack, G.J., Wilson, A.M., Miller, J.D., 2008. Spread and persistence of a rugulosin-producing endophyte in *Picea glauca* seedlings. Mycol. Res. 112, 731–736.

Sumarah, M.W., Miller, J.D., 2009. Anti-insect secondary metabolites from fungal endophytes of conifer trees. Nat. Prod. Commun. 4, 1497–1504.

Sumarah, M.W., Puniani, E., Blackwell, B.A., Miller, J.D., 2008b. Characterization of polyketide metabolites from foliar endophytes of *Picea glauca*. J. Nat. Prod. 71, 1393-1398.

Sumarah, M.W., Puniani, E., Sorensen, D., Blackwell, B.A., Miller, J.D., 2010. Secondary metabolites from anti-insect extracts of endophytic fungi isolated from *Picea rubens*. Phytochem. 71, 760–765.

Sun, X., Guo, L., 2012. Endophytic fungal diversity : review of traditional and molecular techniques. Mycology 3, 65–76.

Tanney, J., Douglas, B., Seifert, K.A., 2015. Sexual and asexual states of some endophytic *Phialocephala* species of *Picea*. Mycologia 5514, 1–32.

Tanney, J.B., 2016. A taxonomic and phylogenetic investigation of conifer endophytes of eastern Canada. PhD Thesis, Department of Biology, Carleton University, Ottawa.

Tanney, J.B., McMullin, D.R., Green, B.D., Miller, J.D., Seifert, K.A., 2016. Production of antifungal and antiinsectan metabolites by the *Picea* endophyte *Diaporthe maritima* sp. nov. Fungal Biol. 120, 1448–1457.

Thomas, D.C., Vandegrift, R., Ludden, A., Carroll, G.C., Roy, B.A., 2016. Spatial ecology of the fungal genus *Xylaria* in a tropical cloud forest. Biotropica 48, 381–393.

Tudzynski, B., 2014. Nitrogen regulation of fungal secondary metabolism in fungi. Front. Microbiol. 5, 1–15.

Van Rensburg, C.E.J., van Straten, A., Dekker, J., 2000. An in vitro investigation of the antimicrobial activity of oxifulvic acid. J. Antimicrob. Chemother. 46, 847–863.

Vanek, Z., Soucek, M., 1962. Factors determining the biosynthesis of griseofulvin and similar substances. Folia Microbiol. 7, 262–265.

Visagie, C.M., Houbraken, J., Frisvad, J.C., Hong, S.B., Klaassen, C.H.W., Perrone, G., Seifert, K.A., Varga, J., Yaguchi, T., Samson, R.A., 2014. Identification and nomenclature of the genus Penicillium. Stud. Mycologia 78, 343–371.

Walton, J.D., 2000. Horizontal gene transfer and the evolution of secondary metabolite gene clusters in fungi: A hypothesis. Fungal Genet. Biol. 30, 167–171.

Wang, M., Zhou, H., Wirz, M., Tang, Y., Boddy, C.N., 2009. A thioesterase from an iterative fungal polyketide synthase shows macrocyclization and cross-coupling

activity, and may play a role in controling iterative cycling through product off loading. Biochem. 47, 6288–6290.

Wang, L.W., Xu, B.G., Wang, J.Y., Su, Z.Z., Lin, F.C., Zhang, C.L., Kubicek, C.P., 2012. Bioactive metabolites from *Phoma* species, an endophytic fungus from the Chinese medicinal plant *Arisaema erubescens*. Appl. Microbiol. Biotechnol. 93, 1231–1239.

Wicklow, D.T., 1981. Interference competition, in: The Fungal Community. pp. 265–274.

Wicklow, D.T., Jordan, A.M., Gloer, J.B., 2009. Antifungal metabolites (monorden, monocillins I, II, III) from *Colletotrichum graminicola*, a systemic vascular pathogen of maize. Mycol. Res. 113, 1433–1442.

Wicklow, D.T., Joshi, B.K., Gamble, W.R., Gloer, J.B., Dowd, P.F., 1998. Antifungal metabolites (monorden, monocillin IV, and cerebrosides) from *Humicola fuscoatra* traaen NRRL 22980, a mycoparasite of *Aspergillus flavus* sclerotia. Appl. Environ. Microbiol. 64, 4482–4484.

Williams, S.T., Vickers, J.C., 1986. The ecology of antibiotic production. Microb. Ecol. 12, 43–52.

Wolf, J.C., Mirocha, C.J., 1973. Regulation of sexual reproduction in *Gibberella zeae* (*Fusarium roseum "graminearum"*) by F-2 (Zearalenone). Can. J. Microbiol. 19, 725–34.

Zeng, L., Jin, H., Lu, D., Yang, X., Pan, L., Cui, H., He, X., Qiu, H., Qin, B., 2015. Isolation and identification of chemical constituents from the bacterium *Bacillus* sp. and their nematicidal activities. J. Basic Microbiol. 55, 1239–1244.

Zhou, H., Qiao, K., Gao, Z., Vederas, J.C., Tang, Y., 2010. Insights into radicicol biosynthesis via heterologous synthesis of intermediates and analogs. J. Biol. Chem. 285, 41412–41421.

Appendix I- Summary of endophyte collection and preliminary antimicrobial screening

Isolate code	Species	Host/Source	Collection site	Bioassay result		Extract Mass (mg)
				S. cerevisiae	*M. violaceum*	
NB-505-6K	*Lophodermium* cf. *piceae*	*Picea rubens* endophyte	Fundy National Park, NB	0	0	46.0
NB-505-7J	*Lophodermium* cf. *piceae*	*Picea rubens* endophyte	Fundy National Park, NB	1	1	75.1
NB-505-9L	*Lophodermium* cf. *piceae*	*Picea rubens* endophyte	Fundy National Park, NB	0	1	44.7
NB-487-3J	*Lophodermium* cf. *piceae*	*Picea rubens* endophyte	Fundy National Park, NB	0	0	19.9
NB-437-2E	*Lophodermium* cf. *piceae*	*Picea rubens* endophyte	Little Lepreau, NB	0	2	93.3
RS10-8E	*Pseudoplectania* cf. *nigrella*	*Picea rubens* endophyte	Fundy National Park, NB	0	0	15.5
RS10-3B	*Lachnellula cf. calyciformis*	*Picea rubens* endophyte	Fundy National Park, NB	1	1	102.2
RS10-7G	*Rhizosphaera kalkhoffii*	*Picea rubens* endophyte	Fundy National Park, NB	0	0	49.6
437-10C	*Lophodermium* cf. *piceae*	*Picea rubens* endophyte	Little Lepreau, NB	0	0	50.0
437-2A	*Pseudoplectania* cf. *nigrella*	*Picea rubens* endophyte	Little Lepreau, NB	0	0	29.8
334-21H	*Sordariomycete* sp.	*Picea rubens* endophyte	Doaktown, NB	0	1	50.0
392-3M2	*Cornibusella ungulata* gen. et sp. nov.	*Picea rubens* endophyte	Fundy National Park, NB	0	0	140.0
392-3M	*Collophora* sp.	*Picea rubens* endophyte	Fundy National Park, NB	2	2	80.3
334-1B	*Melanconis* cf. *alni*	*Picea rubens* endophyte	Doaktown, NB	0	0	50.0
437-8C	*Myxocyclus cenangiodes*	*Picea rubens* endophyte	Little Lepreau, NB	1	1	22.0
RS10-9K	*Setomelanomma* cf. *holmii*	*Picea rubens* endophyte	Fundy National Park, NB	0	0	50.0
488-6B	*Lachnellula* cf. *subtilissima*	*Picea rubens* endophyte	Fundy National Park, NB	0	0	48.8
437-8J	Rhytismatales sp.	*Picea rubens* endophyte	Little Lepreau, NB	0	0	29.5

285-3E	Rhytismatales sp.	*Picea rubens* endophyte	Doaktown, NB	0	0	33.5
RS10-14I	*Cornibusella ungulata* gen. et sp. nov.	*Picea rubens* endophyte	Fundy National Park, NB	1	1	35.5
NB-277-9C	*Micraspis acicola*	*Picea rubens* endophyte	Doaktown, NB	0	0	20.5
NB-638	*Hysterostegiella typhae*	Apothecia on dead sheath of *Typha* sp.	Orleans, ON	0	0	15.0
NB-632	*Lophodermium* cf. *piceae*	Apothecia on *Picea rubens* needles in litter layer	Little Lepreau, NB	0	0	8.2
RS10-9I	*Gloeopycnis protuberans* gen. et sp. nov.	*Picea rubens* endophyte	Fundy National Park, NB	1	1	35.2
RS10-90	cf. *Aquapoterium*	*Picea rubens* endophyte	Fundy National Park, NB	2	0	115.4
RS9-7B	*Gloeopycnis protuberans* gen. et sp. nov.	*Picea rubens* endophyte	Fundy National Park, NB	0	0	32.3
JMRC12214	*Mollisia cinerea* ex-epitype	Apothecia on decaying wood	Jena, Germany	0	0	18.9
NB-285-4E	*Coccomyces* sp.	*Picea rubens* endophyte	Doaktown, NB	0	0	42.7
NB-649	*Phialocephala biguttulata* sp. nov.	Apothecia under decaying bark of *Pinus strobus* windfall	Ottawa, ON	0	0	21.2
RS10-14I	*Cornibusella ungulata* gen. et sp. nov.	*Picea rubens* endophyte	Fundy National Park, NB	1	1	35.5
RS9-7J	*Calvophomopsis rubensicola* gen. et sp. nov.	*Picea rubens* endophyte	Fundy National Park, NB	0	0	18.0
421-12A	cf. *Pterula*	*Picea rubens* endophyte	Little Lepreau, NB	0	0	26.6
334-3B	*Pileospora picea* gen. et sp. nov.	*Picea rubens* endophyte	Doaktown, NB	0	0	25.3
NB-630	*Tryblidiopsis* sp. nov.	Apothecia on self-pruned *Picea glauca* branch	Dunsford, ON	0	1	39.0
NB-250-4I	cf. Rosaphaeria sp.	*Picea mariana* endophyte	Maugerville, NB	0	1	128.1
NB-644-1	*Lophodermium resinosum* sp. nov.	Fallen *Pinus resinosa* secondary needles on ground	Prescott and Russell Co., ON	0	0	76.4
NB-739	*Cistella* cf. *acuum*	Apothecia on fallen brown *Picea rubens* branch tip	Fundy National Park, NB	0	1	14.6
NB-636	*Xenopolyscytalum pinea*	Conidiophores on *Pinus strobus* needles in litter layer	Stittsville, ON	1	2	10.0
NB-469	*Phialocephala amethystea* sp. nov.	On bark of fallen *Acer saccharum* branch	Fundy National Park, NB	0	1	30.5
NB-285-4C	Rhytismatales sp.	*Picea rubens* endophyte	Doaktown, NB	0	0	24.1

RS10-4J	*Ophiognomonia* sp.	*Picea rubens* endophyte	Fundy National Park, NB	0	0	15.3
505-12I	*Micraspis acicola*	*Picea rubens* endophyte	Fundy National Park, NB	0	0	335.8
RS10-12A*	Thysanophora sp.	*Picea rubens* endophyte	Fundy National Park, NB	0	2	54.2
RS10-14G*	*Thysanophora* sp.	*Picea rubens* endophyte	Fundy National Park, NB	2	2	26.9
NB-589*	*Thysanophora* sp.	Isolated from conidiophores on *Picea rubens* needle	Fundy National Park, NB	0	0	136.7
NB-236-7B*	*Nectria dacryocarpa*	*Picea mariana* endophyte	Grand Lake Meadow, NB	0	2	49.6

* Screened in another study, and selected for further investigation in this thesis
0 = No activity observed
1= <2 mm zone of inhibition in Oxford disc assays
2= >2mm zone of inhibition in Oxford disc assays

Appendix II- Supplementary chromatograms

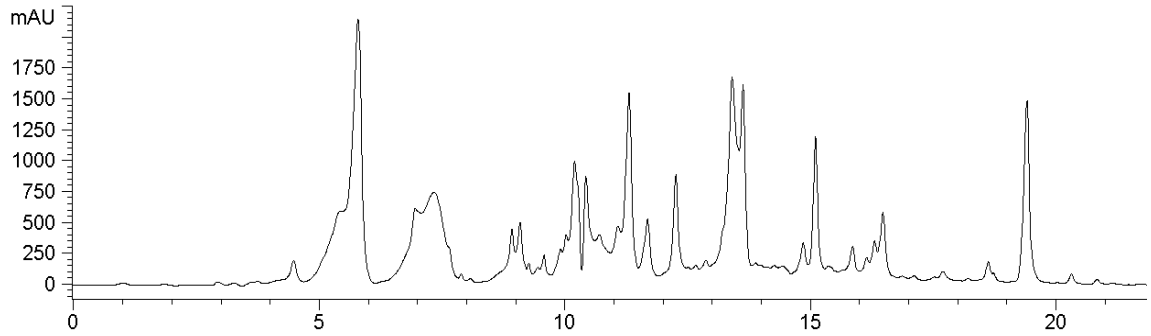

Figure A1. HPLC chromatogram of fraction 6 from *N. dacryocapa* (DAOMC 251709) at 320 nm.

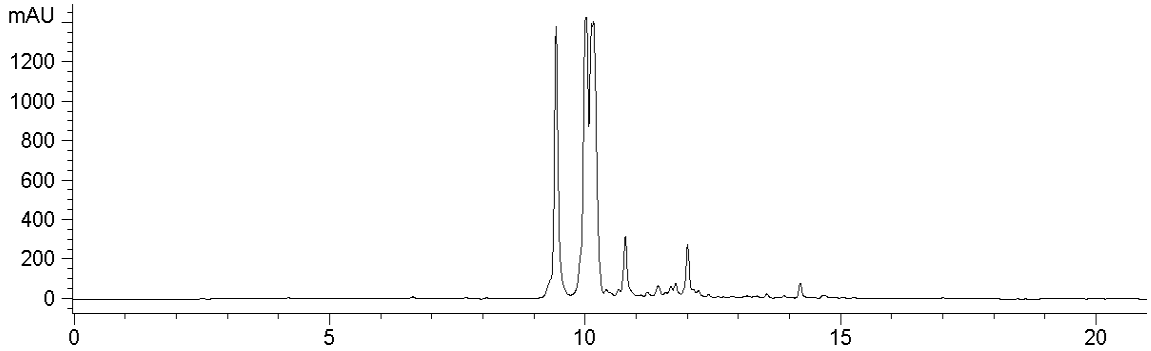

Figure A2. HPLC chromatogram of fraction 10 from *N. dacryocarpa* (DAOMC 251709), at 320 nm.

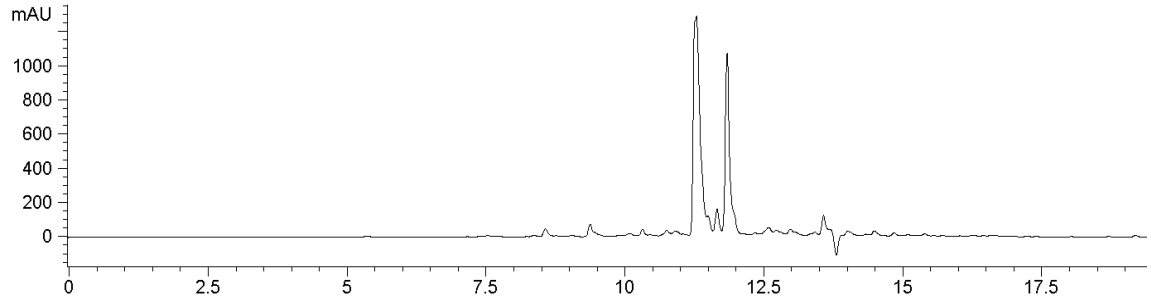

Figure A3. HPLC chromatogram of fraction 11 from *N. dacryocarpa* (DAOMC 251709), at 254 nm

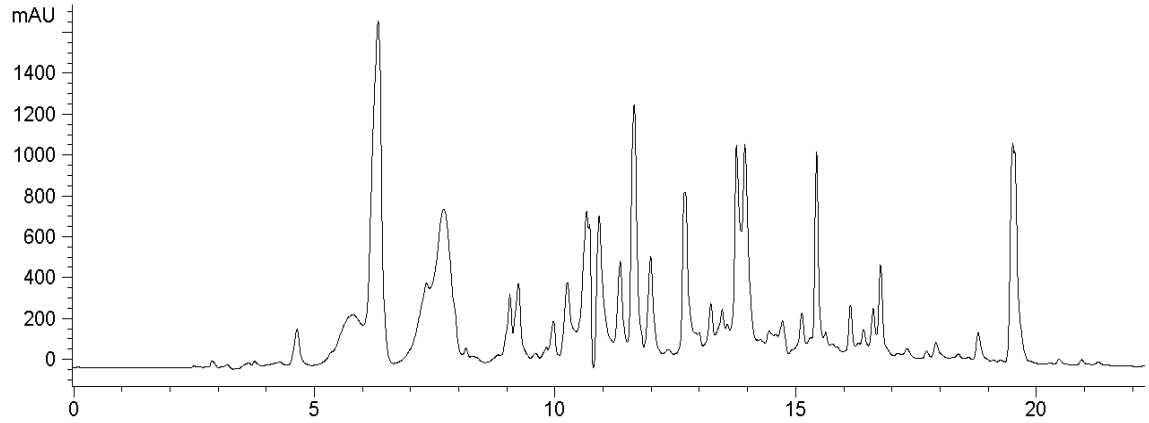

Figure A4. HPLC chromatogram of *P. glaucoalbidum* (RS10-14G DAOMC 251707), fraction 7 at 220 nm.

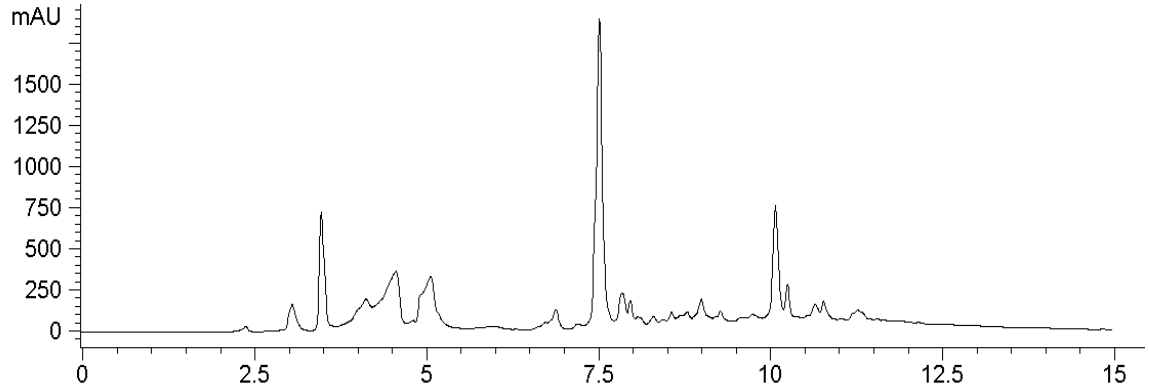

Figure A5. HPLC chromatogram illustrating the major metabolite (**4, 5**) produced by *P. glaucoalbidum* (NB-589, DAOMC 251708), at 254 nm.

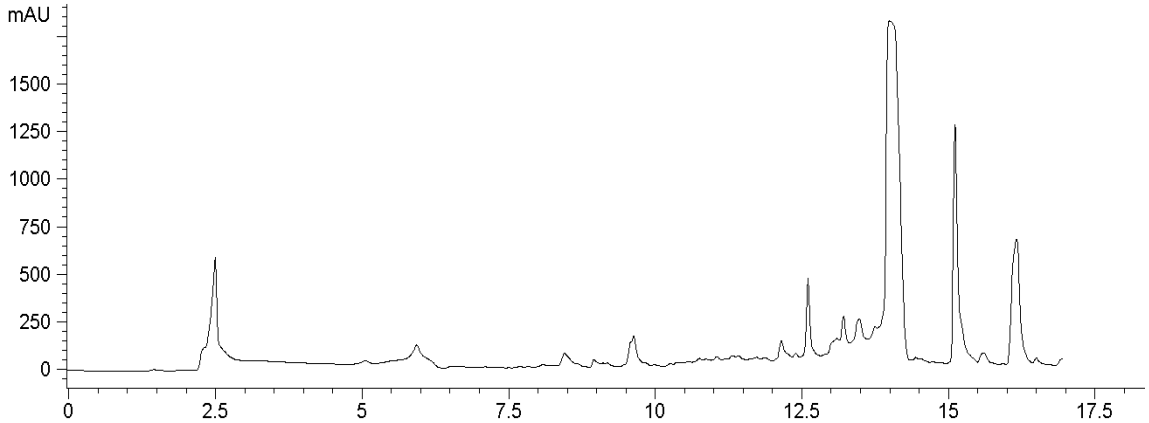

Figure A6. HPLC chromatogram of *L*. cf. *calyciformis* fraction 4 and 5 combined at 220 nm.

Appendix III- Secondary metabolite structures and ^{1}H and ^{13}C NMR spectra

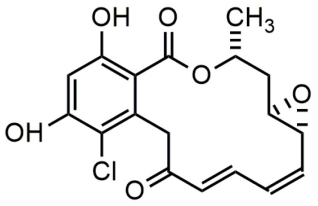

Figure A7. Structure of Radicicol (**1**)

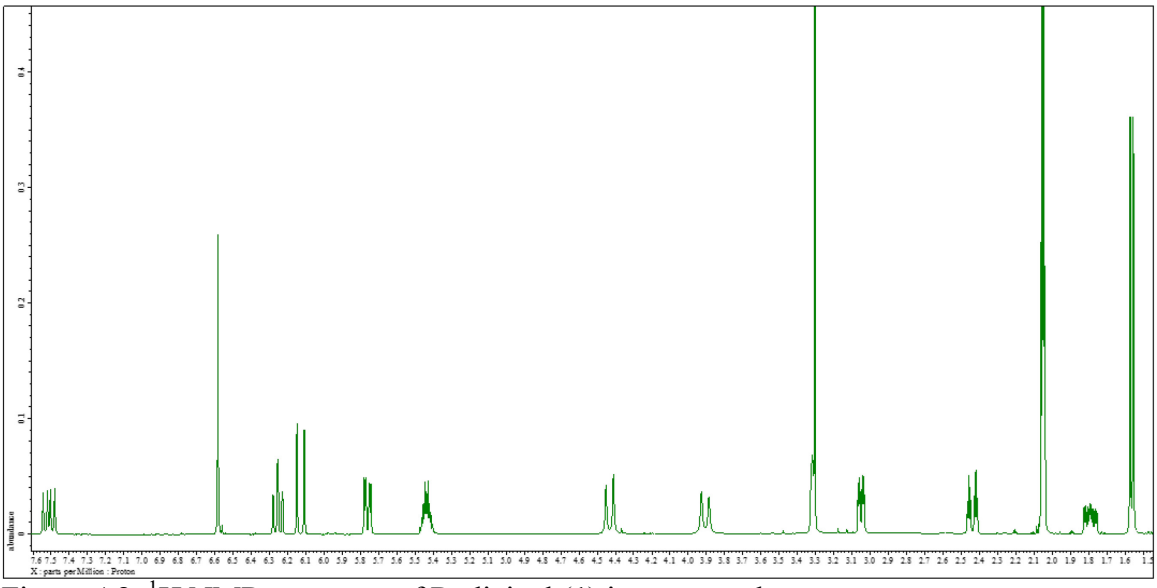

Figure A8. ^{1}H NMR spectrum of Radicicol (**1**) in acetone-d_6.

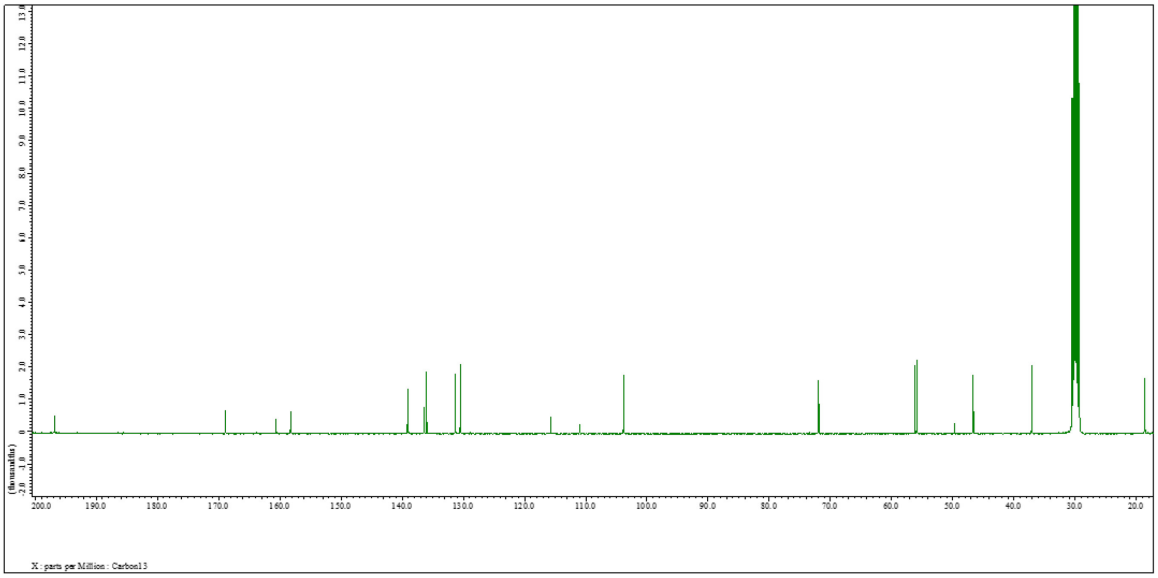

Figure A9. ^{13}C NMR spectrum of Radicicol (**1**) in acetone d_6.

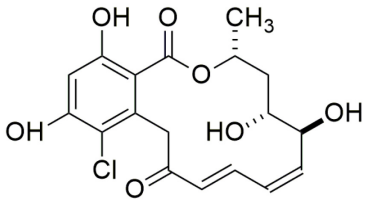

Figure A10. Structure of Radicicol B (**2**) in acetone-d_6.

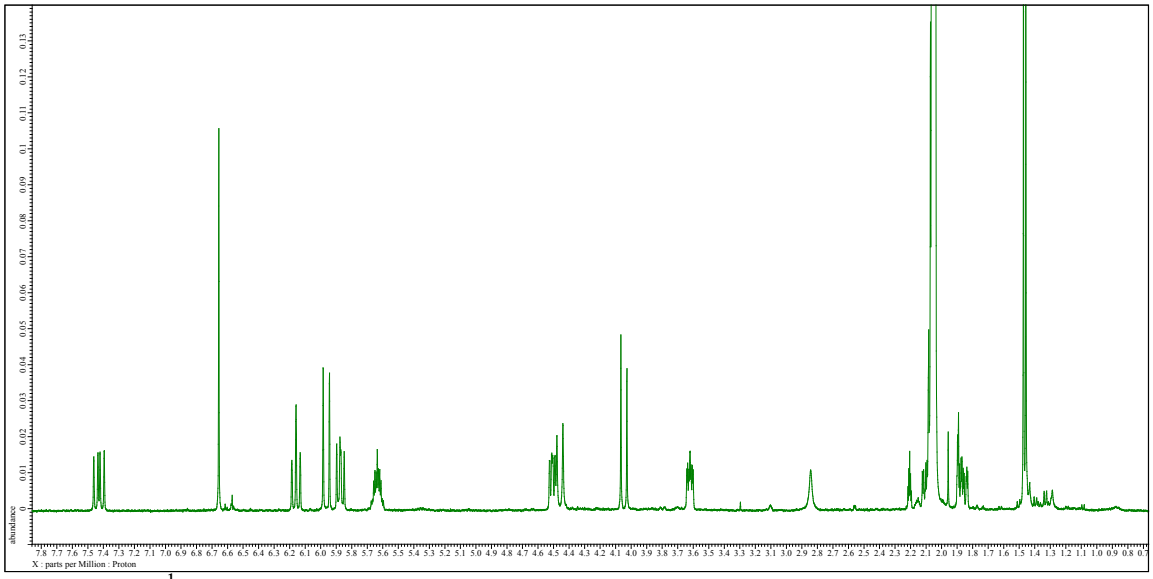

Figure A11. ^{1}H NMR of Radicicol B (**2**) in acetone-d_6.

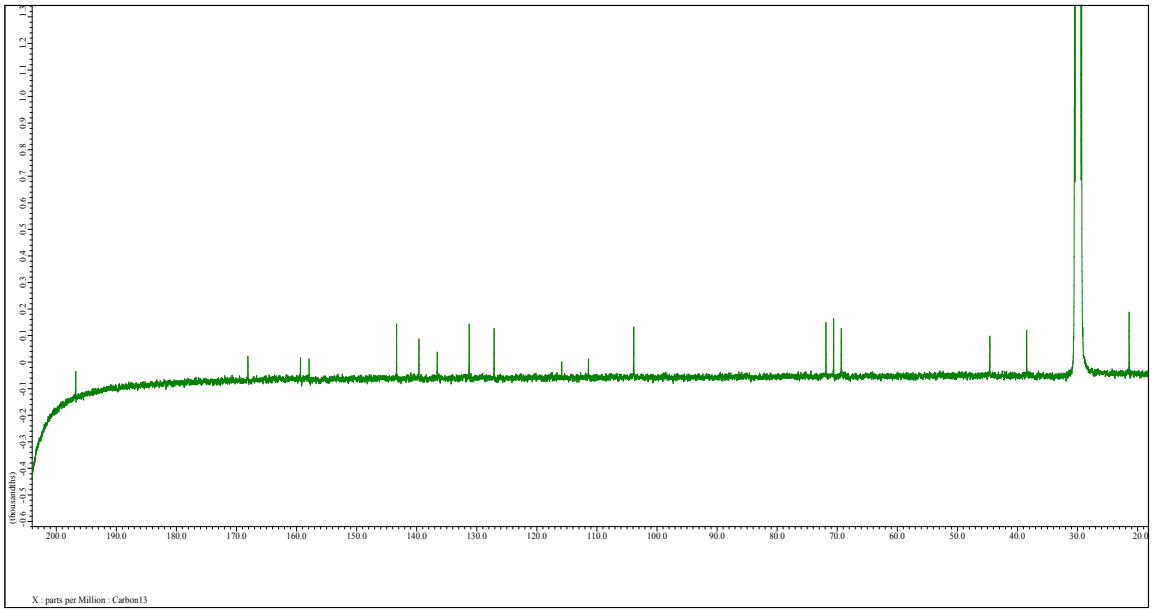

Figure A12. ^{13}C NMR spectrum of Radicicol B (**2**) in acetone-d_6.

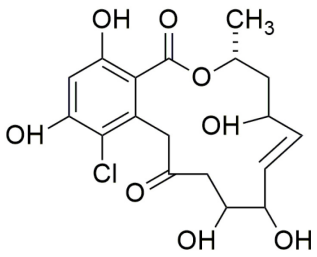

Figure A13. Structure of Radicicol C (**3**).

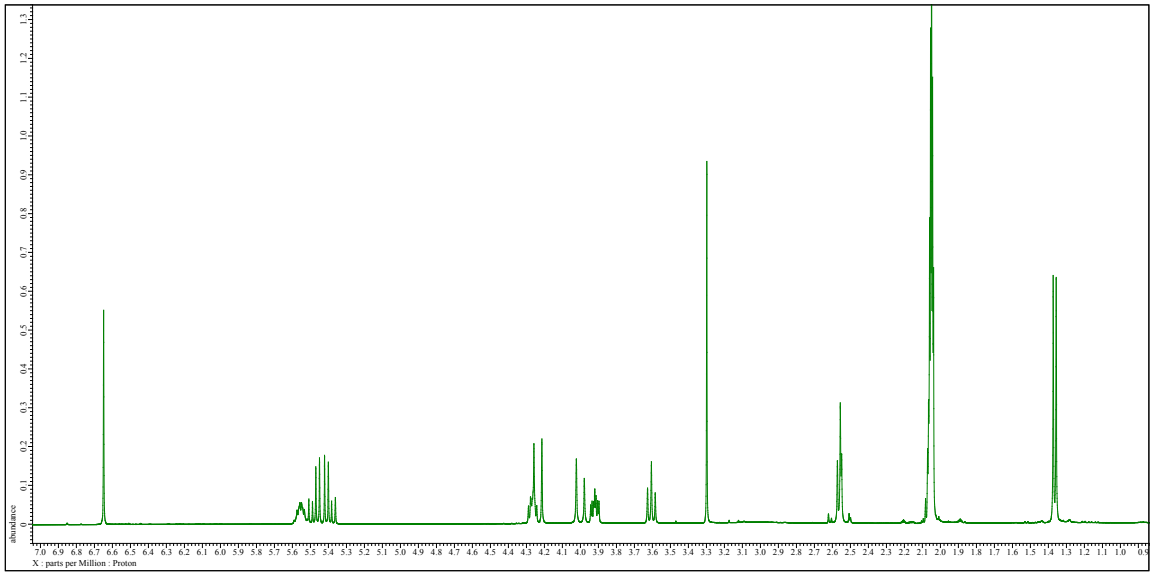

Figure A14. ^{1}H NMR spectrum of Radicicol C (**3**) in acetone-d_6.

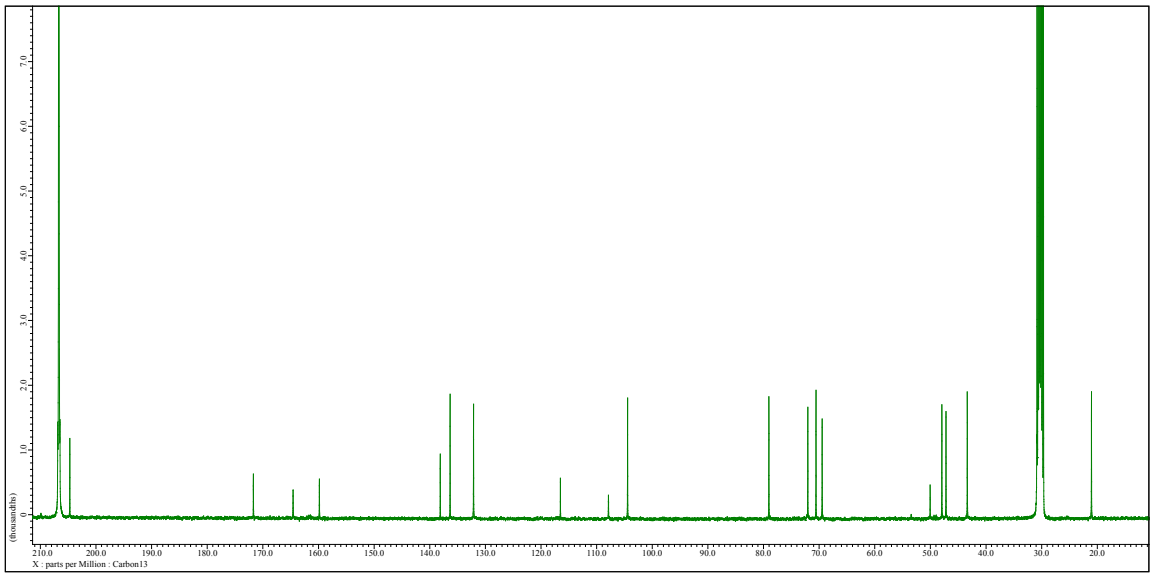

Figure A15. ^{13}C NMR spectrum of Radicicol C (**3**) in acetone-d_6.

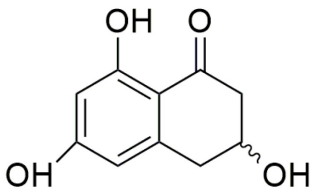

Figure A16. Structure of Scytalone (**4**,**5**)

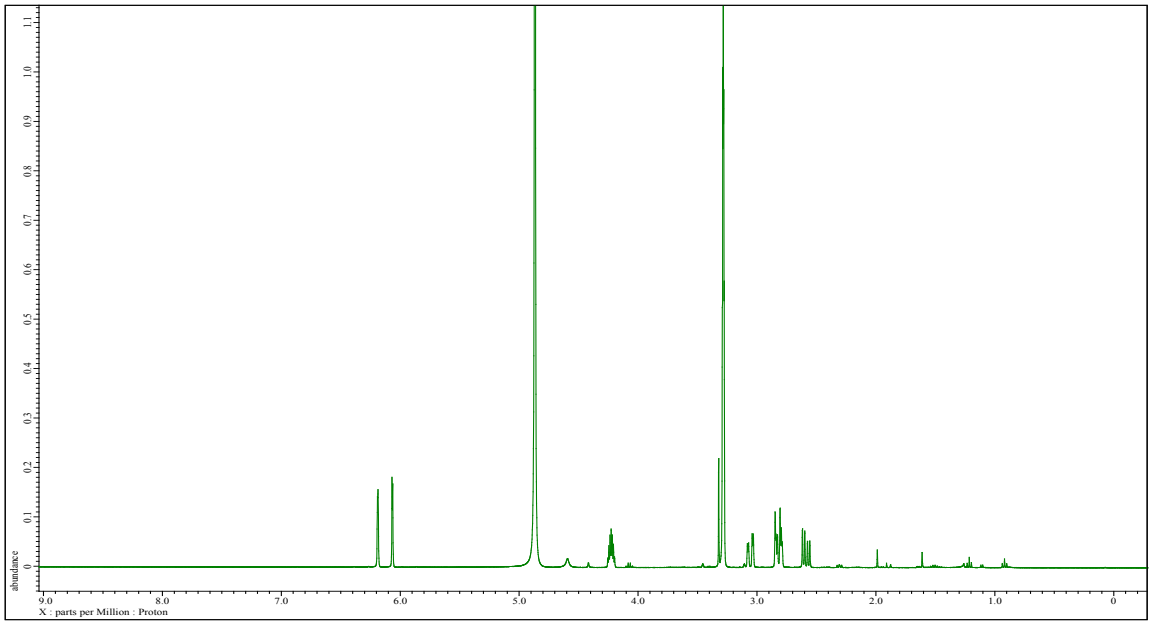

Figure A17. ^{1}H NMR of Scytalone (**4**, **5**) in CD_3OD, produced by *P.* cf. *glaucoalbidum*, NB-589.

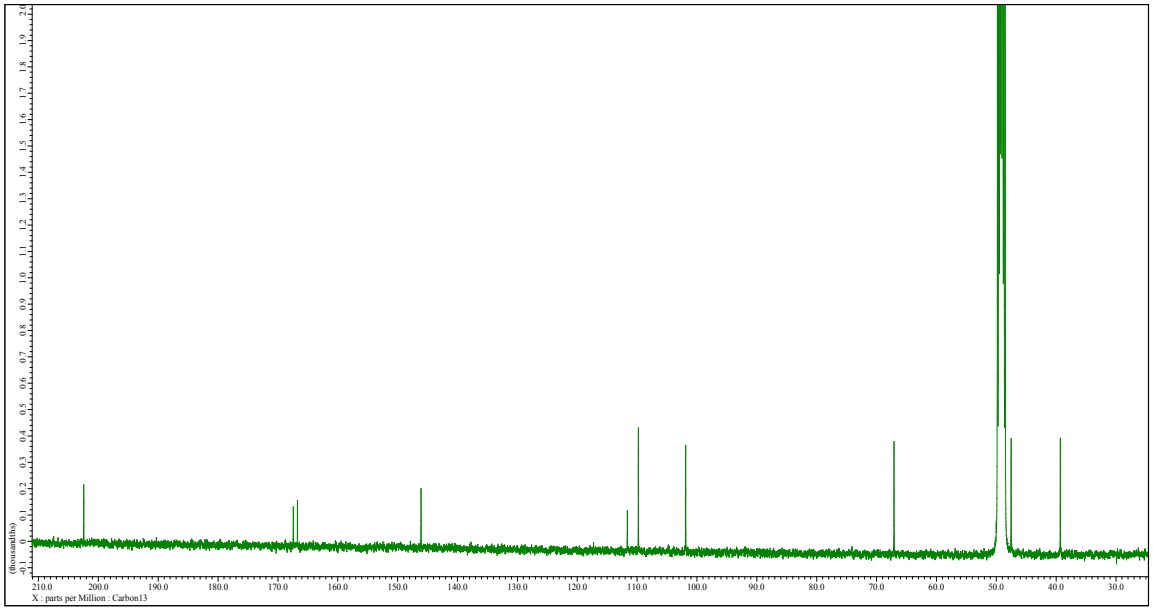

Figure A18. ^{13}C NMR spectrum of Scytalone (**4**, **5**) in CD_3OD, produced by *P.* cf. *glaucoalbidum*, NB-589.

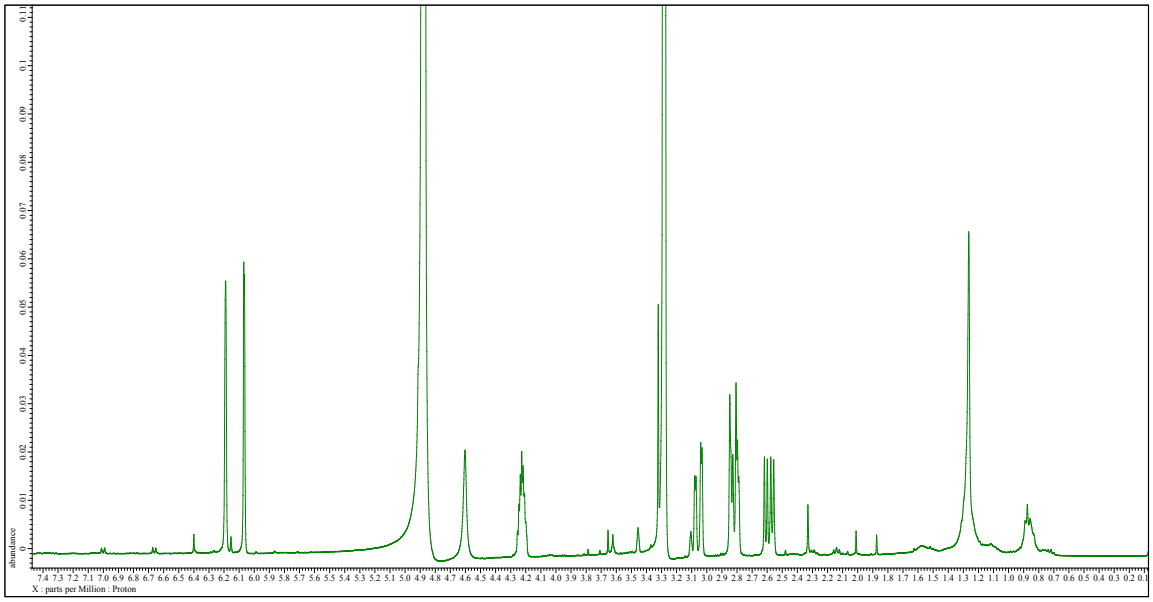

Figure A19. ^{1}H NMR of Scytalone (**4**, **5**) in CD_3OD produced by *P.* cf. *glaucoalbidum*, RS10-14G.

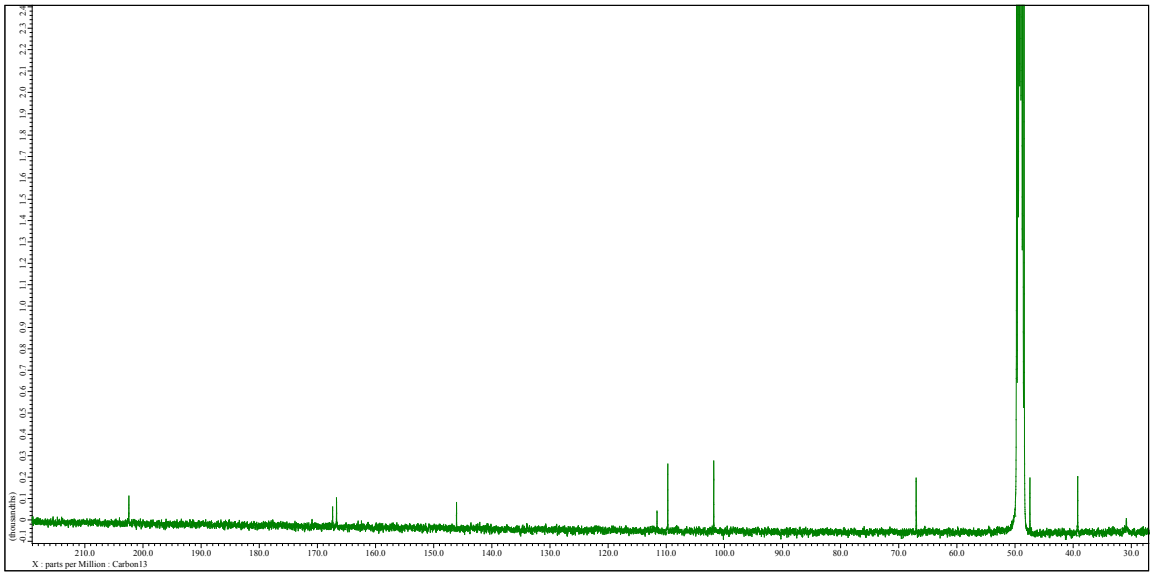

Figure A20. ^{13}C NMR spectrum of Scytalone (**4**, **5**) in CD_3OD, produced by *P.* cf. *glaucoalbidum*, NB-589.

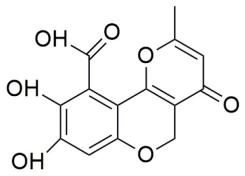

Figure A21. Structure of Citromycetin (**6**).

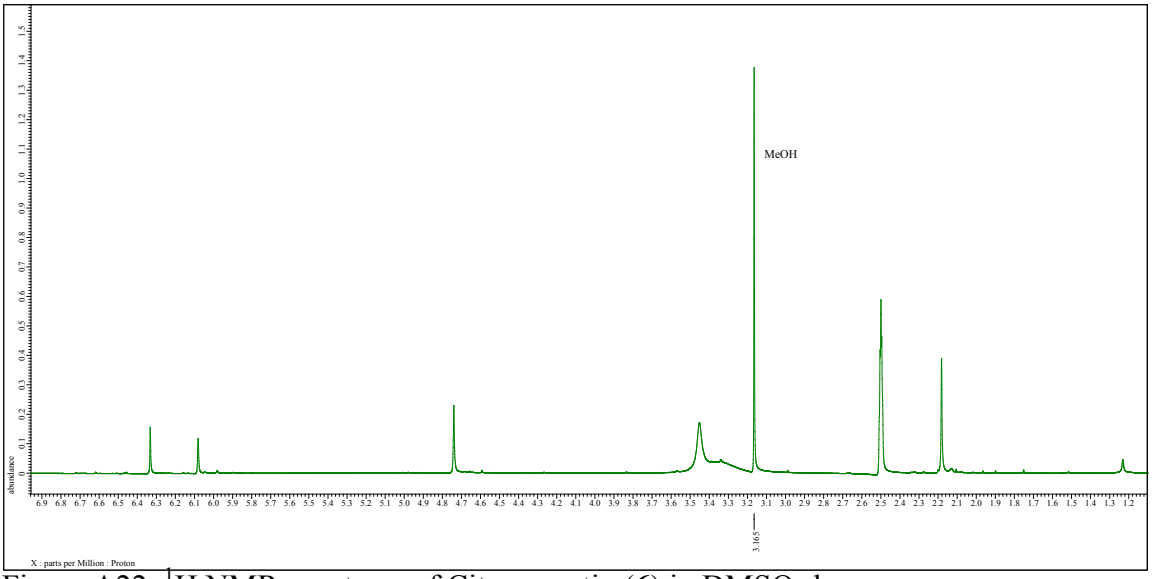

Figure A22. ^{1}H NMR spectrum of Citromycetin (**6**) in DMSO-d_6.

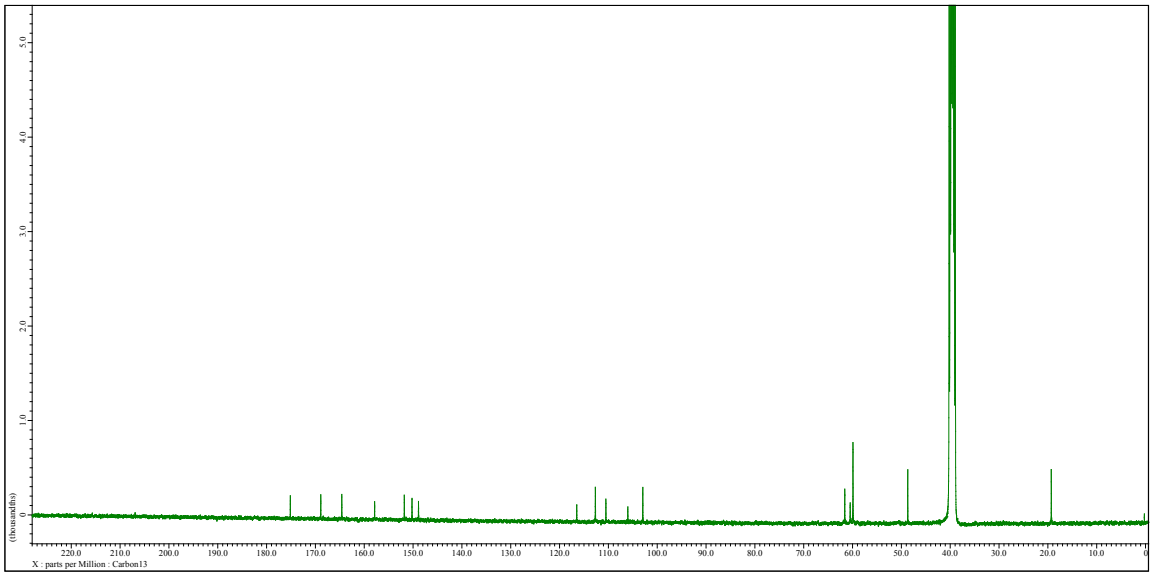

Figure A23. ^{13}C NMR spectrum of Citromycetin (**6**) in DMSO-d_6.

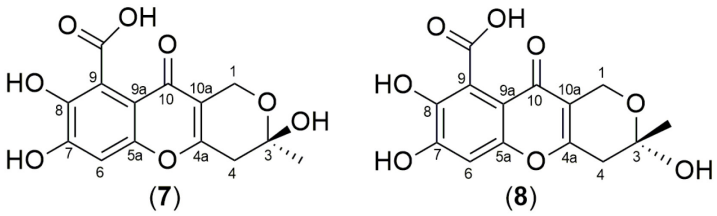

Figure 24. Structure of fulvic acid (**7**, **8**).

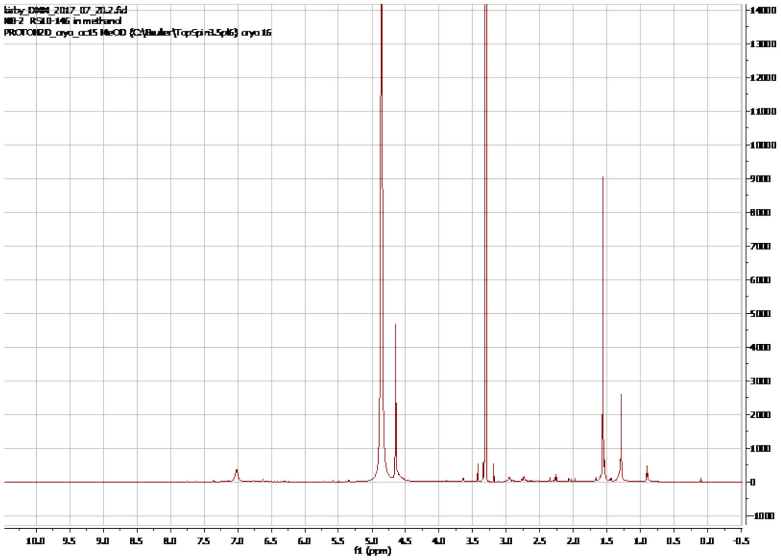

Figure 25. ^{1}H NMR spectrum of fulvic acid (**7**, **8**) in CD_3OD.

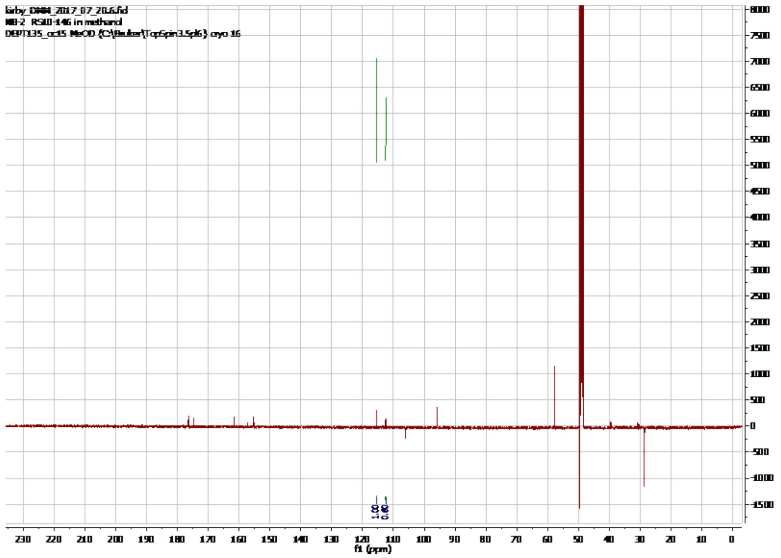

Figure 26. ^{13}C NMR spectrum of fulvic acid (**7**, **8**) in CD_3OD.

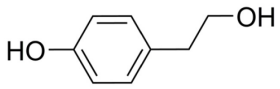

(**9**)

Figure A27. Structure of tyrosol (**9**).

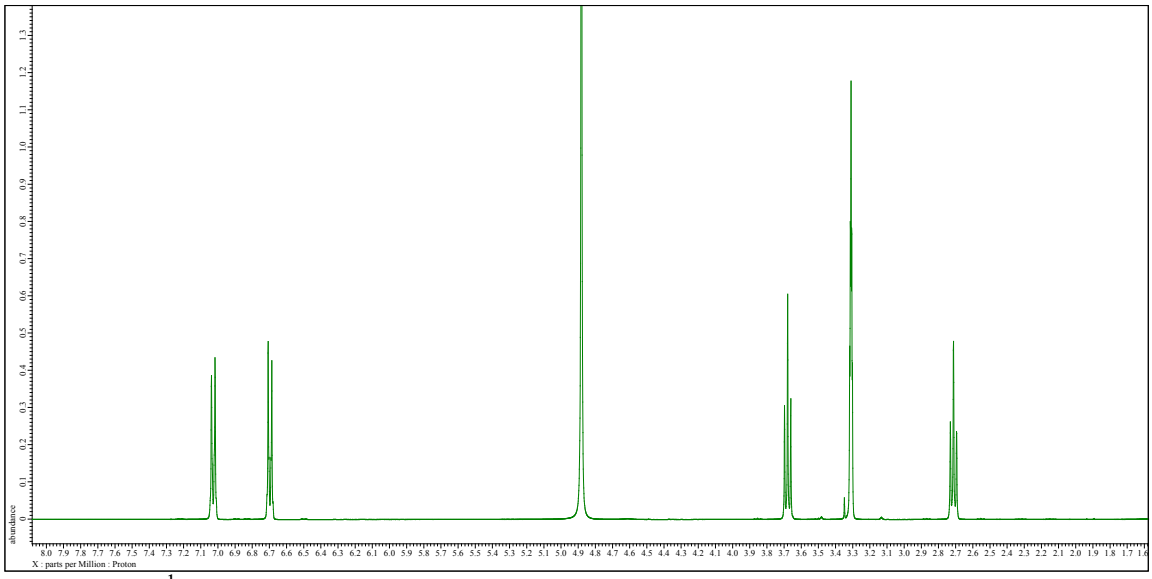

Figure A28. ^{1}H NMR spectrum of tyrosol (**9**) in CD_3OD.

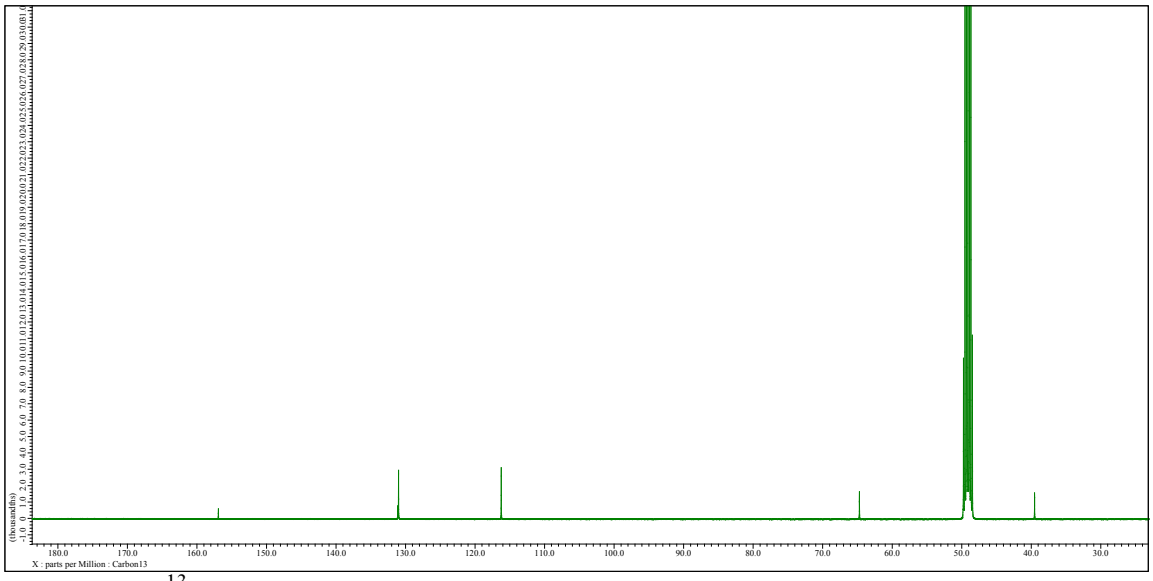

Figure A29. ^{13}C NMR spectrum of tyrosol (**9**) in CD_3OD.

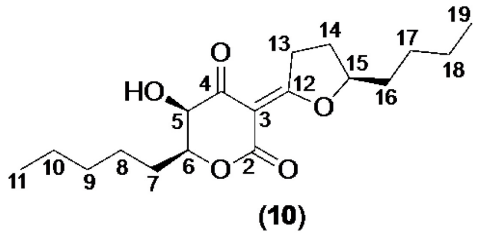

Figure A30. Structure of lachnellulone (**10**) isolated from *Lachnellula* cf. *calyciformis*.

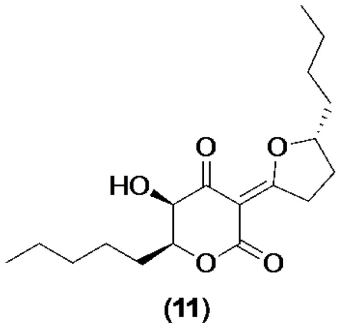

Figure A31. Structure of iso-lachnellulone (**11**) isolated from *Lachnellula* cf. *calyciformis*.

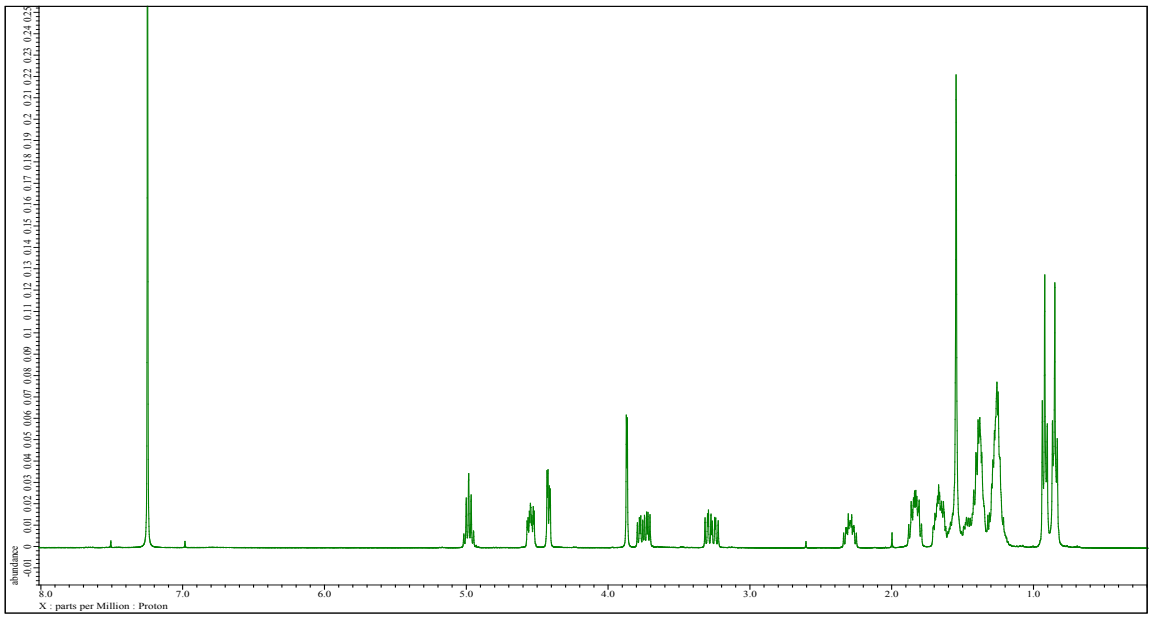

Figure A32. ^{1}H NMR spectrum of lachnellulone (**10**), with minimal amounts of iso-lachnellulone (**11**) in $CDCl_3$.

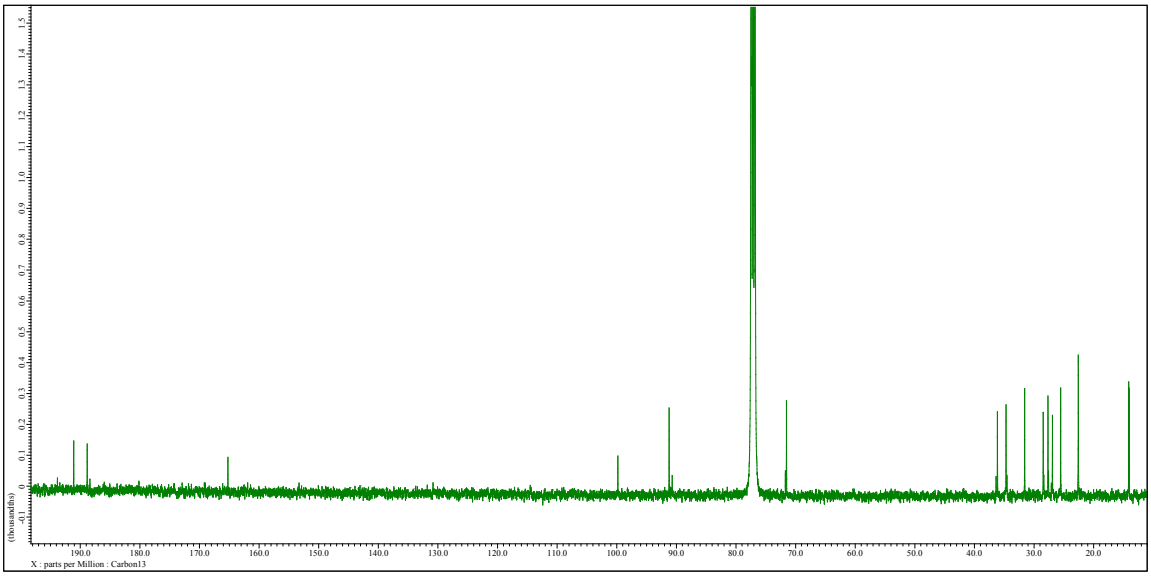

Figure A33. ^{13}C NMR spectrum of lachnellulone (**10**) and minor amounts of iso-lachnellulone (**11**) in $CDCl_3$.

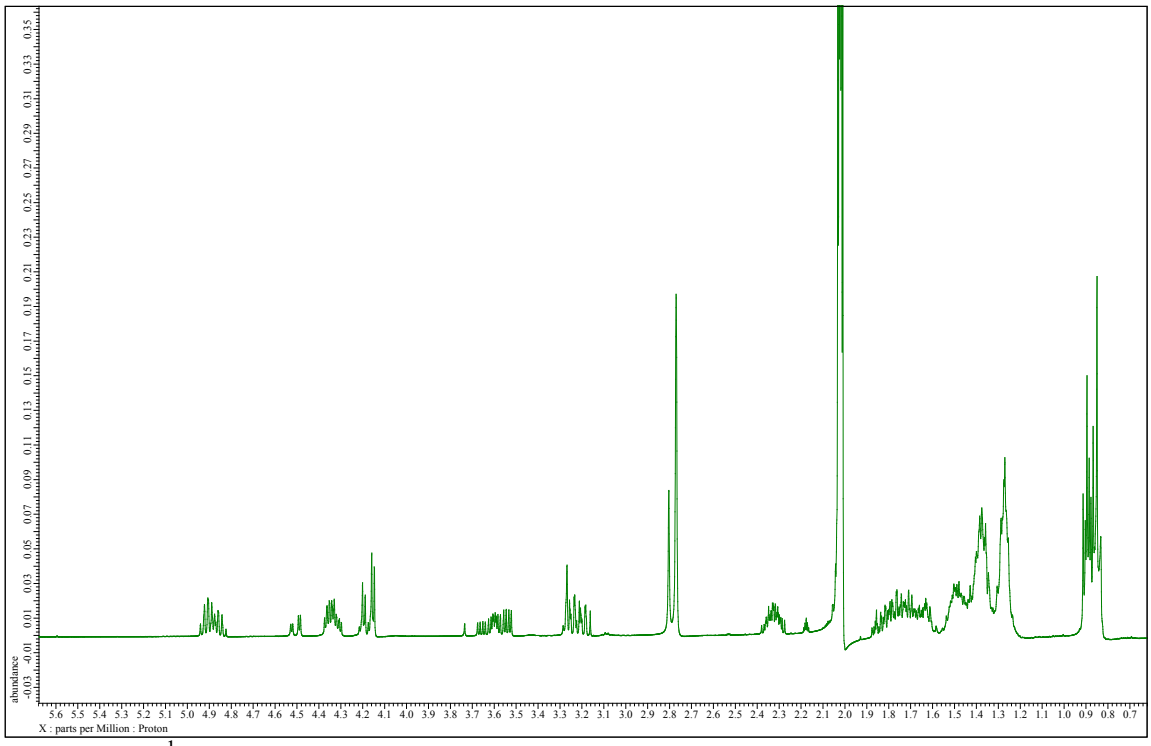

Figure A34. ^{1}H NMR spectrum of lachnellulone (**10**) and iso-lachnellulone (**11**) in Acetone-d_6, in approximately equivalent amounts.

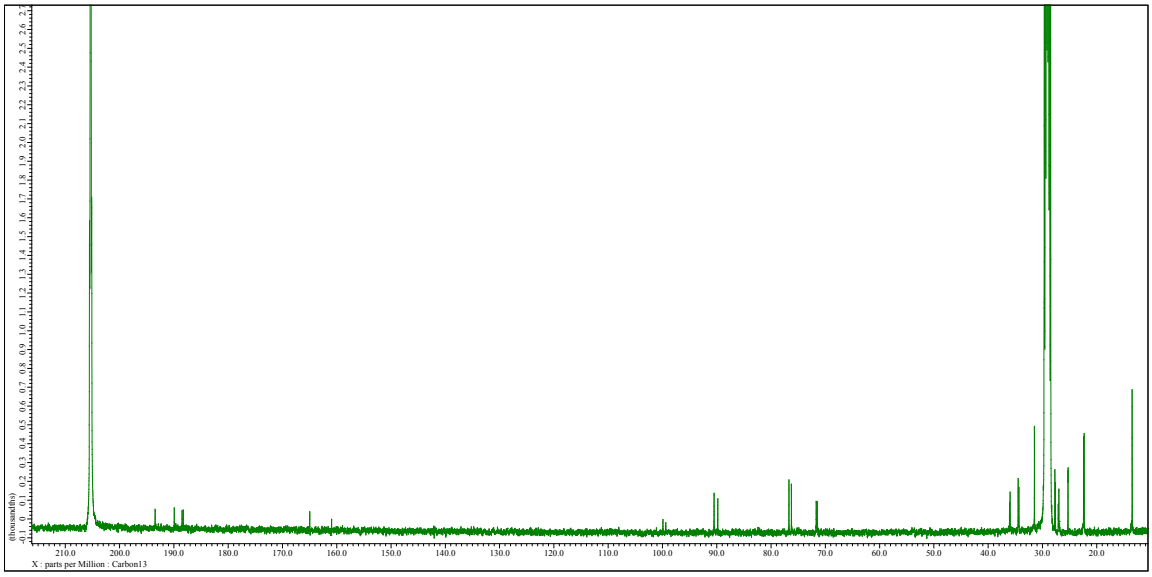

Figure A35. ^{1}H NMR spectrum of lachnellulone (**10**) and iso-lachnellulone (**11**) in CD_3OD, in approximately equivalent amounts.

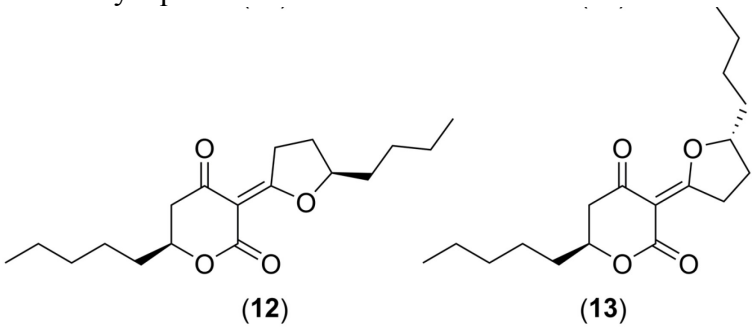

(**12**) (**13**)

Figure A36. Structures of new compounds from *Lachnellula* cf. *calyciformis* (**12**, **13**).

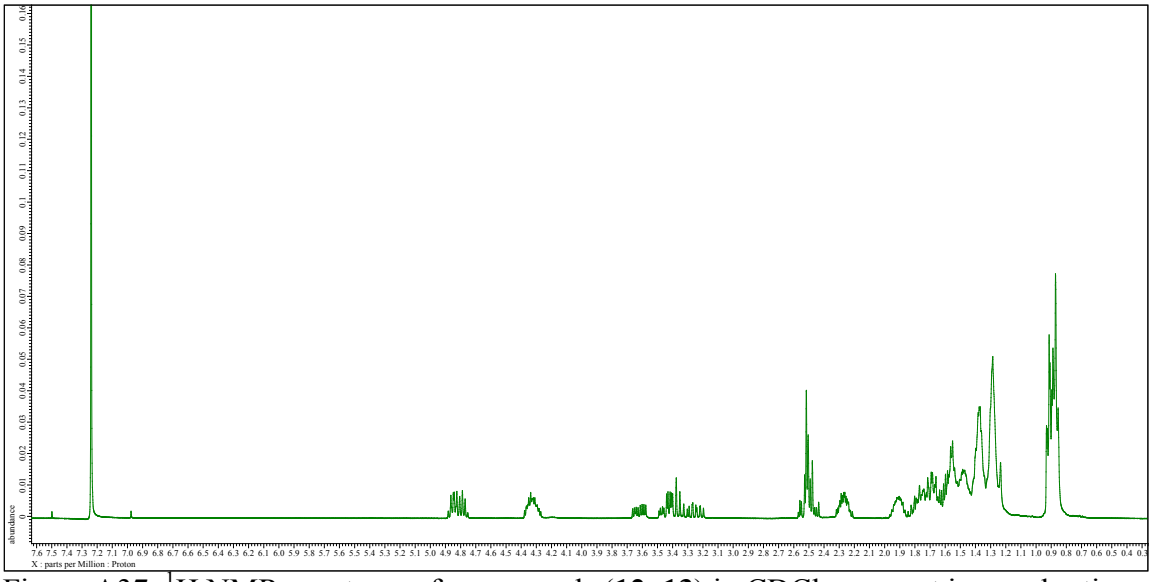

Figure A37. ^{1}H NMR spectrum of compounds (**12**, **13**) in $CDCl_3$, present in equal ratios.

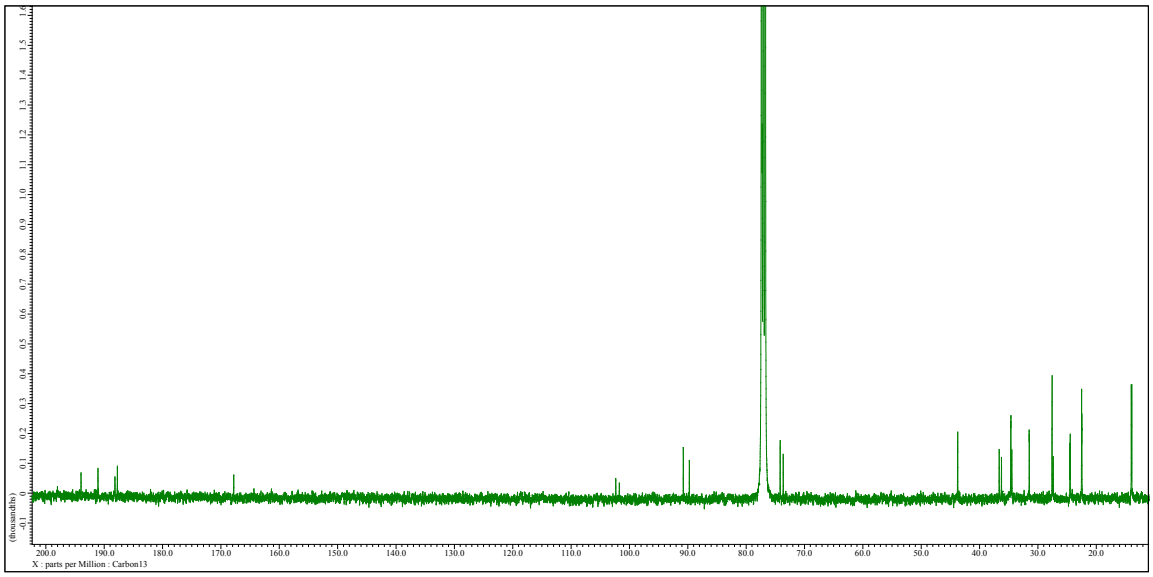

Figure A38. ^{13}C NMR spectrum of compounds (**12**, **13**) in $CDCl_3$ present in equal amounts.

Appendix IV- Phylogenetic variation between *Penicillium* cf. *glaucoalbidum*

BenA

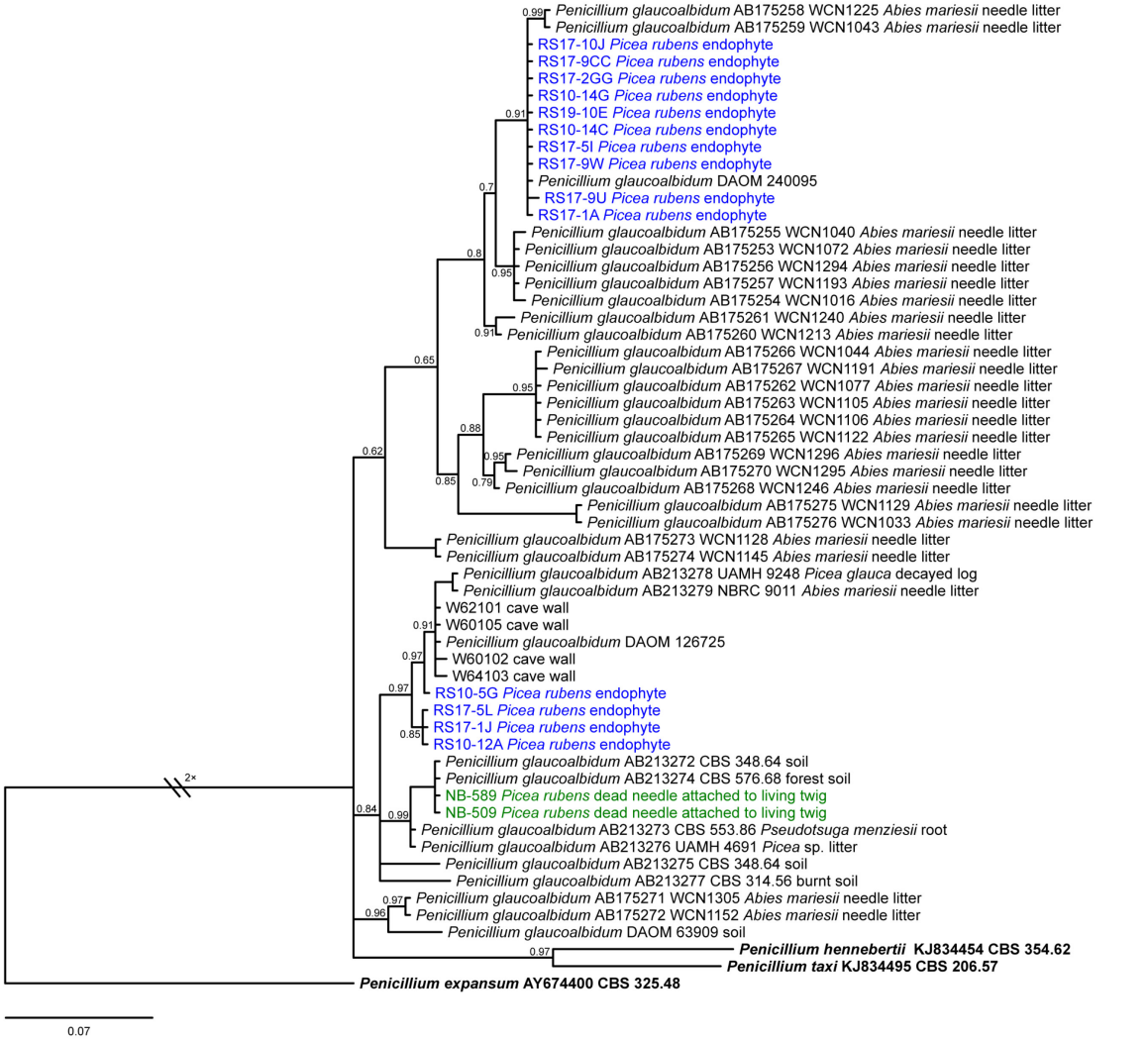

Figure A39. *P.* cf. *glaucoalbidum* species belonging to the Thysanophora sect., based on concordance between β-tubulin gene sequences.

Appendix V- IR spectrum of Tyrosol (9)

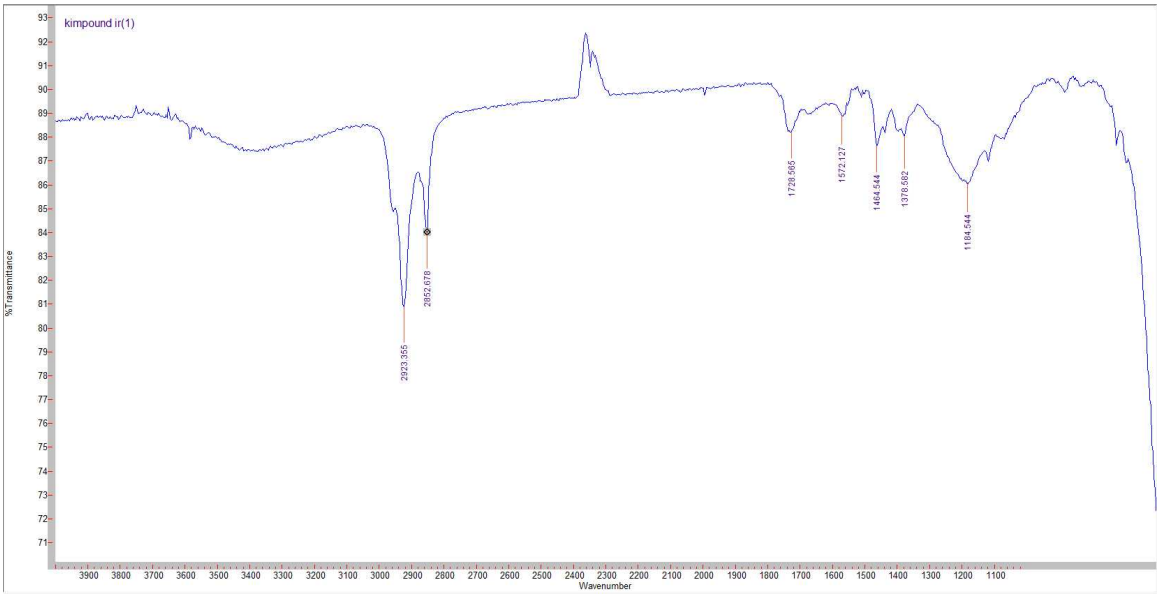

Figure A40. IR spectrum of tyrosol (**9**) prepared on a sodium pellet.